Universidad Miguel Hernández de Elche
Programa de Doctorado en Neurociencias Instituto de Neurociencias UMH-CSIC

The neural control of body symmetry, and an automated high-resolution pupae counting device

Memoria de Tesis Doctoral presentada por:
Roberto Santoro
-2023-

Directora de Tesis:
María Domínguez Castellano

Sant Joan d'Alacant, 16 de noviembre de 2022

La presente Tesis Doctoral, titulada "The neural control of body symmetry, and an automated high-resolution pupae counting device", se presenta bajo la modalidad de tesis convencional con el siguiente indicio de calidad:

Title: AUTOMATED HIGH-RESOLUTION PUPAE COUNTING DEVICE
Publication Number: WO/2022/090589
Publication Date: 05.05.2022
Inventors: R. Santoro, V. Rodríguez, M. Domínguez
International Filing Date 30.10.2020
Applicants: CONSEJO SUPERIOR DE INVESTIGACIONES CIENTIFICAS
PatentScope: https://patentscope.wipo.int/search/en/detail.jsf?docId=WO2022090589
DIGITAL.CSIC: http://hdl.handle.net/10261/286067

Sant Joan d'Alacant, 16 de noviembre de 2022

To whom it may concern,

The doctoral thesis entitled "The neural control of body symmetry, and an automated high-resolution pupae counting device" has been written and developed by me, Roberto Santoro.
This thesis is presented in a conventional format. It is based on experimental studies undertaken at the Neuroscience Institute of Alicante during the PhD program in neuroscience of the Miguel Hernández University.
Yours sincerely,

Sant Joan d'Alacant, 16 de noviembre de 2022

La Dra. "María Domínguez Castellano", directora de la tesis doctoral titulada "The neural control of body symmetry, and an automated high-resolution pupae counting device"

INFORMA:

Que D. "Roberto Santoro" ha realizado bajo mi supervisión el trabajo titulado "The neural control of body symmetry, and an automated high-resolution pupae counting device" conforme a los términos y condiciones definidos en su Plan de Investigación y de acuerdo al Código de Buenas Prácticas de la Universidad Miguel Hernández de Elche, cumpliendo los objetivos previstos de forma satisfactoria para su defensa pública como tesis doctoral.

Lo que firmo para los efectos oportunos, en …… a ……. de …….. de 202….

Directora de la tesis

Dra. "María Domínguez Castellano"

Sant Joan d'Alacant, 16 de noviembre de 2022

La Dra." Elvira De la Peña García", Coordinadora del Programa de Doctorado en n Neurociencias del Instituto de Neurociencias de Alicante, centro mixto de la Universidad Miguel Hernández (UMH) y de la Agencia Estatal Consejo Superior de Investigaciones Científicas (CSIC),

INFORMA:

Que D. "Roberto Santoro" ha realizado bajo la supervisión de nuestro Programa de Doctorado el trabajo titulado "The neural control of body symmetry, and an automated high-resolution pupae counting device" conforme a los términos y condiciones definidos en su Plan de Investigación y de acuerdo al Código de Buenas Prácticas de la Universidad Miguel Hernández de Elche, cumpliendo los objetivos previstos de forma satisfactoria para su defensa pública como tesis doctoral.

Lo que firmo para los efectos oportunos, en …… a ……. de …….. de 202….

Dra. "Elvira De la Peña García"
Coordinadora Programa de Doctorado en Neurociencias.

Financiación/Subvención/Beca:

Este trabajo de Tesis Doctoral ha sido posible gracias a una beca predoctoral de Formación de Personal Investigador (FPI), financiada por el Ministerio de Economía y Competitividad (MINECO) con referencia BES-2016-077689, un contrato de titulado superior en actividades técnicas y profesionales financiado por el Ministerio de Ciencia e Innovación, y un contrato de apoyo técnico a la investigación financiado a través del programa PROMETEO. La investigación ha sido financiada por los siguientes proyectos:

“Crecimiento y Cáncer: De los Mecanismos a las Aplicaciones Terapéuticas”
Ref: BFU2015-64239-R
“Genetic Robustness, Systemic and Local Effectors, and their Implications in Cancer (RESYST)”
Ref: PID2019-106002RB-I00
“Redes Genéticas y Mecanismos de Cáncer y Metástasis (CancerMEC y TERAP)”
Ref: PROMETEO/2017/14


CSIC
UNIVERSITAS
Miguel Hernández
INSTITUTO DE NEUROCIENCIAS


EXCELENCIA
SEVERO
OCHOA

Table of contents

Abbreviations

CNS: Central Nervous System

VNC: Ventral Nerve Cord

SEZ: Subesophageal Zone

PG: Prothoracic Gland

Ilp8: Insulin-Like Peptide 8

Lgr3: Leucine-rich repeat-containing G protein-coupled receptor 3

Lgr4: Leucine-rich repeat-containing G protein-coupled receptor 4

comm: commissureless

CINs: Commissural interneurons

robo1: roundabout 1

robo2: roundabout 2

robo3: roundabout 3

cAMP: Cyclic adenosine monophosphate

GCaMP6m: genetically encoded fluorescent Ca[2+] indicator

ACs: Adenylyl cyclase

rut: rutabaga

Ptth: Prothoracicotropic hormone

IPCs: Insulin-producing cells

TrpA1: Transient receptor potential cation channel A1

AS: Antisymmetry

DA: Directional asymmetry

FA: Fluctuating asymmetry

RA: Random asymmetry

FAi: Fluctuating asymmetry index

MAT: Match-maker

GAT: Give-and-take

foxo: Forkhead box, sub-group O transcription factor

JH: Juvenile hormone

TH: Tyrosine hydroxylase

Table of figures

Resumen

La biología del desarrollo estudia el cambio de un organismo a través del tiempo. Los metazoos pasan por varias fases de crecimiento estereotipadas en cada especie. Para los insectos holometábolos, los pasos más críticos son el desarrollo embrionario, las etapas larvales, la metamorfosis y, finalmente, la edad adulta. Ser capaz de definir correctamente la duración de estas diferentes fases permite a los científicos descubrir los factores que determinan el destino del desarrollo de dicho organismo.

La primera parte de la tesis trata sobre un invento que permite conocer el momento exacto de pupa de cada una de las larvas de Drosophila en los tubos.

En la introducción, escribiré sobre los antecedentes de la invención. También presentaré como se hace el experimento de forma manual, y su historia. El pasado es fundamental para no subestimar este experimento y su utilidad. También revisé la principal solución automatizada en la literatura. Finalmente, en la sección de resultados, describiré el proceso inventivo que nos lleva a la versión real del prototipo.

Mostraré un ejemplo de un experimento grabado cada veinte minutos (los normales son cada cuatro/ocho horas) y los videos producidos por el robot. En la última sección de los resultados, describiré un método utilizado en la fotografía *rollout* para recrear imágenes 2D de un objeto cilíndrico. Finalmente, en la discusión, explicaré las ventajas de nuestro robot frente a otros competidores y cuál será la siguiente fase de este proyecto.

Los organismos del reino animal difieren en dimensiones y formas. A pesar de tales diferencias, la maquinaria molecular central es similar. Aun así, sabemos que un elefante es grande y un ratón es pequeño, y toda su progenie será muy similar entre individuos de la misma especie. Además, un hecho es que somos bilaterales y que nuestras manos, piernas, pies, son en general simétricos. Aunque nuestros brazos y piernas (y el resto del cuerpo) pueden crecer durante dieciocho años, produciendo miles de millones de células, el resultado final es notablemente simétrico. La segunda rama de esta tesis te introducirá a un mundo de formas y simetrías.

Esta introducción es un viaje por el reino animal. En primer lugar, intentaremos comprender qué diferencia a las especies entre sí. Continuaremos con una analogía entre la presencia de neuronas en los *phyla* y la presencia de simetría externa (radial y bilateral). Luego navegaremos por las asimetrías animales, donde algunas regiones del cuerpo se apartarán de la perfecta simetría bilateral. De los

ejemplos de asimetrías, introduciré los conceptos básicos de mi tesis, que son la asimetría fluctuante y el estudio de la homeostasis del crecimiento. También introduciré uno de los factores molecular que determina el crecimiento contralateral del sistema nervioso en desarrollo y por qué este tiene una íntima relación con la simetría de los rasgos corporales bilaterales.

En la sección de resultados, presentaré datos para comprender cómo las proyecciones contralaterales de las interneuronas son necesarias para el control del crecimiento homeostático, y como afectarán la simetría bilateral del cuerpo. Luego, intentaremos obtener el circuito mínimo para la homeostasis del crecimiento seleccionando cuidadosamente un subconjunto de neuronas de crecimiento homeostático. Finalmente pasaremos a la caracterización fisiológica de estas neuronas y su papel en el mantenimiento de una perfecta simetría bilateral. En la discusión, relacionaré nuestros resultados con el estado del arte y describiré un posible modelo para tales descubrimientos.

Summary

Life is the property that distinguishes living organisms from inanimate matter, defined as the capacity for growth, reproduction, and response to stimuli outside or from within the organism. These properties have *time* in common. One stone will remain a stone after one hundred years, but an organism will not be the same. Life has an intimate relationship with progress and change.

Developmental biology studies the changes of an organism through time. For holometabolous insects, such as *Drosophila melanogaster*, the most critical step is the onset of metamorphosis. Determining the timing of such a crucial milestone with precision entitles scientists to uncover factors and stressors that may accelerate, delay, prevent or cause an untimed transition and exploit the alteration to screen for compounds and medicines that restore timed development and health.

The measurement of the timing of metamorphosis has been performed manually since the beginning of the past century. Recently, interest in automatizing this laborious and time-consuming task has led to several reports on possible automated solutions. However, none of the solutions achieve the precision of manual quantification, and none are scalable. In the first section of my thesis, I will present the robot flyGear. This robot fully automates the measurement of developmental timing for larvae and pupa of *Drosophila melanogaster and more*, achieving more precision than manual scoring and is scalable. I extensively tested the accuracy and its uses in different scenarios. The technology is now patented and highly user-friendly. I will describe how the technology was developed and illustrate how flyGear can precisely track pupation and the preceding wandering behaviour in a developmental timing experiment.

Living organisms are highly reactive to environmental perturbations and mutations that can affect developmental timing and growth. Yet, they are also robust, capable of withstanding substantial variations in size and producing perfectly symmetrical bodies. This is remarkable if one considers that the body and parts like legs can grow for eighteen years, producing billions of cells. The final outcome is remarkably precise, as illustrated by body symmetry.

The second section of my thesis will present new molecular and cellular mechanisms involved in maintaining body symmetry. The preface is a journey through the animal kingdom and species with or without bilateral external symmetry (radial and bilateral). First, I will discuss animal asymmetries, where some regions of the body depart from the perfect bilateral symmetry, which have a genetic basis. Then, I will discuss body asymmetries as pathological departures (fluctuating asymmetry) of expected

bilateral symmetric parts. I will introduce the basic concepts of the experimental subject of this thesis, the geometric morphometric methods, and the genes used to decipher the circuit and logic ensuring the symmetry of bilateral body traits.

The results section shows that commissural interneurons convey information between the left and right parts of the central nervous system (CNS) to ensure bilateral body symmetry. Next, I will describe the MAT (Match-maker) and GAT (Give-and-take) neurons that form the core circuit that controls bilateral symmetry homeostasis. To conclude, I will present ex vivo calcium recording and in vivo electrical manipulation of these neurons and a model of how these neurons correct mismatches and maintain perfect bilateral symmetry.

"Yes, man is mortal, but that would be only half the trouble. The worst of it is that he's sometimes unexpectedly mortal—there's the trick!"

— Mikhail Bulgakov, The Master and Margarita

Introduction

flyGear

The automation of experimental tasks to increase precision and productivity

Automating some routine manual tasks in the laboratory will be standard in the coming years. Considerable time will be saved, and researchers will have more control over their experiments by using their mobile phones and apps to set up experiments, their progress, or check on animal welfare.

The fruit fly *Drosophila melanogaster* is one of the most used insects in research on growth (Texada, Koyama and Rewitz, 2020), development (Garcia-Bellido, Ripoll and Morata, 1973; Rubin, 1988), neurogenetics (Nériec and Desplan, 2016), obesity (Musselman and Kühnlein, 2018; Chatterjee and Perrimon, 2021), and physiology of 'puberty' (Hariharan, 2012; Pan, Connacher and O'Connor, 2021). The adult fruit fly is a favourite model organism for behavioural and neuroimaging studies, and the automation of standard behavioural experiments has been progressing rapidly in recent years. For example, several methods have been published for the automated climbing assay (Podratz *et al.*, 2013; Cao *et al.*, 2017; Aggarwal, Reichert and VijayRaghavan, 2019; Spierer *et al.*, 2021), which measures motor performance in adult flies by exploiting the innate negative geotaxis of fruit flies when startled. The climbing assay has a broad use in investigations of *Drosophila* models of Alzheimer's disease (Cao *et al.*, 2017), Huntington's disease (Lambrechts, Faber and Sibon, 2017), and ageing (Jones and Grotewiel, 2011). All these climbing systems are produced by different laboratories, and they lack a unification method to address the locomotor disfunctions.

A major automated system for measuring *Drosophila* locomotion do exist and is fabricated by a little company called TriKinetics (TriKinetics, internet site). The most used tool from TriKinetics is the *Drosophila Activity Monitor* or DAM system. It works by counting the activity of single flies by the interference of the fly with infra-red light. The DAM system is used to study, among many other things, the circadian rhythms (Sarov-Blat *et al.*, 2000; Chen *et al.*, 2014; Yamaguchi *et al.*, 2022). Citing these articles, I'm just scraping the surface of one of the most used automation methods in the fruit fly field. In fact, this method is so widely utilized that there are growing number of software for analysing these data (Gilestro and Cirelli, 2009; Cichewicz and Hirsh, 2018; Geissmann *et al.*, 2019).

A very interesting hardware for studying the feeding behaviour in the fruit flies is the flyPAD (Itskov *et al.*, 2014). This is a device for automating feeding behaviour in individual flies and it uses the proboscis extension response and a sensor as an indicator of food intake *in vivo* and capable of capturing critical aspects of this behaviour in response to stress, diet, illness, or changes in internal state *in vivo* (Itskov *et al.*, 2014). The apparatus is based on the interaction between the proboscis of a fly and the food and is detected as a change in capacitance between two electrodes, where one electrode is under where the fly stands, and the second is where the food is placed (Itskov *et al.*, 2014). Many studies utilize the flyPAD for measuring food intake in a variety of conditions, like for studying high-sugar diet

effects (van Dam *et al.*, 2020), or to assaying the neural basis of satiety (Musso, Junca and Gordon, 2021).

Although the existence of various automatized assays, many scientific works with flies rely upon manual-performed, and time-consuming experiments, and very few automations are covering the growth stage of the fruit fly. Many attempts of automation in the fly world are amateurish and far away from the precision that science requests.

During my Ph.D., and for the three first years in my free time, I envisioned and developed a robot prototype. Then, the ball starts to roll down, and nowadays, we are developing a must-have robot for future research in Drosophila.

In the following sections, I will introduce flyGear, a robot that automates the count of wandering larvae and pupae.

Background of the invention flyGear

The beginning of sexual maturation (called metamorphosis in insects, and its equivalent, puberty, in mammals) is the most critical transition in the life history of an organism, which maximizes its reproductive success and adaptation to the environment (Tennessen and Thummel, 2011; Barredo *et al.*, 2021). The critical signal triggering the onset of sexual maturation or puberty is still unknown in most animal species, and as a consequence, the control of this process is the subject of intense research (Barredo *et al.*, 2021).

There is an enormous interest in clinical factors causing early initiation or delay in the transition between the juvenile and adult stages (Abreu and Kaiser, 2016; Das *et al.*, 2017; Lam *et al.*, 2021). The juvenile growth and the age of sexual maturation show plasticity and adaptation in response to distinct environmental conditions and endogenous factors, such as poor nutrition, diseases, infections, mutations, a tumour, or endocrine disruptors in flies (Smith-Bolton *et al.*, 2009a; Tennessen and Thummel, 2011; Garelli *et al.*, 2012), and humans (Lam *et al.*, 2021). The delay or acceleration of this transition can have a negative and persistent impact on the final height and fertility (Chan, Feld and Jonsdottir-Lewis, 2019), and it is a risk factor for obesity (Lam *et al.*, 2021) and certain cancers (Day *et al.*, 2017; Hur and Giovannucci, 2020). The onset of sexual maturation varies from individual to individual within a species. Genetic factors and environmental conditions, such as changes in temperature, length of day (seasons), nutrition, and endocrine disruption or diseases, influence the onset of sexual maturation or metamorphosis/puberty (*Reproductive health in young male adults with chronic diseases in childhood*, 2013).

In both children and insects, juveniles do not enter sexual maturation until they are competent and have acquired adequate development and growth. Toxic substances in the environment, such as plastic (bisphenol A), pollution, or recurrent infections, undernutrition, and diseases such as tumours and unknown genetic factors, can slow development and impair growth, ultimately delaying puberty age and metamorphosis in insects (Sedlmeyer and Palmert, 2002).The rate of development is also an essential parameter in studies of drugs' efficacy or toxicity. Several high-efficiency drug screening studies recently exploited the fruit flies for pre-clinical models of neurodegenerative and cancer diseases (Wang *et al.*, 2016; Villegas *et al.*, 2018; Bangi *et al.*, 2019; Su, 2019).

These are, in part, some of the motivations that brought us to develop a better approach for studying the time of sexual maturations, hoping that such improvement will eliminate many critical constraints that are limiting the performances and results in our experiments.

The developmental timing experiment in the history

The studies about growth, sexual maturations, and how the genes were affecting those physiological processes were understudied until the beginning of the 20th century. The first attempt to compute growth's phases with time in insects was performed by W.W. Alpatov in 1929. He counted the numbers of animals passing through the various development phases of *Drosophila* development (**Figure 1A**) (Alpatov, 1929).

The time through which an holometabolous insect grows and moults, and finally pupates, was used as readout of the growth rate from the second decade of the 20th century (Alpatov, 1929, 1930). The first mutant presenting a developmental delay was the *vestigial* mutation in *Drosophila melanogaster* (Alpatov, 1930). Seventeen years later this experiment became much more common. In an article on Nature of 1946, Marguerite Vogt described the inhibitory effects of *corpora cardiaca* and *corpus allatum* in *Drosophila hydei* by publishing a developmental timing experiment with the same graphic as the present investigation (**Figure 2B**) (Vogt, 1946). From these starting points, the developmental time experiment was used in many other studies, becoming one of the most studied processes for understanding animal growth and sexual maturation.

Let me describe the principle of the experiment in the following paragraph. The life cycle of *D. melanogaster* is highly stereotyped. At 25 °C, with adequate diet, and humidity, *D. melanogaster* wild-type lifecycle takes 10 days, from egg-laying to adult (**Figure 1A**). Larval stages consist of three instars (L1 to L3) separated by two moults, and these larval stages are equivalent to the childhood, juvenile, and adolescent stage in humans.

The commitment to sexual maturation or metamorphosis only occurs when the third instar larvae surpass a specific bodyweight called critical weight (Mirth, Truman and Riddiford, 2005). After this weight checkpoint, larvae feed and grow for another 24 to 26 hours and then exit the food and initiate a wandering stage (around 12 hours) until they find a dry, dark place to pupate (**Figure 1B**). The critical weight and transition from feeding to wandering stage and pupae and puberty onset in children are affected by similar environmental and neuroendocrine factors (Juarez-Carreño *et al.*, 2021; Pan, Connacher and O'Connor, 2021), making *D. melanogaster* a suitable animal model for these studies.

The manual experiment starts with an egg-laying chamber, where flies can lay eggs for four hours. After 24 or 48 hours, the researcher takes the larvae from the plate and put them into standard fly tubes (**Figure 1B**). The number of L1 larvae per tube depends on the tube dimension and the quantity of food inside the tube. It is recommended not to harvest too many flies inside to prevent overcrowding, that will negatively affect the development time. The experiment is performed by counting every 8 hours the number of pupae in each tube for several days.

Because of the nature of this assay, conducting large scale experiments became unfeasible. In fact, it is difficult to find in the literature studies with screenings where the phenotype tested is the time to pupariation. Possible automatic solutions to overcome these limitations exists, and I will introduce them in the next chapter.

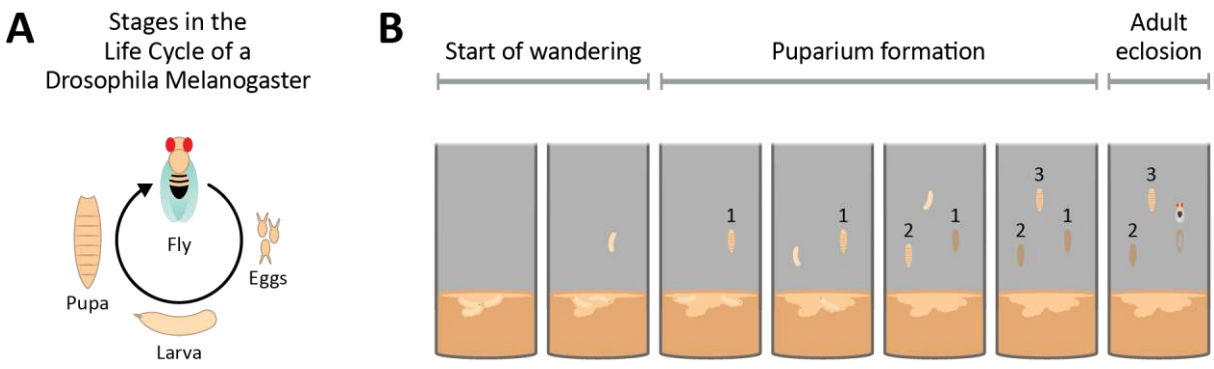

Figure 1. The life cycle of Drosophila melanogaster and the developmental timing experiment.

(**A**) The life cycle of D. melanogaster is about 10 days at 25°C, from eggs laying to adult's eclosion. (**B**) The developmental time experiment starts when the L3 larvae are starting to change from the feeding behaviour to the wandering. In this period the larvae are looking for a dark and dry place where start the pupariation. This period of pupariation starts from the 96 hours safter eggs laying till 140 hours in WT animals. Finally, after 4/5 days of metamorphosis the adult will hatch.

A

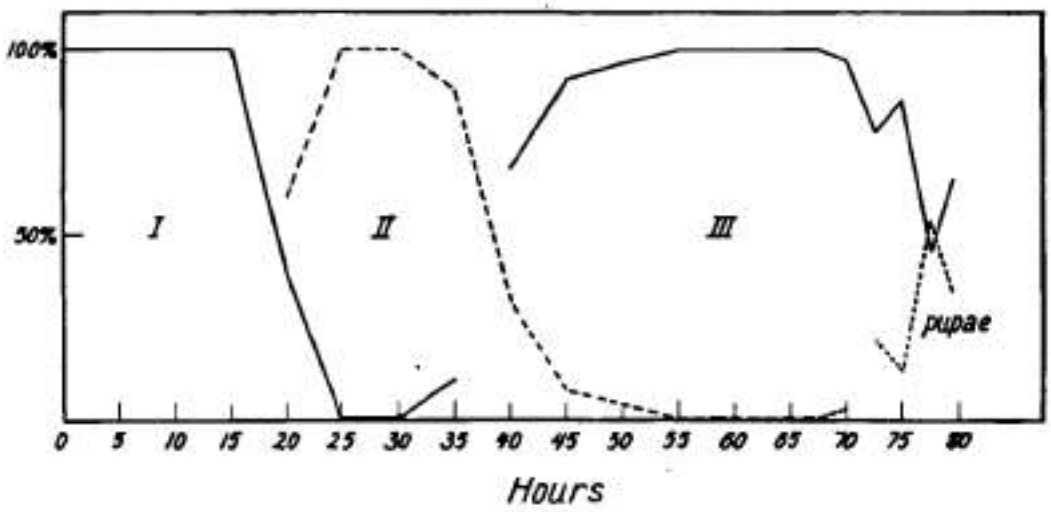

Fig. 11 Graphs of the passage of one larva from one stage to another. First experiment. Based on data of table 4.

B

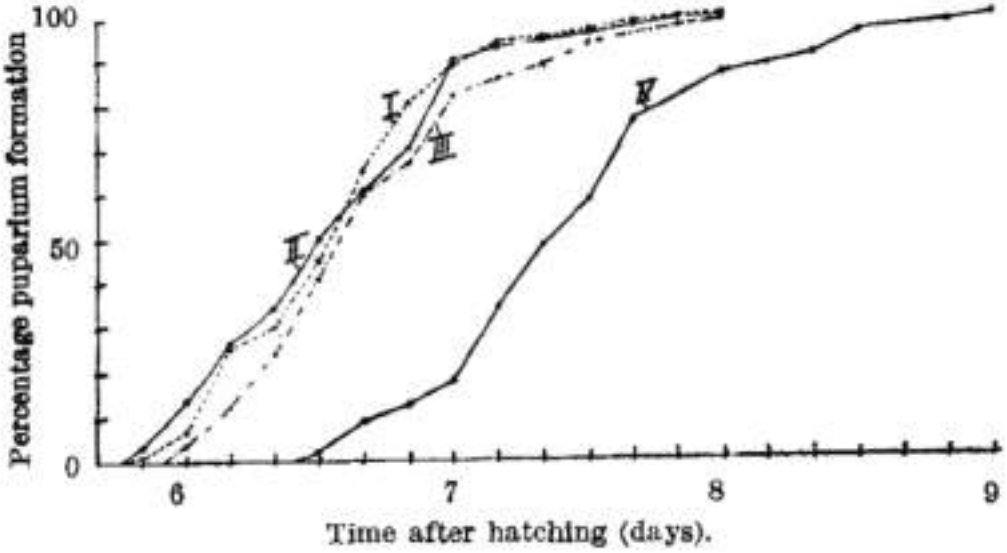

PERCENTAGE DISTRIBUTION OF TIME OF PUPARIUM FORMATION.
I = control series. Mean = 6·62 ± 0·04 days (n = 119).
II = fat body series. Mean = 6·62 ± 0·06 days (n = 61).
III = corpora allata series. Mean = 6·75 ± 0·06 days (n = 58).
IV = corpora cardiaca series. Mean = 7·51 ± 0·07 days (n = 56).

Figure 2. Developmental timing in the history.

(**A**) One of the first (or the first) attempts to plot the percentage of larvae passing from one instar to another, and the time to pupariation of *Drosophila melanogaster* (Alpatov, 1929). (**B**) The second example of a contemporary graph, showing the delay in pupariation caused by the implants *of corpora cardiaca* in WT larvae of *Drosophila hydei* (Vogt, 1946).

Why automates the counting of developmental timing?

Manual counting is currently the standard for this experiment (Su, 2019). There are many factors that made this method obsolete in the nowadays, and would make automatic counting an important improvement:

1. The automatic task is faster and non-interfering with the circadian cycle of the animals.
2. Enable high-throughput screening of thousands of flies for identifying antitumor drugs or longevity studies. This is a technical challenge and unsatisfied demand (Su, 2019).
3. With automation, one can store videos for future reanalysis and score multiple animal parameters co-varying with developmental timing. The records are also helpful in keeping standards, and record proof of the phenotype reported.
4. One can have developmental and morphometric data from a single experiment (there is even the possibility to measure the dimensions of the animals, body composition and behaviour).

To improve accuracy, scale up this manual task, and increase productivity, we decided to develop a method that would automate the counting, would be respectful of circadian rhythms, as accurate as manual counting and, would be able to perform high-throughput experiments. Furthermore, it would be, scalable for industrial uses, and much more informative.

The actual solution: automate developmental timing using culture wells

In 2020, two new articles reported possible solutions for development time automation, although none of these solutions reached manual accuracy and scaling the number of animals was either not possible or was too expensive. For example, Ki-Hyeon Seong et al. solution uses 96- or 384-well microplates inserted into a scanner (Seong *et al.*, 2020a) (**Figure 3**). Here, the researchers place the embryos one by one in each well, which is tedious, and then place the microplate inside the scanner, which acquires time-lapse images and finally analyse the output with a custom algorithm. The system works well, but it has significant limitations:

1. The intense light from the scanner can severely modify the animals' circadian behaviour.
2. The confined space of the well can affect the health of the individual flies, and their feeding since the food dries out.
3. They can’t use the standard food. This render more difficult the comparisons with other experiments performed with the standard food.
4. Watery food creates moisture and fog that clouds the glass and occludes the image.
5. The final images are not high quality.

Another article published in the 2020 present the same technical problems (Schumann and Triphan, 2020a). The added values of these two papers are that they can track the various larval moulting, and not only wandering and pupariation, as our robot can do. Both methods are based on the use of multi-well plates, as it is normally performed for cell-based methodologies. This is the biggest limitation. The wells are not studied to allow the whole development of the flies. It is evident from the paper of Schumann and Triphan that the difference of nine days (nine days!!) between the first pupa and the last one in a cohort of 33 animals. Instead, the maximum differences with the flyGear, in a cohort of 72 animals between the first and the last pupa is only 26 hours (**Figure 11**). The data obtained with the last method have significant measurement errors, so they are not suitable for experiments requiring accurate development time measurement.

In our laboratory the developmental timing has been studied, for at least, ten years (Garelli *et al.*, 2012). Nowadays, we are innovating an old experiment by applying 21st century technology. In the results section we will explain the new method, from the first version to the latest ones. We will compare it with the latest competitors, and we will see an example of its use.

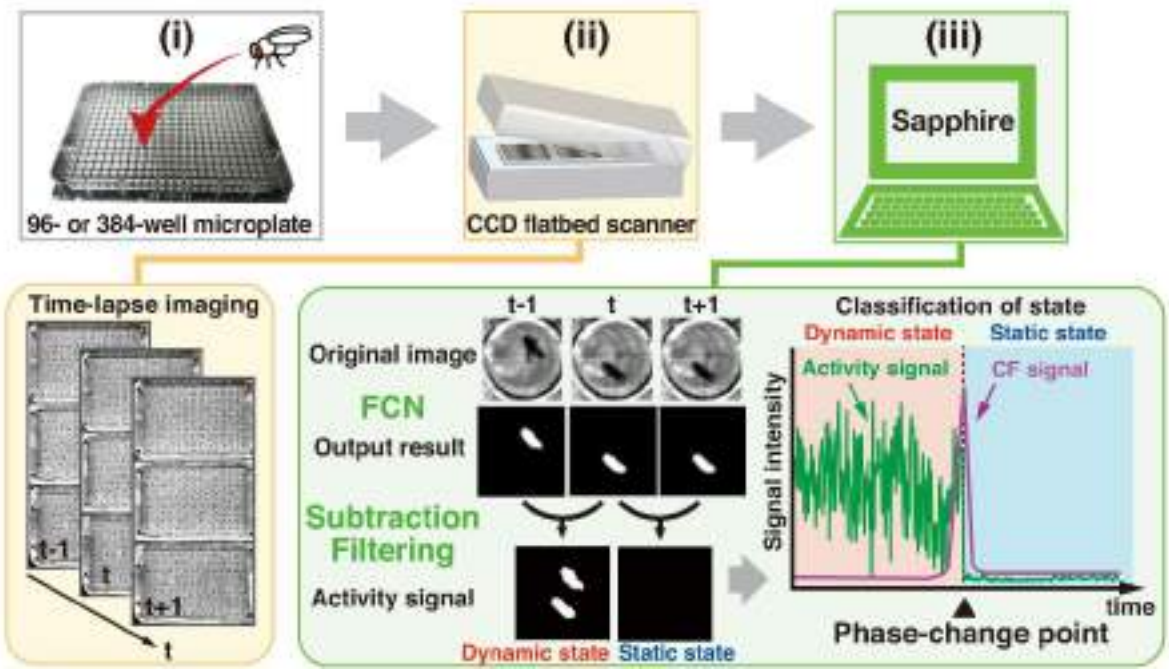

Figure 3. An example of automation of the developmental timing experiment.

This is the workflow of the automation of the developmental timing, Siu Kang and colleagues use a 96/384-well microplate to accommodate every embryo, then they do time-lapse images using a scanner, and with a custom algorithm they count the numbers of animals (Seong *et al.*, 2020a).

The neural substrates and circuitry logic for body symmetry-assurance

The study of animal growth control

Why can we distinguish a dolphin from a whale or a *Drosophila melanogaster* from a *Drosophila simulans*?

Many of the species that we know, or can define as species, have most individuals similar to each other. That is not a surprise. They have, to a great extent, similar shapes and dimensions. So in many cases, we can define a species or recognize it as so by looking at its external characteristics. This is an obvious observation, but it is of great value for understanding this understudied field, the study of growth control.

The study of animal growth control is a branch of biology that focuses on understanding how animals regulate their growth and development. This includes studying the genetic and hormonal mechanisms that control growth, as well as the environmental factors that can influence growth. Researchers in this field aim to gain a better understanding of the processes involved in animal growth and development, and how animals reach their final shape and dimension, which can have important implications for understanding human development and disease.

There are many research fields for such a theme; here, we focus on developmental stability. In fact, although we know that many germline mutations cause illness, many more have no effect on an animal's fitness. This is because the development of an organism is highly controlled and resistant to external or internal perturbations. This concept is called “canalization” and was presented for the first time eighty years ago by Waddington (Waddington, 1942).

The concept of canalization and developmental stability

“Developmental *reactions as they occur in organisms submitted to natural selection*, are in general canalized. That is to say, they are adjusted so as to bring about one definite end-result regardless of minor variations in conditions during the course of the reaction” (Waddington, 1942).

If we take, for example, a population of wild-type *Drosophila melanogaster* is much less variable than a mutant population (Waddington, 1942). The penetrance of many genetic mutations is not 100%, the fact is that the organisms are not canalized towards the mutations we have selected for. Moreover, the absolute precision of the WT strains is incredibly constant in the maintenance of his phenotype, despite little changes in temperature, food, contaminations, etc. Canalization is the capacity of a developmental system to counteract unwanted changes. That will bring the final shapes and proportions of the system unchanged.

There is not a single definition of canalization, as it has been changed over the years. Moreover, two other definitions, the developmental stability and the developmental homeostasis are used many times. There are little differences and the lack of an unequivocal definition of those concepts, so I believe that all the three definitions are part of the same group. Developmental stability could also be seen like a subgroup of canalization because it refers to symmetrical body parts that are growing in the same environment. In this thesis I will use mostly the last two definitions as synonyms of the major concept of canalization that I have defined above in this paragraph. In the next paragraph I will show some examples of canalization in various models.

The hidden control of symmetric body traits

Our limbs grow through all the embryonic development until the end of puberty. It is astonishing that after eighteen years of development, they have the same proportion, shape, and dimension (Wolpert, 2010). How is this achieved? How could two independently growing appendages reach this level of near-perfect bilateral symmetry? Developmental biologists have struggled to answer these questions over the last two hundred years.

Most living organisms on earth show some type of symmetry (Manuel, 2009). Very few animals' phyla do not present evident symmetry, such as the *Porifera* (sponges, but some of them could be radially symmetric) and *Placozoa* (some of the simplest animals), among others (Manuel, 2009)(**Figure 4**). On the other hand, animals have radial or bilateral symmetry (bilateral account for the 99% of all living species of animals) in the vast majority of the cases (Finnerty *et al.*, 2004). Traditionally, at least about bilateral symmetry, it seems evident that the evolutive advantage of having two matching sizes is to move in an environment. Moreover, the first type of something definable as a neuron was found in phyla that present symmetrical species (*Ctenophora*, *Cnidaria*, and *Bilateria*) (Kristan, 2016) (**Figure 4A**). The usual working definition of a neuron is a cell that transmits information from one cell (or from a stimulus) to one or many other cells via synapses. One useful marker for neurons is their morphology having long, thin processes. Another valuable marker is the presence of voltage-gated channels (NA_V, CA_V, K_V) (**Figure 4A**). Even some prokaryotic organisms have genes homologous to voltage-gated channels (probably for controlling intracellular ions and water). Then, these genes become more neuron-specific. In fact, during the evolution of clades that present neurons, there has been an expansion of these families of genes (**Figure 4A**). However, the origins of the first neuron are still elusive (Kristan, 2016).

Near-perfect bilaterally symmetric traits are those in which the perfect symmetry of the traits is functional. For example, our legs are highly symmetrical because we use them to walk around and run. Another example is our face. The more a face is symmetric, the more we consider it beautiful (Perrett

et al., 1999). The notion of symmetry of functional traits is also true in the most primitive bilateral species, like the order of *Amphioxiformes*. For example, the species that are obligate filter feeders maintain the symmetry of their gills. Conversely, the species that are facultative feeders show less symmetry in the numbers of gills (Larouche-Bilodeau, Guilbeault-Mayers and Cameron, 2020). All this means that organisms tend to have perfect symmetry in traits that are under evolutive constraints.

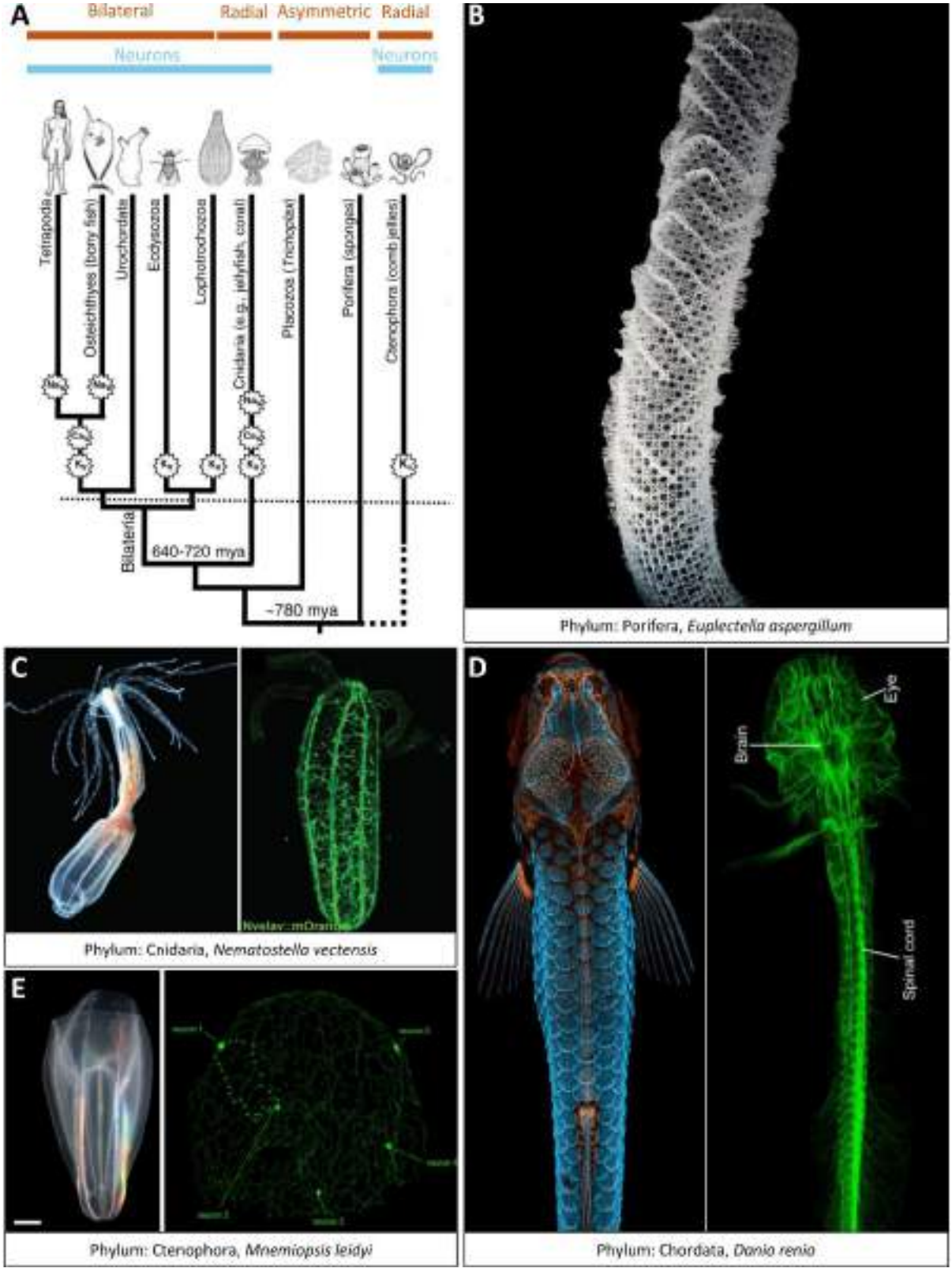

Figure 4. The evolution of symmetry and neurons in metazoan.

(**A**)Evolutionary tree indicating some of the major events in the evolution of neurons, mostly through gene duplications, of the genes producing voltage-gated channels selective for potassium (Kv), calcium (Cav), and sodium (Nav) ions (modified from: Kristan, 2016). (**B**) The siliceous skeleton of a glass sponge. (**C**) Image of adult cnidarian *Nematostella* polyp (left), and his neural net (right). (**D**) The image of a zebrafish with scales (blue) and lymphatic system (orange) (from Nikon Small World competition) (left), and the α-TUBB3 staining of the central nervous system (right). (**E**) Image of the ctenophore(left), and its neural net of the cydippid developmental stage (right). All the images are not in scale.

Asymmetries in biology

There are many exceptions to the rule of symmetry. First, I will review the two main types of asymmetries found in biology. Then, I will cover in a separate section the third type of asymmetry, Fluctuating Asymmetry (FA), being the principal subject of my thesis.

The animals' asymmetries fall mainly into two categories: 1) directional asymmetry (DA) (**Figure 5A**), where one side of the body presents a fixed asymmetry, and 2) random asymmetry, where either the left or the right part could be asymmetric, defined as antisymmetry (AS) (**Figure 5B**) (Palmer, 1996). These two types of asymmetries are different because it is easier to make the two-side different than to define a left side and a right side. The two subjects present different developmental histories. The AS is a random environmental signal that triggers a different development of one side (**Figure 5C**, **E**). Instead, in DA, there is an already present positional signal that is different among the two bilateral sides of the body, which will change the development of one side (**Figure 5D**, **F**) (Palmer, 1996).

I will expose in this thesis just a couple of examples of the many found in nature. This is because they are not the main scope of my thesis, neither of the introduction (but they also have interesting developmental insights that will be relevant for the discussion of the results). I found interesting the example of antisymmetry of the claws in snapping shrimps *Alpheus armillatus* (Mellon and Stephens, 1978; Palmer, Strobeck and Chippindale, 1994). These shrimps are asymmetric in their claws; one remains smaller (the pincer) than the other (the snapper). The snapper is used to fight with other individuals of the main species. Interestingly, upon removal of the nerve of the snapper claw the contralateral (the pincer) becomes snapper (Mellon and Stephens, 1978). This result is an example of different developmental and regenerative programs could work through the nervous system.

Antisymmetry seems to be stochastic, with no heritable basis (Palmer, 2009). On the other hand, it seems that DA, or fixed symmetry, is hereditable. An example of DA are flatfishes. Flatfishes have highly asymmetrical skulls, with both eyes placed on one side of the head (Friedman, 2008). Another type of DA is found in the arrangement of some internal organs of many mammals. Mammals, like many other vertebrates have the heart on the left. A mutation in the mouse *iv* is causing the random left-right position of the heart (Palmer, 2009).

I presented here just a small fraction of all the literature about asymmetry in animals. So, If you are interested in such argument, I really advise you to check this web page (*Palmer Home Page*, 2019).

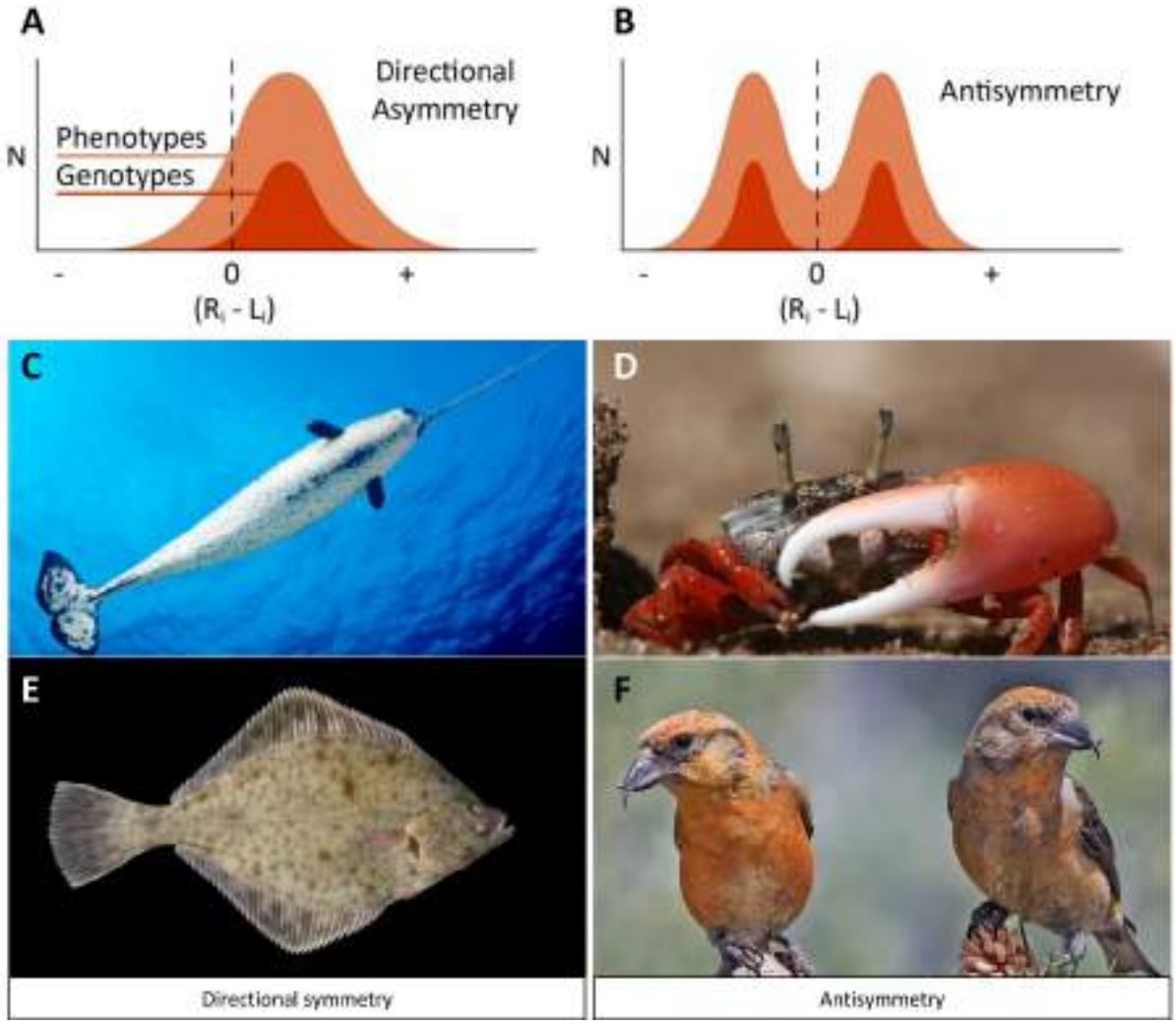

Figure 5. Asymmetries in biology.

(**A**) A "pure" form of bilateral asymmetry is the directional asymmetry, where most individuals have a predisposition for one side. (**B**) Another "pure" form is the antisymmetry, where half of individuals are left bias, and half right bias. (**C**) Narwhals' males present directional asymmetry in a canine tooth, while the other remains vestigial. (**D**) The claw of fiddler crab is an example of antisymmetry. (**E**) Another example of directional asymmetry is the flat fish, where there is the orbital migration of one eye during growth. (**F**) A second example of antisymmetry in the birds of the species *Loxia Leucoptera*.

Fluctuating asymmetry as measure of developmental stability

I am going to write about the last type of asymmetry, Fluctuating Asymmetry (FA), in this separate section because it is one of the main topics of my thesis (**Figure 6A**, **B**).

FA is mainly used to assess the effects of developmental stability in a population (**Figure 6C**) (Palmer and Strobeck, 1986; Debat and Peronnet, 2013). FA reflect a minor, non-directional variation, from otherwise perfect bilateral symmetry (Palmer and Strobeck, 1986; Palmer, 1994; Graham *et al.*, 2010). The left and right symmetric parts of the body develop together; they have the same genetics and grow in the same environmental condition. In theory, the values of the left minus right of the two bilaterally symmetrical body parts should have a difference near zero. If this condition is matched, it should mean that the developmental stability in this animal is maximal. Computing the (left – right) value for a large population, you will obtain a gaussian distribution (**Figure 6D**) (Palmer and Strobeck, 1986; Graham *et al.*, 2010). The larger the distribution, the bigger the value of FA (**Figure 6E**).

FA has also some limitations, for example it can be inflated by measurements errors that could be bigger that the real left-right difference. Moreover, DA could be inflating the values of pure FA. It is important to visually check the gaussian distribution (and performing normality tests), it must have skewness near to zero (symmetric distribution), with *kurtosis* values near to zero. For example, kurtosis lower than zero (platykurtic distribution) could hide AS (Palmer and Strobeck, 1986).

FA has been used for assessing developmental stability since the 1950s. FA was used as a measure of developmental stability in many studies using the fruit fly (Debat *et al.*, 2011; Colombani, Andersen and Léopold, 2012; Garelli *et al.*, 2012; Vallejo *et al.*, 2015).

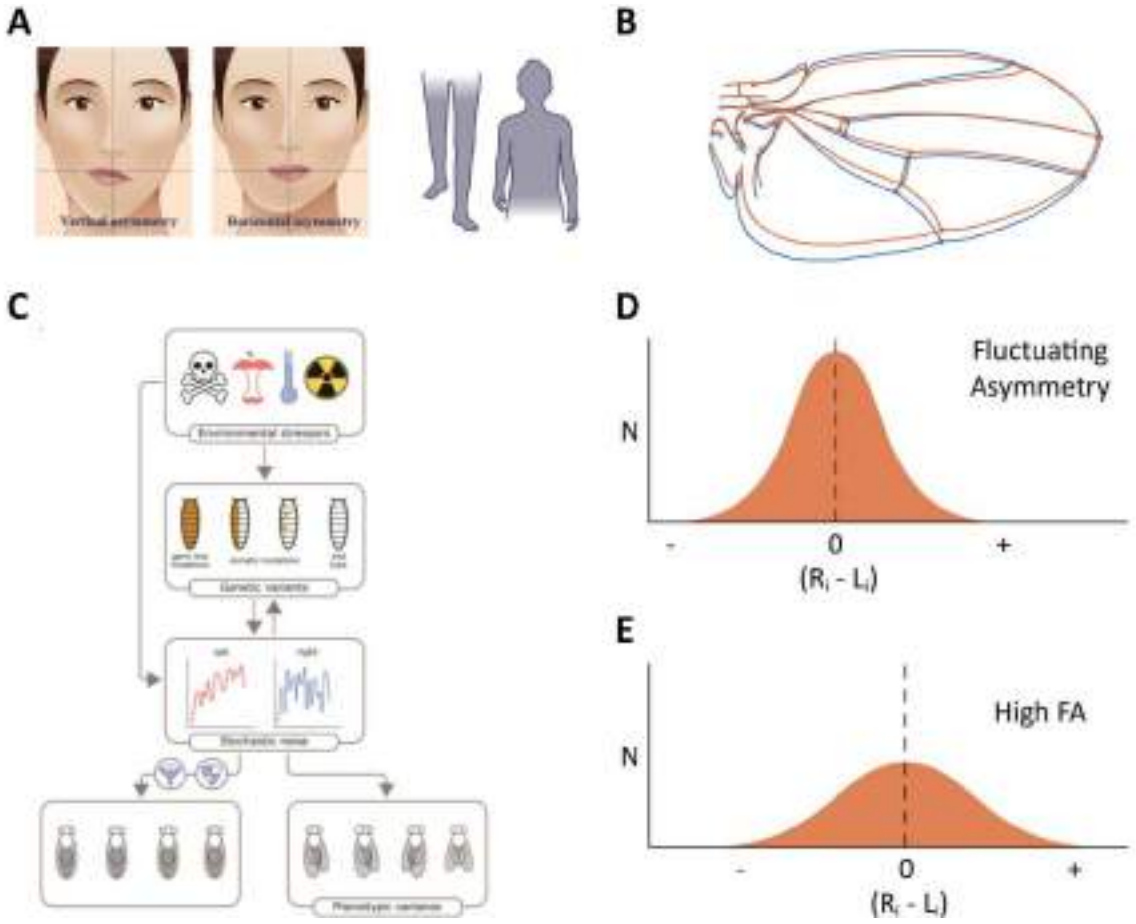

Figure 6. Fluctuating asymmetry.

(**A**, and **B**) Deviations from perfect symmetry in humans and flies. (**C**) Flies may acquire mutations that can be expressed in a mosaic state (brown dots) or inherited from one of the parents (all brown). Stochastic noise may cause gene expression fluctuations and variability in growth between the left and right sides. Environmental factors may cause changes in gene expression by genetic and non-genetic effects. Biological noise can cause replication errors that result in mutations and thus it may also contribute to somatic mutations. (**D**) Fluctuating asymmetry is a population index where the left minor right values will form a bell-shaped curve with mean of zero. (**E**) In a population that loses the buffering control, for a mutation, or for environmental factors, the bell-shaped curve will be flattened with more individual displaying high left-right differences.

Autonomous and systemic control of organ growth

Autonomous control of organ growth is essential for determining their unique shape and size (Domínguez and Casares, 2005). However, paired organs such as wings and limbs, and those that work together, like the retina and lenses, require a more coordinated approach to grow in a matched size despite their independent growth. Moreover, controlling growth also demands corrective and compensatory measures to address deficiencies caused by injuries or mutations (Bryant and Levinson, 1985; Smith-Bolton *et al.*, 2009). Although the neural and systemic mechanisms that ensure perfect bilateral symmetry and proportionality remain poorly understood, systemic controlling the growth of organs and compensating for an injury requires a set of evolutionarily conserved systemic hormones and growth factors.

The three major hormone systems in *Drosophila melanogaster* — ecdysteroids, juvenile hormone, and insulin-like peptides - work together to achieve systemic control of growth (Texada, Koyama and Rewitz, 2020). Insulin-producing cells in the brain produce three specific ILPs (ILP2, ILP3, and ILP5) that promote growth control. These ILPs are released into the neurohemal organ *corpus cardiacum* in response to signals reflecting nutrient and energy status and input from other neurons (Brogiolo *et al.*, 2001; Texada, Koyama and Rewitz, 2020). Brain-derived ILPs are then released into the haemolymph, acting on a single insulin receptor to stimulate cell growth and nutrient storage. In addition, the fat body produces an insulin growth factor (IGF)-like peptide, ILP6, that also promotes growth via the single InR (Texada, Koyama and Rewitz, 2020).

Ecdysteroids, which are primarily responsible for inducing moulting, also play a role in regulating size. The prothoracic endocrine gland produces the pro-hormone α-ecdysone, which is converted into several ecdysteroids, among which the 20-hydroxyecdysone (20E) is the most intensely investigated (Richards, 1978; Pan, Connacher and O'Connor, 2021). While the exact role of 20E in growth control is still debated, silencing the shade gene, which encodes the enzyme converting alpha-ecdysone into 20E, delays growth and results in smaller pupae, implying that ecdysone signalling promotes larval growth (Buhler *et al.*, 2018). Other authors have shown that silencing the ecdysone receptor (EcR) in the fat body causes larger pupae, implying that ecdysone signalling inhibits systemic growth; however, the effect is only seen under certain nutritional conditions (Colombani *et al.*, 2005).

The sesquiterpenoid juvenile hormone (JH) also regulates body size, the development of specific tissues, and reproductive maturation (Mirth, Truman and Riddiford, 2005; Jindra, Palli and Riddiford, 2013; Vallejo *et al.*, 2022). In many insects, JH prevents metamorphosis until the right body size or weight is achieved, while ecdysone promotes metamorphosis. In *Drosophila melanogaster*, the role of

JH in preventing metamorphosis is less relevant or unclear as available mutations in JH receptors do not accelerate metamorphosis (Nijhout, 2003).

The activity of these hormones is coordinated through a complex signalling network that involves feedback loops and crosstalk between different pathways and which are not yet fully understood, particularly the regulation of JH signalling and production. Garelli et al. (2012) and Vallejo et al. (2015) found that injury-induced developmental delay also caused the dampening of these three hormone systems. Moreover, Colombani et al. (2015), Garelli et al. (2015), and Vallejo et al. (2015) found that neurons producing the receptor of the novel insulin-like peptide ILP8 (called Lgr3) make direct connections with PTTH-producing cells, thereby directly modulating the production of ecdysone and developmental timing in response to injuries and tumours (**Figure 7**, **F**). Vallejo et al., (2015) also found that ILP8-Lgr3 neurons also make direct connections with insulin-producing cells and modulate the transcription of ILP3 but not other ILPs. How the ILP8-Lgr3 system modulates the levels of JH was unclear, but this Thesis work uncovers that some Lgr3 neurons in the R19B09 ensemble make direct connections with the *corpus allatum* (data not shown). This endocrine gland produces the juvenile hormone (Richard *et al.*, 1989). Consistently, dysregulation of these pathways can lead to developmental delays, abnormal growth, and body size.

However, whether and how a delicate balance of these hormones and signals is required to ensure a perfect bilateral symmetry remains yet to be discovered. Identifying the core Lgr3 neurons that mediate bilateral symmetry control is paramount to understanding the interplay of these hormones and input signals and how they work together to ensure how organs grow and mature.

Autonomous and systemic compensatory organ growth

Under proper conditions, the growth of a developing organism follows a regular path. In humans, illness, malnutrition, and other environmental conditions could affect this typical path. After the children recover from an illness or malnutrition causing growth perturbation, accelerated growth occurs to compensate for the deficiency until the genetically encoded final size is attained (Tanner, 1963). This burst of growth is defined as "catch-up growth" (Tanner, 1963, 1981) . The paediatrician J. Tanner hypothesised that children have a genetically defined size and that this size setpoint in the brain enables growing children to achieve their correct size and compensate for growth perturbations. Using a different setup, which involved perturbation of growth of a bilateral side, Baron and co-workers suggested that compensatory growth is not controlled systemically or by the brain but through an autonomic growth control involving senescence of the bone or counting cell divisions (Baron *et al.*, 1994).

Catch-up growth led to the idea that a size setpoint in the brain or "sizostat" enables a body metric (Tanner, 1986). The "sizostat" hypothesis posits that: there is a neuroendocrine control of growth, where the growing body releases hormones that are related to its growth, and the neuroendocrine organs (the "sizostat") increase the expression of its receptors with time (Tanner, 1981, 1986). In this model, if an insult like malnutrition causes growth retardation, the hormones expressed by the growing body will not be enough to bind all the receptors of the "sizostat". So, the "sizostat" will continue the production of a second growth hormone. Finally, the excess of growth hormone will accelerate the growth after the insult has concluded, explaining the catch-up growth (Tanner, 1963, 1981, 1986). Recently, we have reported that after a period of starvation, *Drosophila melanogaster* larvae recover from the growth retardation by accelerating growth or catch-up growth, and we provided evidence that this control is on the endocrine gland *corpus allatum*, involving the relaxin receptor Lgr4 (Vallejo *et al.*, 2022, and data not shown).

The alternative hypothesis to the “sizostat” promulgated by Baron and co-workers suggest that injury to an organ is compensated autonomously —the "growth plate hypothesis" (Baron *et al.*, 1994). Although this hypothesis seemingly challenges Tanner's "sizostat" theory, these authors deal with different growth problems, one involving a local injury and body symmetry and the other involving a growth deficiency that affects the whole body and catch-up growth (Baron *et al.*, 1994).

Analogous to the "growth plate hypothesis", studies in *Drosophila melanogaster* led to the hypothesis that injury to imaginal discs, like the wing discs, can be compensated via organ autonomous mechanisms. However, several authors found that such injury caused developmental delay and systemic retardation of global growth (Bryant and Levinson, 1985; Halme, Cheng and Hariharan, 2010). These authors proposed that control is intrinsic and extrinsic to the injured organ. Still, the systemic signal produced by the injured organ that delays developmental time and inhibits global growth was only recently discovered in Drosophila melanogaster (Colombani, Andersen and Léopold, 2012; Garelli *et al.*, 2012).

Roselló-Díez *et al.* (2018), using mice and an elegant tool for genetic manipulation of left-right sides separately, showed concert integrations of the autonomous and systemic controls, unifying Tanner’s and Baron's theories. These studies in mice also imply that the systemic insulin-like signals that control body symmetry and responses to injury in the fruit fly may be universal mechanisms of compensating and ensuring perfect growth control and proportionality. The findings of the gene Ilp8 will be introduced in the following chapter.

Ilp8 and the systemic growth control

During the last ten year, studies in the *Drosophila melanogaster* found a gene that explains the mechanism of the catch-up growth (Colombani, *et al*., 2012; Garelli *et al.*, 2012a, 2015, p. 3; Colombani *et al.*, 2015, p. 3; Vallejo *et al.*, 2015), and the unification of the "sizostat" and the "growth plate hypothesis" (**Figure 7**) (Garelli *et al.*, 2012b; Boone *et al.*, 2016; Boulan *et al.*, 2019).

Ilp8 gene was discovered independently by two groups (Colombani *et al.*, 2012; Garelli *et al.*, 2012). One of which performed a screen for suppressors of the pupation delay elicited by imaginal disc injury (Colombani *et al*., 2012). The other group discovered Ilp8 as a gene upregulated in tumour eye discs as assessed using microarray technology and then realized that the secreted peptide has homology to the insulin and relaxin-like family, thereby given the name Ilp8 for insulin-like peptide 8 (Ferres-Marco *et al.*, 2006; Garelli *et al.*, 2012). During an insult of an imaginal tissue, *Ilp8* is up regulated and produces a delay in the pupariation by causing a delayed transcription of the genes *disembodied* and *phantom* (Garelli *et al.*, 2012a). Moreover, the KO of *Ilp8* increases FA in these animals (**Figure 7A**, **B**). These experiments support the vision where a secreted molecule acts as a signal to maintain developmental stability against perturbations (**Figure 7**, **F**). Subsequent studies demonstrated that the gene *Lgr3*, encoding a leucine-rich-repeated containing G protein-coupled receptor, is the receptor for the peptide ILP8. When the receptor is knocked down from the Lgr3 neurons it rescues the normal pupariation time, even in the presence of *Ilp8* overexpression (Colombani *et al.*, 2015, p. 3; Garelli *et al.*, 2015; Vallejo *et al.*, 2015). *Lgr3* mutant flies have a high increase of FA. Moreover, just the removal of the gene in the brain (*elav-Gal4>Lgr3*^{RNAi}) (**Figure 7C**) or from a neural sub-population found in a Lgr3 enhancer (*R19B09>Lgr3*^{RNAi}), induced high levels of FA (Colombani *et al*., 2015; Vallejo *et al.*, 2015). These experiments argue in favour of a vision where a central neuroendocrine control regulates growth after a perturbation, by responding to a peptidergic signal from the periphery of the growing organism. This is the basis of the "sizostat" hypothesis.

Moreover, Ilp8 regulates the growth of the wings imaginal discs and the allometric growth of the other organs (Boulan *et al.*, 2019). Finally connecting the "sizostat" hypothesis with the "cell-nonautonomous" growth inhibition.

Lgr3 and the systemic growth control

Although all the knowledges relative to *Ilp8*, we know less about its receptor, Lgr3. As said before, Lgr3 is a leucine-rich repeated-containing G protein-coupled receptor (GPCR). It is a conserved receptor with two mammalian homologs named LGR7 and LGR8(Van Hiel *et al.*, 2015).

Like many GPCRs, Lgr3 is expressed at low levels in the fly's tissues. Previous studies have shown that Lgr3 was a constitutively active receptor. The receptor induced a strong cAMP response when transfected in mammalian cells (HEK 293) (Van Hiel *et al.*, 2015). *In vivo*, however, this constitutive activity was not evident. The induced cAMP seems correlated with the concomitant high levels of its ligand, ILP8, bringing evident activations of two pairs of bilateral cells in the central brain of the wandering larvae, with few signs of activity without the overexpression of *Ilp8* (Garelli *et al.*, 2015, p. 3; Vallejo *et al.*, 2015). Males and females have differential expressions of this GPCR, with more expression in the former (Van Hiel *et al.*, 2015).

The expression of *Lgr3* is in the central nervous system, and the neurons expressing *Lgr3* are connected with the homeostatic regulators such as the Insulin Producing cells (IPCs) and the PTTH neurons (**Figure 7E**) (Colombani *et al.*, 2015; Garelli *et al.*, 2015; Vallejo *et al.*, 2015). Enhancer lines of *Lgr3* are also expressed in ovaries of the adult flies (Liao and Nässel, 2020).

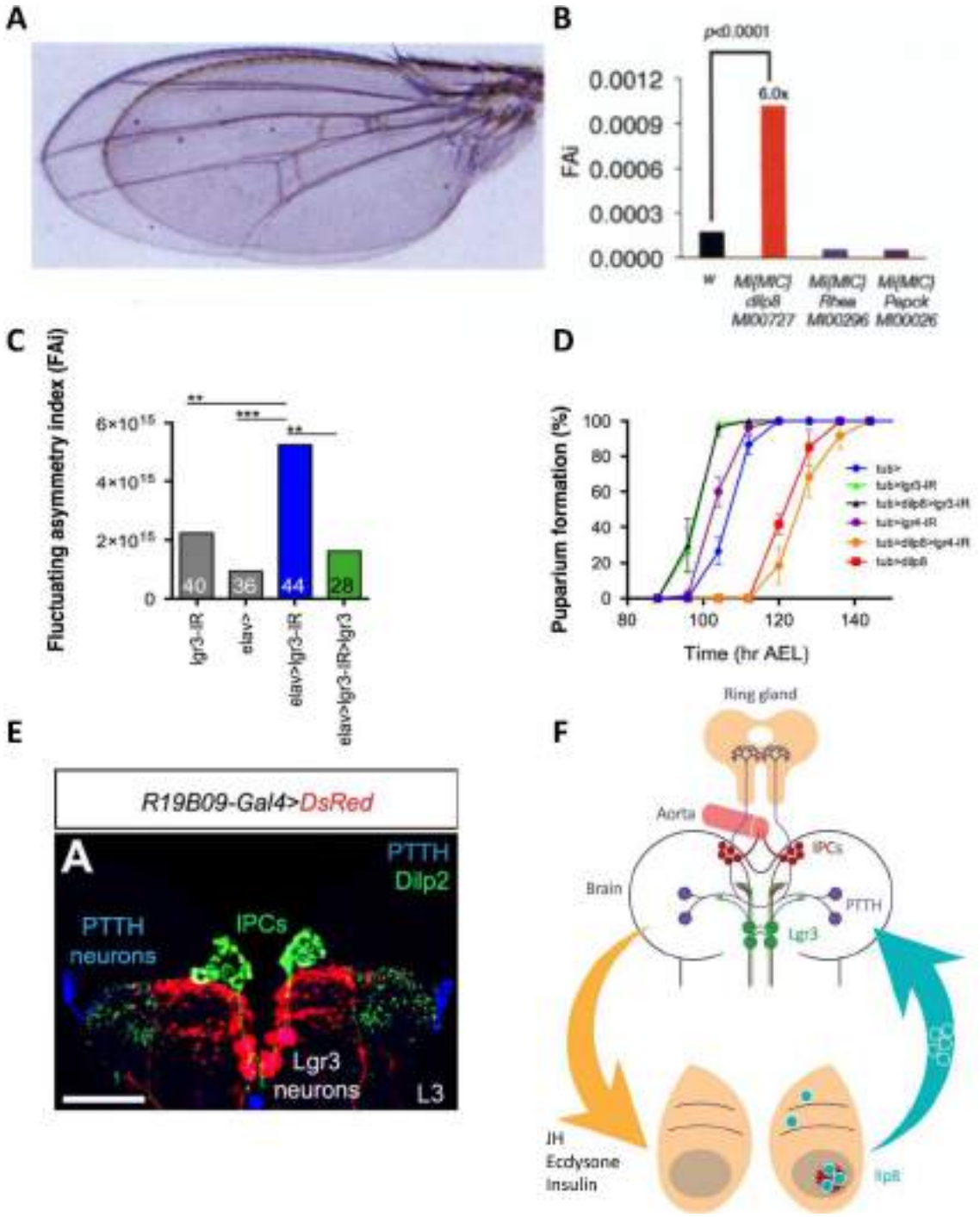

Figure 7. Ilp8 and Lgr3 in the systemic growth control.

(**A**) Individual KO for Ilp8 showing high left-right asymmetry. (**B**) Deviations from symmetry are measured by a fluctuating asymmetry index (FAi) in flies deficient for the hormone Ilp8 receptor in neurons. (**C**) Flies with the knock-down of Lgr3 in the brain (blue Histogram) show high fluctuating asymmetry (FA). (**D**) The knock-down of Lgr3 rescue de pupariation delay cause by Ilp8. (**E**) Neural network underlaying the Ilp8-Lgr3 homeostatic growth control. (**F**) The expression of Ilp8 declines as maturation proceeds but its expression is acutely increased when grow is disturbed. Circulating Ilp8 levels signal the brain the amount of time needed to recover and complete growth by activating two pairs of symmetric Lgr3 neurons in the central brain. These neurons connect with the insulin-producing cells and the PTTH-producing cells and other neurons yet-to-be identified to attenuate growth and maturation to compensate and attain the correct size.

The importance of the commissures in metazoans and the split-brain

Bilaterally symmetric animals represent more than 99% of all living multicellular animal species (Finnerty *et al.*, 2004). In bilateral animals, the integration of left-right inputs is crucial, at least, for sensory and motor functions (the central pattern generator) (**Figure 8B**) (Lanuza *et al.*, 2004; Suárez, Gobius and Richards, 2014). This integration works because the left and right sides of the nervous system are connected. These connections are known as commissures.

Commissures are present throughout vertebrate and invertebrate species; similar molecular mechanisms for the development of contralateral projections argue in support of a common bilateral ancestor (Xu *et al.*, 2021). Nevertheless, the function of commissure was a mystery until the mid of the 20th century. There was a general line of thought for the crucial functions of the *corpus callosum*, the prominent human commissure, in coordinating the activity of the two hemispheres. Nevertheless, the actual observations on the effect of complete surgical section or of total agenesis of the *corpus callosum* in man and other animals have indicated a surprising absence of deficit (Myers and Sperry, 1958). It was only with the seminal work of Roger Sperry and colleagues that we started to understand the basics of the *corpus callosum* and the commissures' functions of split-brain patients (**Figure 8A**) (Myers and Sperry, 1958; Gazzaniga, 2005).

As outlined at the beginning, one conserved bilateral function across mammals and insects that relies on commissural projections is the central pattern generator (Kjaerulff and Kiehn, 1996; Comer *et al.*, 2019). In mice, the loss of a particular commissural neural population disrupts the left-right rhythmicity of the central pattern generator (**Figure 8B**) (Lanuza *et al.*, 2004; Comer *et al.*, 2019). In *Drosophila*, the silencing or activation of the population of the conserved commissural interneurons also disrupt the this pattern of neural activity that drive rhythmic and stereotyped motor behaviours (Heckscher *et al.*, 2015).

The Robo signalling in the regulation of contralateral projections

The roundabout signalling pathway is one of the conserved axonal path-finding routes across species (Dickson and Gilestro, 2006; Cárdenas *et al.*, 2018). *robo* was initially discovered in the fruit fly in screening for commissural path-finding defects (**Figure 8D**, centre) (Seeger *et al.*, 1993; Mitchell, 2018). Robo proteins prevent axons to cross the midline, where a source of slit protein is present (**Figure 8C**) (Dickson and Gilestro, 2006). In *Drosophila* three *robo* genes are known, namely *robo1*, *robo2*, and *robo3* (Dickson and Gilestro, 2006). Despite their names, only *robo1* is well conserved from flies to vertebrates (Dickson and Gilestro, 2006). *Commissureless* (*comm*) was also identified in the same genetic screening as *robo* (**Figure 8D**, right) (Seeger *et al.*, 1993). In contrast with *robo*, no axons were

able to cross the midline (Seeger *et al.*, 1993). In *Drosophila*, Comm binds Robo in the ER and brings it to the proteasome (Myat *et al.*, 2002). When *comm* is expressed, Robo proteins are not able to reach the axonal tip, so the growth cone can cross the midline and grows contralaterally (Keleman *et al.*, 2002). Although *comm* appears to not be conserved, a functional homologous has been found in human, meaning that Robo's intracellular trafficking is maintained through evolution (Justice, Barnum and Kidd, 2017).

Slit protein, the ligand of Robo, is expressed in the midline of the ventral nerve cord and protocerebrum. Moreover, Slit protein is also present in the mushroom bodies of the larval brain (Oliva *et al.*, 2016). Oliva et al. found that overexpression of *robo2* is sufficient to prevent the midline crossing of dorsal cluster neurons, and eventually, they will innervate the ipsilateral optic lobe in the adult brain (Oliva *et al.*, 2016).

In humans, mutations in the *ROBO3* gene cause a syndrome known as horizontal gaze palsy with progressive scoliosis (HGPPS) (Jen *et al.*, 2004). People affected by this syndrome show, among other defects, profound scoliosis 1, which is a sign of fluctuating asymmetry in humans (Graham and Özener, 2016). Mutation of the human functional homolog of *comm*, the *PRRG4* gene, is associated with the autistic features of WAGR syndrome (Justice, Barnum and Kidd, 2017). High fluctuating asymmetry is often seen in autistic children (Graham and Özener, 2016). Autism is also associated with *corpus callosum* defects and *ROBO* mutations (Justice, Barnum and Kidd, 2017). Progressive scoliosis of children with *ROBO3* mutations, which is associated with defective decussation of certain brainstem neuronal systems, led us to hypothesise that contralateral communication of Lgr3 neurons may be important for maintaining perfect bilateral symmetry.

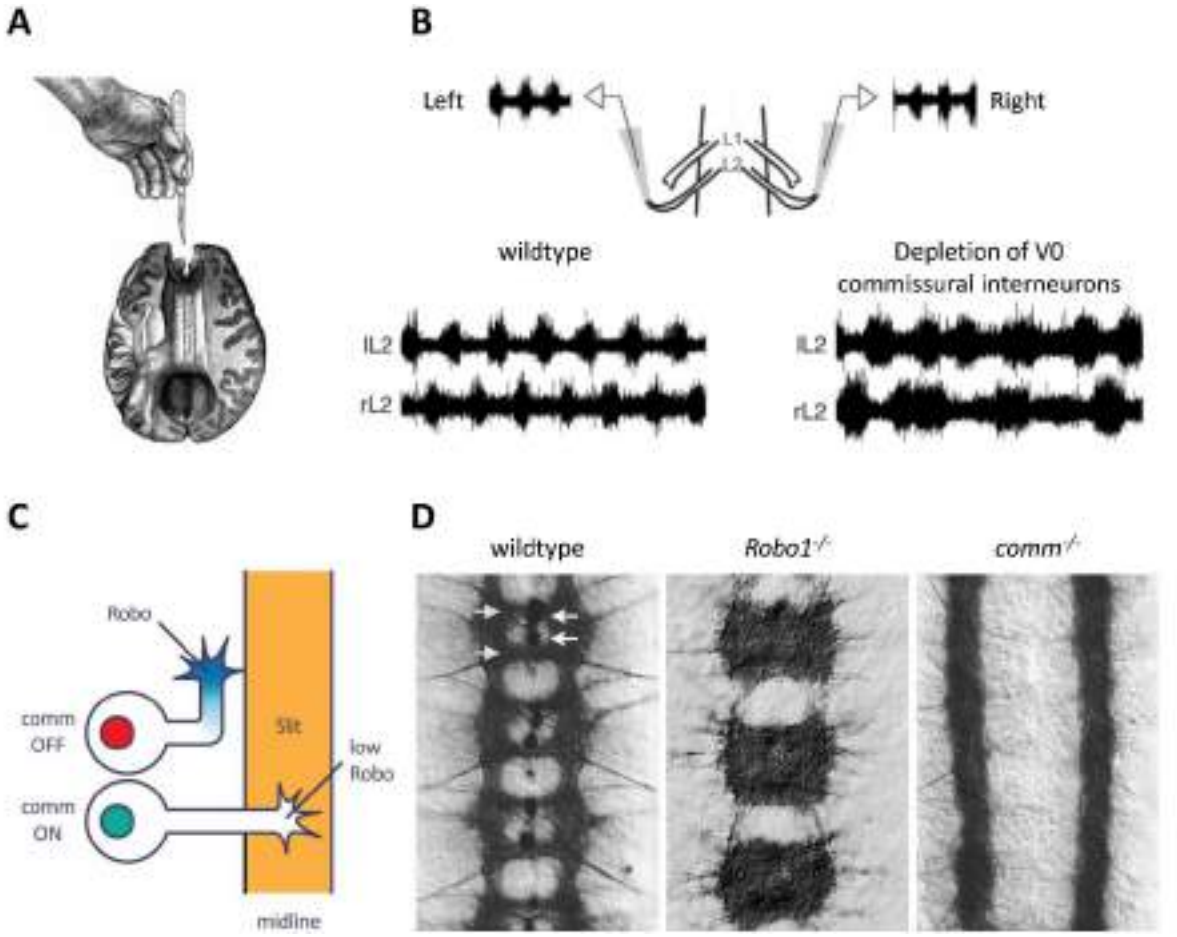

Figure 8. The importance of the commissures, and a conserved pathway for their development.

(**A**) The split-brain is conceived by severing the *corpus callosum*. (**B**) The importance of commissural interneurons in the central pattern generators (modified from (Lanuza *et al.*, 2004)). (**C**) Simplified version of the robo pathway during the formation of the central nervous system. (**D**) The embryonic central nervous system of *D. melanogaster* in the wildtype forms an anterior and a posterior commissure for every segment. In *robo1* mutant, axons are continuously crossing the midline. In *comm* mutant the axons never cross the midline.

The Adenylyl cyclase genes in the fruit fly

The Lgr3 receptor response to Ilp8 is strongly coupled to cAMP stimulation (Vallejo *et al.*, 2015). This second messenger molecule is synthesized from ATP by membrane-bound enzymes called adenylyl cyclases (ACs), activated by G-protein coupled receptors (GPCRs) (Lee, 2015). In mammals, nine AC genes exist (Hurley, 1999). In *Drosophila*, there are ten AC genes (Cann, Chung and Levin, 2000). The genes ACXC, ACXB, ACXA, and ACXE are repeated in tandem in the second chromosome, and the ACXD is in the third chromosome. All these five genes are expressed primarily in the male germline of the fruit fly (Cann, Chung and Levin, 2000).

Rutabaga (*rut*) encodes a membrane-bound $Ca2^{+}$/calmodulin-activated AC (Levin and Reed, 1992). *rut* plays key roles in regulating behavioural, neuroanatomical, and electrophysiological plasticity (Kyriacou and Hall, 1984; Heisenberg *et al.*, 1985; Han *et al.*, 1992; Zhong, Budnik and Wu, 1992; Heisenberg, 2003) . The rut gene is expressed in a brain region called the mushroom body, which plays a critical role in memory formation both in the larva and adult fly (Levin and Reed, 1992; Davis, 1993; Zars, 2000).

The gene AC76E is expressed in a highly restricted pattern throughout fly development, including the *corpus allatum* (CA), the endocrine gland that produces the juvenile hormone (JH) (Mattila *et al.*, 2009). JH was discovered around the 1940s using transplantation experiments, where the cuticle adjacent to the site of the implant of the *corpus allatum* retains the imaginal characteristics (Wigglesworth, 1940, 1947; Vogt, 1946). Moreover, the gene AC76E is also present in the gastric cecum, and the Malpighian tubules (Mattila *et al.*, 2009), which acts as the mammalian kidneys (Singh and Hou, 2009). The expression of *AC76E* is regulated by FoxO (Mattila *et al.*, 2009), a negative regulator of the Insulin/PI3KAKT pathway discovered in *C. elegans* (Ogg *et al.*, 1997) (Kops *et al.*, 1999). However, silencing *AC76C* did not rescue the FoxO-mediated control of loss cAMP (Mattila *et al.*, 2009), suggesting other ACs may mediate the effects of FoxO. As possible downstream signalling in the Lgr3 cascade, it should be tested in the regulation of the developmental delay induce by ILP8.

Objectives

The objectives are split into two groups. The first is about the prototype with a market-oriented purpose. Then, the second group relates to the scientific goals of the thesis.

flyGear

1. Create a functional prototype for the automation of the developmental timing experiment.
2. Build a workflow for the analysis of the images.
3. Validate the application of the prototype in several scenarios of experiments.
4. Protect the invention with a patent.
5. Implement the prototype: Its design, software, accuracy, and applicability uses in high-economic industrial sectors like insect farming and pest control.
6. Bring the prototype to the real world: Go to the market.

The neural substrates and circuitry logic for body symmetry-assurance

1. Find the downstream signals mediating Ilp8 functions.
2. Ilp8 in left-right symmetry: Continuous monitoring of growth or development checkpoint?
3. Define the role of left-right communication within the Lgr3 neural ensemble.
4. Define the minimal circuit for the integration of left-right information.
5. Assess temporal requirements for the Ilp8-Lgr3 system: does the brain continuously monitor growth or a single checkpoint?
6. Single circuit or multiple circuits for Ilp8 functions?

Materials and Methods

Drosophila melanogaster strain used in the thesis

Short name	Source	Reference Number
R19B09-Gal4	Bloomington *Drosophila* Stock Center	RRID:BDSC_48804
tsh-Gal4	Bloomington *Drosophila* Stock Center	RRID:BDSC_3040
ilp3-Gal4	Bloomington *Drosophila* Stock Center	RRID:BDSC_52660
Ptth-Gal4	Vallejo et al. 2015	N/A
Tub-Gal4;Tub-Gal80	gift from Luis García Alonso	N/A
UAS-Lgr3-RNAi	Bloomington *Drosophila* Stock Center	RRID:BDSC_36887
UAS-Comm-RNAi	Bloomington *Drosophila* Stock Center	RRID:BDSC_28381
UAS-Robo2oe	Oliva et al. 2016	N/A
UAS-Robo3oe	Oliva et al. 2016	N/A
TrpA1	Bloomington *Drosophila* Stock Center	RRID:BDSC_26264
Piezo-RNAi	VDRC stock center	CG44122
tsh-Gal80	Lab collection	
UAS-mCD8-GFP	Vallejo et al. 2015	N/A
UAS-GCaMP6m	Bloomington Drosophila Stock Center	RRID:BDSC_42748
Tub-Ilp8	Vallejo et al. 2015	N/A
UAS-Ilp8-RNAi	Bloomington Drosophila Stock Center	
CRE-F-luc	Vallejo et al. 2015	N/A
UAS-Comm-RNAi	VDRC stock center	V-39018
MCFO1	Bloomington Drosophila Stock Center	RRID:BDSC_64085
MCFO2	Bloomington Drosophila Stock Center	RRID:BDSC_64086
MCFO5	Bloomington Drosophila Stock Center	RRID:BDSC_64089
UAS-Ilp8-RNAi	VDRC stock center	V-112161
Trans-Tango	Bloomington Drosophila Stock Center	RRID:BDSC_77124
R46B11-Gal4	Bloomington Drosophila Stock Center	RRID:BDSC_50254
R19B09-LexA	Bloomington Drosophila Stock Center	RRID:BDSC_52539
R35E05-Gal4	Bloomington Drosophila Stock Center	RRID:BDSC_48127
R40D06-Gal4	Bloomington Drosophila Stock Center	RRID:BDSC_48616
R40D06-Gal4-DBD	Bloomington Drosophila Stock Center	RRID:BDSC_70212
R42A12-p65-AD	Bloomington Drosophila Stock Center	RRID:BDSC_70929
R35E04-p65-AD	Bloomington Drosophila Stock Center	RRID:BDSC_70933
ChaT-Gal4.7.4,UAS-GFP.S65T	Bloomington Drosophila Stock Center	RRID:BDSC_6793
UAS-ACXD-RNAi	VDRC stock center	V-107396
UAS-ACXB-RNAi (Also known as AC34A)	VDRC stock center	V-104248
UAS-AC76E-RNAi	VDRC stock center	V-51974
UAS-AC76E-RNAi	VDRC stock center	V-106232
UAS-ACXC-RNAi	VDRC stock center	V-105167
UAS-RUT-RNAi	VDRC stock center	V-101759
UAS-amon-RNAi	Bloomington Drosophila Stock Center	RRID:BDSC_28583
UAS-AstA-R2-RNAi	Bloomington Drosophila Stock Center	RRID:BDSC_25935
UAS-RUT-RNAi	VDRC stock center	V-109441
UAS-FRT.stop.mCD8-GFP.H	Bloomington Drosophila Stock Center	RRID:BDSC_30032
8XLexAop2-FLPL	Bloomington Drosophila Stock Center	RRID:BDSC_55820
UAS-DenMark, UAS-syt.eGFP	Bloomington Drosophila Stock Center	RRID:BDSC_33065

Measurement of the developmental timing of pupation

We crossed 50 females and 20 males. After 24-48 hours, flies were transferred to grape juice agar plates with yeast paste and left for 4 hours to allow egg deposition. We set the time "0 hours" after the 4 hours of eggs laying when we removed parental flies. We incubated the eggs for 48 hours at 27°C. After this time, we selected and transferred Second-instar onto 5 mL of Drosophila standard "Iberian" food (20 larvae per tube) and reared at 27°C. We counted the number of pupae every 4-8 hours.

Immunohistochemistry in larval brains

L3 larval brains, were dissected out in cold Phosphate-buffered saline (PBS) buffer and fixed in 4% paraformaldehyde for 20 minutes (Morante and Desplan, 2011). Brains were stained overnight at room temperature with the following primary antibodies: mouse anti-HA, anti-V5, anti-Flag, anti-Myc, anti-Slit, (1/200, DSHB). Secondary antibodies were purchased from Invitrogen and Jackson ImmunoResearch, with 3 hours incubations at room temperature. Finally, the brains were mounted using the bridge method for maintain the 3D structure (Morante and Desplan, 2011).

Super-resolution confocal imaging

Larval brains and fat bodies were mounted in Vectashield mounting medium with DAPI (H-1200, Vector Labs), maintaining their 3D configuration (Morante and Desplan, 2011). Images were obtained on a Zeiss LSM 880 confocal microscope with Airyscan, a module for super-resolution based on an array detector with laser scanning confocal microscopy. The Airyscan images were processed with the Zen Black software. The subsequent analysis, were all done using FIJI (Schindelin *et al.*, 2012).

Temperature shift experiments for removing *Ilp8*

We crossed the 50 virgins flies carrying the Tub-G80^{ts};Tub-Gal4 with 20 males carrying UAS-Ilp8-IR, and with 50 virgins flies W^{118} for the control experiment. We carried an extra control crossing 20 male flies UAS-Ilp8-IR with 50 virgins flies W^{118}. We maintained the mating flies at 25ºC for three days. Then, we flipped the flies every 24 hours for thirteen days, maintaining the resulting offspring at 18ºC. At this temperature the transcriptional repressor Gal80 is not functional. Then, we shift the temperature to 29ºC for repressing the function of Gal4. We shift the temperature we the animal arrives at the desired developmental stage. We assessed the developmental stage by analyzing part of the flies' population of interest with a stereomicroscope. For removing Ilp8 in the lasts developmental phases we did the opposite. We maintained the resulting offspring at 29ºC, and we shift the temperature at 18ºC we the animals reaches the right developmental time point.

Weight and size measurements

For weighing larval flies, 30-45 larvae of each genotype were collected at required developmental stages and weighed using a precision scale.

For larval and pupal volume determination, 10 larvae and pupae of each genotype were collected and photographed with their dorsal side up, and length and width were measured using ImageJ. Volume was calculated according to the following formula $V = (4/3)\ \pi(L/2)*(w/2)^2$ (L, length; w, width).

Geometric morphometric

Acquisition:

Flies from the proper genotype were collected in 96% ethanol. Left and Right wings were mounted with glycerol and photographed using a Zeiss Axiophot with 5X magnification abject. The camera used for the photos was a QIMAGING Micropublisher 5.0 RTV with the software QCAPTURE.
The image size was 2560 x 1920 pixels, in TIFF format.

Landmark digitization:

For landmark digitization were used 15 landmarks in the crossing veins of Drosophila wings. Landmarks of some genotypes were digitized twice for measurement errors. The program used for digitizing the landmarks was tpsDIG.

Size analysis:

Size was measured using the Log of Centroid size (Centroid size: square roots of the sum of the squares of all the landmark from the centroid). Size was also measured using the total wing area.

Shape analysis:

For the shape analysis Procrustes superimposition was used, which is composed from three passages: 1) Change scale so that all the configurations have the same size; 2) Shift the center of gravity to a single point; 3) Rotation to minimize the dispersion of corresponding points. The coordinates of the landmarks obtained by the Procrustes Superimposition only contain variation in shape (Klingenberg, 2010).

Multivariate analysis:

Variation in shape is intrinsically multivariate. To study shape changes of the landmark configuration we used multivariate statistical analysis, like Principal Component analysis and Canonical Variate

Analysis. PCA was used to asses differences between genotypes. For a given experiment we had run the Procrustes Superimposition, generated the Covariance Matrix and run a PCA.
CVA was used to maximize differences of shape grouping the data for genotype*developmental stage.

Fluctuating Asymmetry:

Fluctuating asymmetry denotes small differences between the left and right sides due to random imprecisions in developmental processes (Klingenberg, 2015). To measure size FA we applied a conventional two-way ANOVA. To measure shape FA we applied a Procrustes ANOVA derived from the Procrustes superimposition. Variance of (L-R) was used to calculate size FA using the Log centroid size as measure of the dimension of the wings. For shape asymmetry scores we had made the averages of the Procrustes FA scores of each individual resulting from the Procrustes ANOVA. All datasets passed the D'Agostino-Pearson normality test. Moreover, the data did not present signs of DA and AS. The data presented have a skewness near zero (symmetrical distribution).

Ex vivo calcium imaging

We dissected the 3rd Instar larval brain, and we immediately mounted it in a home-made chip treated with poly-L-lysine solution 0.1% (w/v) (Sigma-Aldrich) in PBS. All the recordings were done using the genetic calcium sensor GCaMP6m (Chen *et al.*, 2013). We immediately imaged the brain for 300 or 360s. We apply 5µL of the desired solution after 120s for stabilizing the baseline of some neuron's bodies. The applied solution remained in the bath until the end of the experiment.

The microscope of choice was a spinning-disk confocal Visitron CSU-W1. We used the sequent parameters for all the recordings: 30 slices of 1.5µM thickness; pixel binning of 2; 50ms of exposure. We used 20x or 40x magnification depending on the experiment, and the resulting acquisition speed was 0.5Hz.

Data processing and analysis of the cell bodies of the 3rd Instar larval brain

We first opened the files with FIJI, and we did the correction of the drift using the plug-in called "correct 3D drift" (Parslow, Cardona and Bryson-Richardson, 2014). Then, we transferred the recording in Imaris (Bitplane), where we used an automated particle tracking algorithm, allowing us to follow the neuron's bodies during the whole length of the video. For some cell's bodies that were difficult to track automatically, we did it manually. The Imaris software identifies every cell body as a spot with a unique identity number, producing a plot with the intensity of the cell over time. We created an extra spot in proximity to the analyzed cell's bodies as background fluorescence. We saved the files as .csv for subsequent analysis.

We performed a downstream analysis using python, normalizing the fluorescence using the formula (Ft-F0)/F0, where Ft is the fluorescence intensity at the time point t, and F0 is the baseline as the average intensity of the first ten frames before the stimulation.

Temperature control with TRPA1

We use TRPA1 ion channel to activate neurons in determined time point during larval development. For the activation of the channel, we change the incubation temperature from 23°C to 29°C. The larval instar was determined by looking the morphology of the jowls in a representative population.

Results

flyGear

The idea of a robot

We developed an automatization of developmental timing inspired by the manual inspection of pupae/flies in the fly vials (**Figure 11A**). The goal was to find a convenient method to record the wandering and pupariation of the flies in their standard tubes.

People, in general, are afraid of changing their methods and try to use newer ones. So the more accessible new technology will be, the higher the probability that the researchers will use it. Accessibility was the goal that we wanted to reach, using the standard tubes was a must.

The idea of the robot flyGear started in 2017 to accelerate and scale up the developmental time experiments. It was not a scale-up since the development of this robot took years because it was a side project. We wanted to develop an easy-to-use automatic solution with user-friendly software analysis. The robot has a capacity for 20 tubes and can be adapted to accommodate standard fly vials of different diameters.

The first iteration

We developed several ideas to create a platform that could rotate 360º with the help of Víctor Rodríguez at the IN electronics facility. The prototype was a circle with 20 holes for the tubes. A microwave oven motor moved this circular platform, and a camera recorded the tubes. However, this device did not work. The microwave motor changed the direction of rotation randomly, and the abrupt changes and movements were far from the clockwork precision expected of a scientific robot. Moreover, having only a central motor, counting the animals was tricky. We were unsatisfied with the prototype, so we decided to make a second one.

The second iteration

We decided to modify the project. We needed more than a single engine to achieve our goal. Moreover, using an Arduino board was the best way to control the movements reasonably and ensure that they were smooth and reproducible. The Arduino Uno board communicates serially with Bonsai, a program that allows many live-video manipulations and the control of several cameras, among many other functions (Lopes *et al.*, 2015). Therefore, we built a robot with two stepper motors connected to an Arduino (**Figure 9A**). We used a laser cutter to build a central circular platform and the components' base. Then we made tubes and camera holders with a 3D printer and positioned a camera in a lateral position that records video and images directed toward the platform. A central motor rotates the platform in front of the camera until a sample tube of interest is in front. An external (second) motor rotates the front sample tube 360º over itself, allowing the camera to record its entire surface (**Figure 9C** and **D**).

We added other details to the device, such as bearings, positioned between the tube holders and the circular platform, allowing smooth rotation. Both the motors (central motor and external motor) and the lighting module comprise a housing that covers them with an internal insulator to protect them from humidity and allow a longer life span of the device. We will also include in the device a lighting module with infrared and white light that illuminates the sample tubes to recreate day and night.

Finally, we created a little software working with the serial monitor of the Arduino board. The software was able to:

1) write the name of the experiment,
2) set the positions with the tube placed,
3) decide to start the recording,
4) decide the time after eggs laying, and
5) set the elapsed time from one recording to another.

The resulting videos were of good quality (full HD resolution) and were easy to recognize larvae pupae and adult fruit flies.

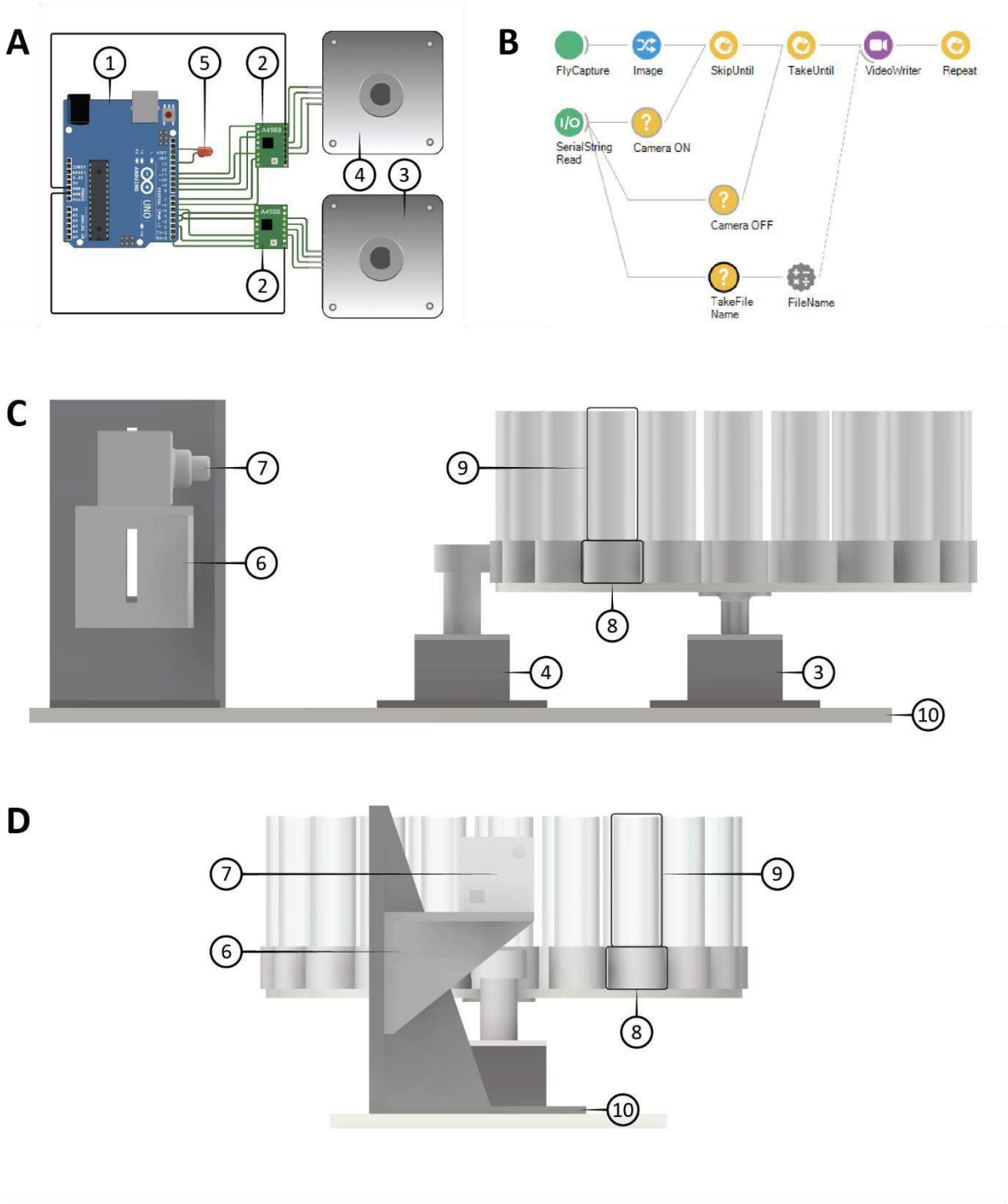

Figure 9. The hardware composition of flyGear.

(A) The basic hardware configuration of flyGear. (B) The Bonsai software controls the camera via serial communication with Arduino. (C) Lateral view of flyGear. (D) Frontal view of flyGear. The components are: 1) Arduino Uno microcontroller; 2) Two SparkFun stepper motors drivers; 3) Principal stepper motor; 4) Second stepper motor; 5) Light source illuminating the tube; 6) Camera holder; 7) Camera; 8) Tube Holder; 9) Standard fly tubes; 10) base.

The analysis of the videos

The final goal of flyGear is to automate all the passages of the developmental time experiments. The last and most challenging task is to perform an accurate automated counting of the animals inside the tubes. The first way we tried was to use a method previously used by a photographer, Justin Kerr, to produce a book of the vessels of the pre-Columbian Maya civilization(Justin Kerr, Maya vase database: An archive of rollout photographs). What he was doing was flattening the whole circumference of the vase (**Figure 10A**). This method, known as rollout photography, is used mainly for archaeological photography (Felicísimo *et al.*, 2018; Felicísimo and Polo García, 2021). We apply this method using a Python code that mimics a slit-scan process found online (*Generating Slit Scan Images in Python - Make Art with Python*, Kirk Kaiser). With little modifications to the original code, we mimicked the slit scan process by creating a slit of the width of one pixel and the length of the entire tube, and we placed it in the centre of the video. For every frame where the tube is rotating, the program takes just one pixel-wide line and sticks them together. The resulting image is a flat version of the rotating tube (**Figure 10B** and **C**). Ideally, this image can be analysed using the segmentation method to find the contours of the object of interest (pupae in this case) (**Figure 10B** and **C**, right panel). Although this method is excellent, we still do not have a fixed pipeline for counting pupae.

We also developed pipeline software to recognize larvae from pupae. We did it using Bosai, a user-friendly software that allows programming in an easy way (Lopes *et al.*, 2015). We used the output videos from the flyGear, converted them to greyscale, and applied a threshold that could detect just the orange-coloured pupae compared with the whitish coloration of larvae (**Figure 10B**). In this way, we demonstrated how much could be easy the recognition of two different developmental stages of Drosophila.

The last method we want to implement is DeepLabCut software (Mathis *et al.*, 2018). Here the idea is to train a neural network with the images of pupae and larvae from the videos and then use this network for counting the animals. In the present day, we have just started this implementation, and it will not be discussed in this thesis.

Finally, after having high-quality videos, we showed several ways in which an automated counting of larvae and pupae could be achieved. More work is needed to automate this counting.

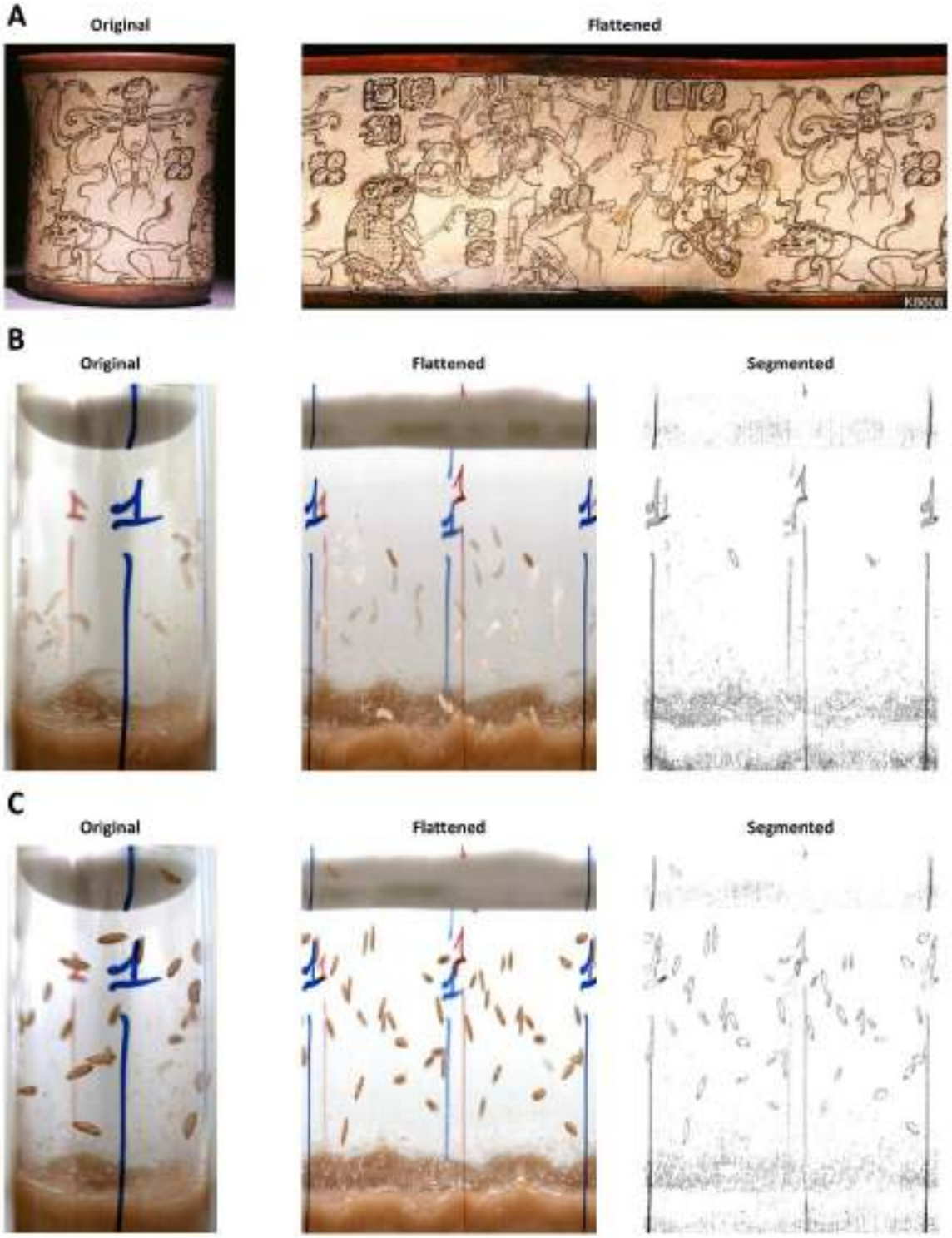

Figure 10. A rollout photography method for the analysis of flyGear videos

(**A**) Example of a maya vase in the original version (left) and the rollout photo of it. (**B**) The original tube at 118 hours and 40 minutes from eggs laying (left), its rollout photo, and the segmented image. (**C**) The original tube at 138 hours and 0 minutes from eggs laying (left), its rollout photo, and the segmented image.

A working proof of the flyGear

The developmental time in Drosophila melanogaster is measured every 4 or 8 hours. Here we present a proof of concept of the flyGear in which the robot records the video every 20 minutes, from 70h AEL to the eclosion of all the flies (Figure 11A and B).

We used flies with the null *Lgr4* mutations (hereafter $Lgr4^{KO}$), created in our laboratory, and the control *yw* flies in which the CRISPR alleles were induced (hereafter *CTRL*) (Vallejo *et al.*, 2022). Lgr4 relaxin receptor belongs to the LGR subfamily of GPCRs (Van Hiel *et al.*, 2015) and is homologous to the human Relaxin Family Peptide receptors RXFP1 (LGR7) and RXFP2 (LGR8) (Hsu, 2003).

We conducted the assay with three tubes per condition. In Figure 11A there is the schematic representation of the experiment. Under them is a QR code of the tube video representing the equivalent developmental phase of the *CTRL* condition. We can measure wandering and pupariation from the movies (Figure 11B). The time with the maximum number of wandering larvae, the wandering peak, was near the median of the distributions of the number of wandering larvae in the time (Figure 11D). In the *CTRL* group, the median was 121.3 hours, and in the $LGR4^{KO}$ group, 117.0 hours (Figure 11C and D). The difference between the two peaks was of 4.3 hours, and it was highly significant (Figure 11C). We also measured the time to pupariation in the two conditions. We saw that the median perfectly equals 50% of the total number of the pupae (Figure 11C). The median pupariation time of the *CTRL* animals was 125.3 hours; in the $LGR4^{KO}$ group, it was 120.7 hours (Figure 11C and E). The elapsed time between the two lines was of 4.6 hours, and it was highly significant (Figure 11C). The difference between wandering and pupariation time in the *CTRL* was 4 hours and 3.7 hours in the $LGR4^{KO}$. Neither the wandering nor the pupariation time have a normal distribution, so we used a non-parametric statistical test to compare groups (Figure 11C).

Here we showed how to utilize flyGear for timing experiments with a high-frequency acquisition. This sensitivity allowed us to find differences in the wandering and pupariation time as little as 4 hours. Moreover, it is easy to compare these results with any experiment as the food and conditions used were the same as in the classical assays. We will include this experiment in a future publication (Vallejo *et al.*, in preparation).

During the past years, we used flyGear extensively. Some of these experiments are in the following chapters of this thesis.

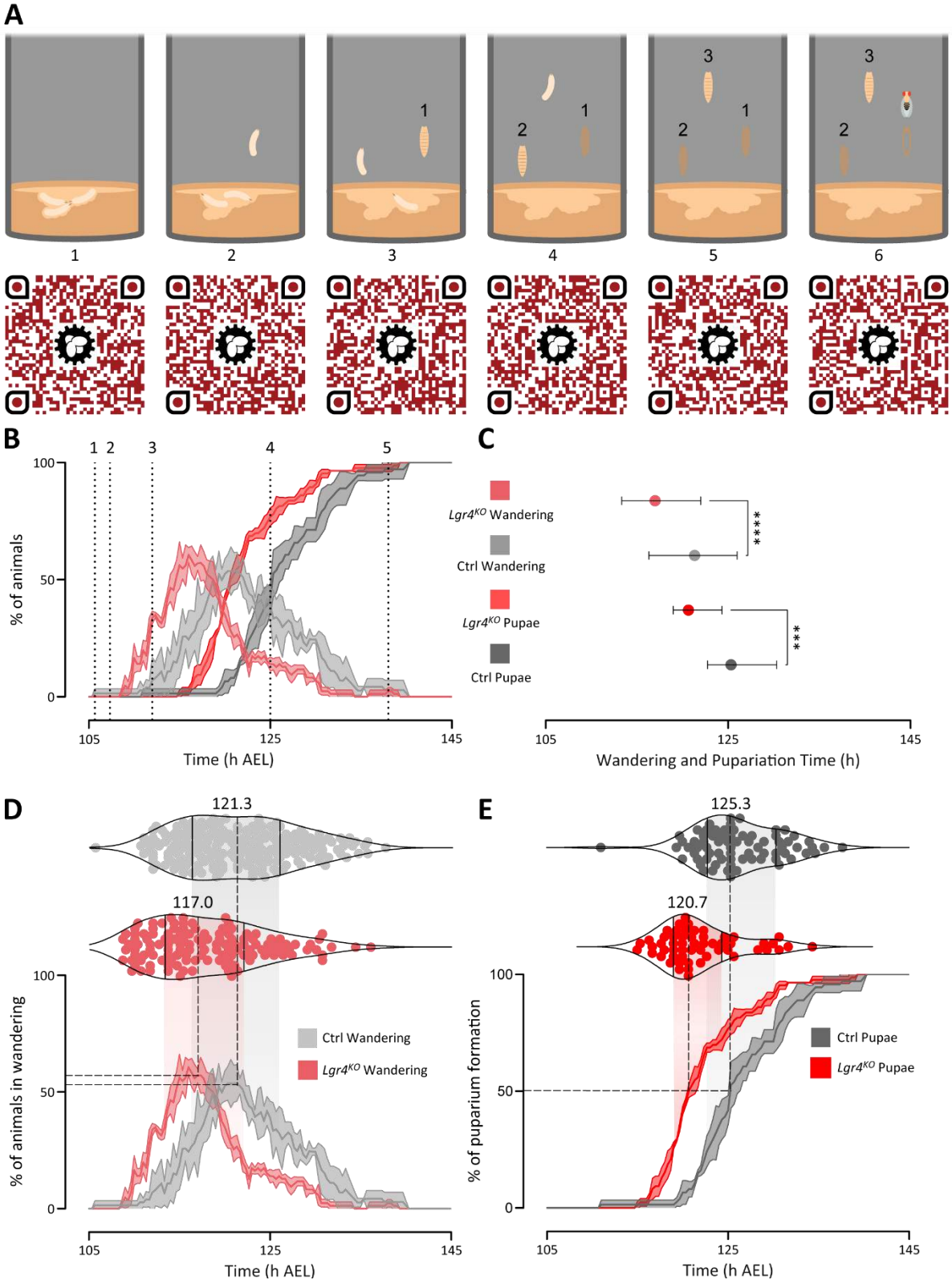

Figure 11. Wandering and pupariation's time measured every 20 minutes of *Lgr4*^{KO} and *CTRL* flies.

(A) The development of the fruit fly illustrated (top), and the QR codes of the corresponding videos of the *CTRL* flies(bottom). (B) The wandering and puparium formation measure every 20 minutes. Dotted lines represent the videos in (A) (C) The median time and the interquartile range of the experiment in (B). (D) The violin plot representation of the wandering phase of the experiment in (B). Note that the distribution of wandering is not normal. (E) The violin plot of the pupariation's time of the experiment in (B). Note that the median equals the 50% of the pupariation.

The neural substrates and circuitry logic for body symmetry-assurance

Adenylate cyclase genes have limited effects in ILP8-Lgr3 mediated developmental delay

We started with studying the downstream signals that could mediate the developmental delay induced by the overexpression of Ilp8. The Lgr3 receptor response to Ilp8 is strongly coupled to cAMP stimulation (Vallejo *et al.*, 2015). This second messenger molecule is synthesized from ATP by enzymes called adenylyl cyclases (ACs), activated by G-protein coupled receptors (GPCRs) (Lee, 2015). To verify that elevated cAMP downstream of ILP8-mediated activation of its receptor Lgr3 is required for ILP8-induced developmental time checkpoint, we screened candidate AC genes for their ability to rescue the ILP8-induced delay in pupation when the candidate AC gene was silenced in Lgr3-expressing neurons using the R19B09-Lgr3 enhancer-Gal4.

Silencing of ACXC and ACXB had no effects on the developmental timing delay induced by ILP8 (**Figure 12A, B**). In contrast, the silencing of ACXD, the ACXs on the third chromosome, partially rescued the development delay caused by the *Ilp8* overexpression (*tub-ilp8*, *R19B09>ACXD*^{RNAi}) (**Figure 13A**). Silencing ACDX alone did not change in the time of pupariation in flies having *R19B09-Gal4>ACXD-IR* (**Figure 13A**).

Because FoxO regulates the expression of the *AC76E* gene, and FoxO has an essential role in the development and organ growth and likely also acts on developmental timing in the insulin/PI3K/AKT pathway (reviewed by Texada 2020), we next tested whether the silencing of this AC gene in Lgr3 neurons may impact developmental timing. We used two independently generated AC76E-RNAi lines (Materials and Methods), and we detected a mild reduction of the ILP8-induced developmental delay with both RNAi constructs (only one line is shown here) (**Figure 13B**). In contrast, silencing FoxO did not rescue the ILP8-induced developmental delay (**Figure 13C**). Thus, the AC76C is required for ILP8-Lgr3 signalling to modulate developmental timing and independent of FoxO.

These data identify two adenylate cyclase, ACXD and AC76C, as possible novel elements in the ILP8-Lgr3 signalling mechanism that triggers the developmental time checkpoint for buffering growth perturbation. Because the results were not stronger enough, we moved to study other aspects of Ilp8-Lgr3 system.

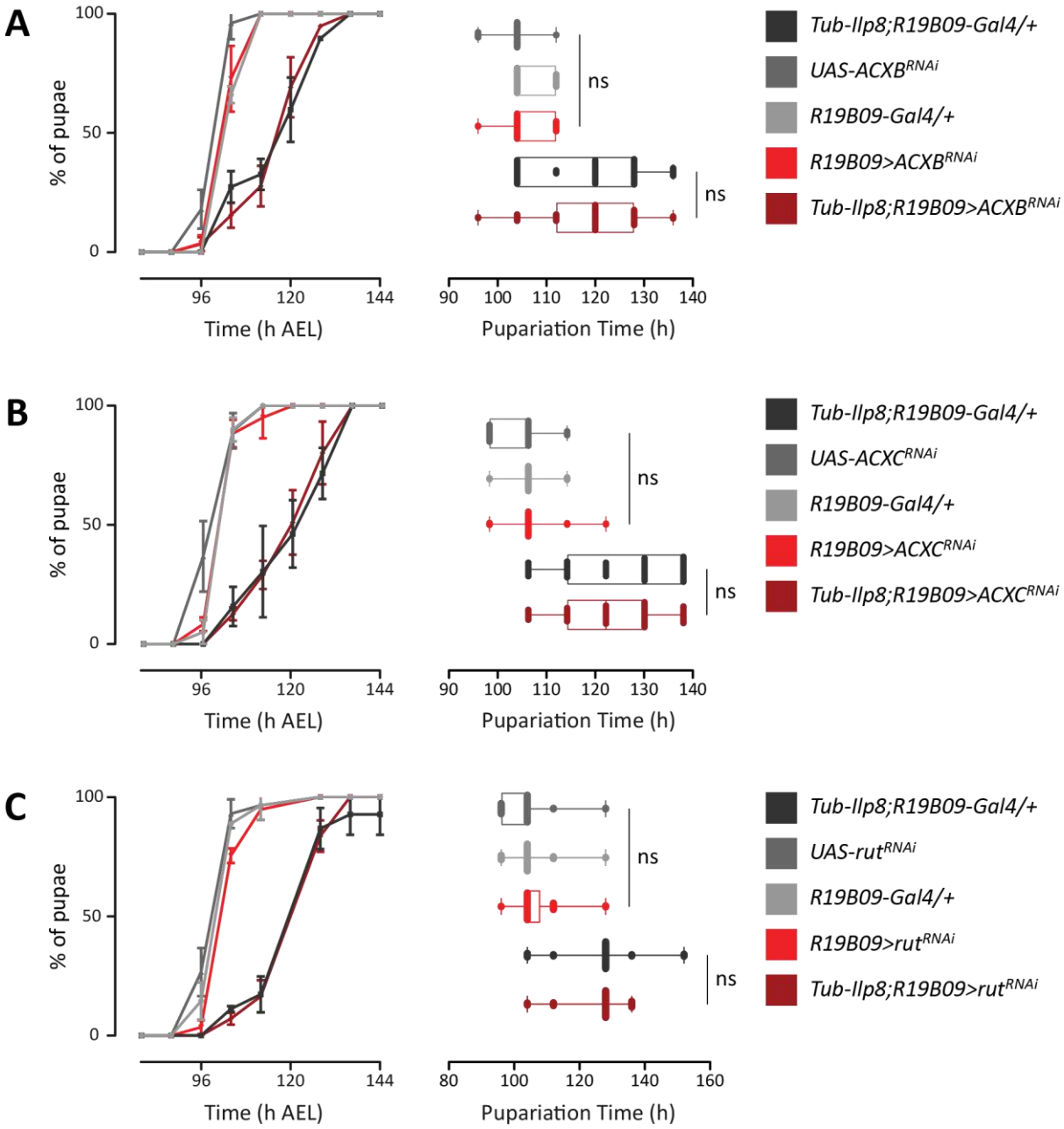

Figure 12. The knock down of adenylate cyclase ACXB, ACXC and rut does not rescue the delay induced by Ilp8.

(**A**) The knock down of *ACXB* have no effect of the delay induced by *Ilp8*. (**B**) The knock down of *ACXC* have no effect of the delay induced by *Ilp8*. (**C**) The knock down of *rut* have no effect of the delay induced by *Ilp8*. For all the graphs on the left the pupariation time in expressed as the percentage of pupae counted every 8h, h AEL (hours After Eggs Laying). The number of animals in each genotype is approximately 60. Each data point represents the mean of three biological replicate, and the bars represent the ±SD (Standard Deviation); The graphs on the right represent the same experiment in the view of box plot, where the box extends from the 25th to 75th percentiles, the whisker from the minimum to maximum, and all the points are shown. The statistical test used was the Kruskal-Wallis's test.

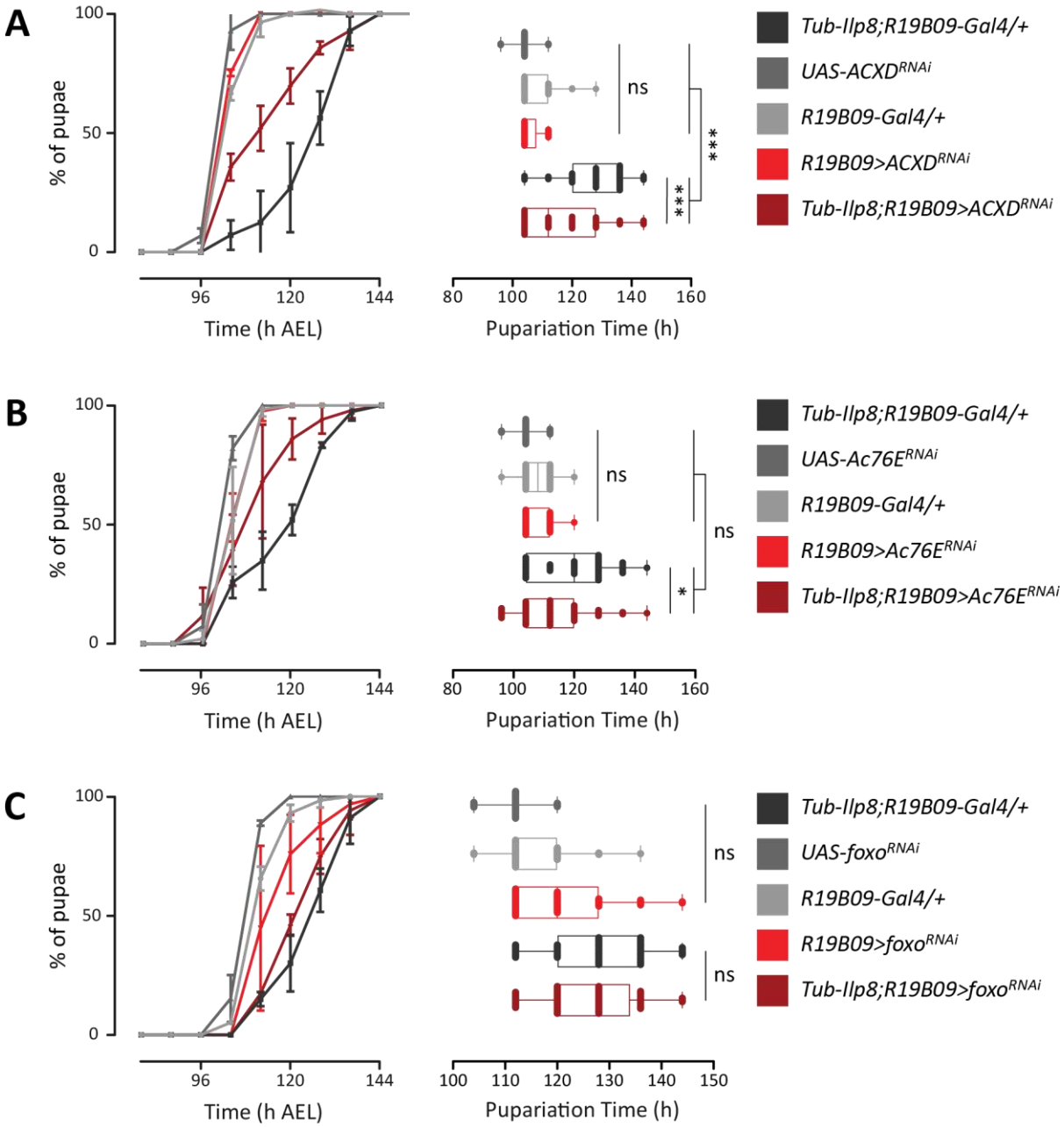

Figure 13. The knock down of adenylate cyclase *ACXD,* or *AC76E* partially recues the delay induced by *Ilp8*.

(**A**) The knock down of *ACXD* significatively reduced the delay induced by *Ilp8* (*** p = 0.0003), but not at the controls time(***p=0.0007). (**B**) The knock down of *Ac76E* partially reduced the delay induced by *Ilp8*(* p = 0.0289), but not at the controls time (**** p=0.0001). (**C**) The knock down of *foxo* have no effect of the delay induced by *Ilp8*, so the induction of *Ac76E* is independent by the activity of FOXO in these neurons. For all the graphs on the left the pupariation time in expressed as the percentage of pupae counted every 8h. The number of animals in each genotype is approximately 60. Each data point represents the mean of three biological replicate, and the bars represent the ±SD (Standard Deviation); The graphs on the right represent the same experiment in the view of box plot, where the box extends from the 25th to 75th percentiles, the whisker from the minimum to maximum, and all the points are shown. The statistical test used was the Kruskal-Wallis's test.

When is Ilp8 necessary for controlling body symmetry?

Flies deficient for Ilp8 cannot buffer minor size variations between bilateral body parts or maintain correct body dimensions and proportionality (Colombani, Andersen and Léopold, 2012; Garelli *et al.*, 2012). This lack of buffering and ability to stabilize size across the body results in higher than normal FA (Garelli *et al.*, 2012). The FA is a population index that measures developmental instability (Garelli *et al.*, 2012b). ILP8 deficient flies also have more varied body sizes (and parts) than control flies (Garelli *et al.*, 2012).

We envisioned maintaining symmetry by continuously monitoring the size and comparing the current size with the expected size requires continuous monitoring of circulating ILP8 (Juarez-Carreño, Morante and Dominguez, 2018). Others have hypothesized that ILP8, which is strongly expressed at the transition between larvae and pupal (Heredia *et al.*, 2021), may act only at the end of development to correct size variation in a checkpoint-like manner (Boulan *et al.*, 2020).

To determine when ILP8 activity is required for maintaining perfect left-right symmetry, we used the TARGET system (McGuire, Mao and Davis, 2004) for accurate temporal control of Gal4 activity. If ILP8 is required in a defined developmental window or checkpoint, we expected that only silencing *Ilp8* during this period would result in high FA, like the effect of *Ilp8* mutants. Instead, a continuous requirement during the larval growth period will be manifested as increased FA when Ilp8 is silenced during the larval growth. The larval epidermis increases only during the larval feeding period and stops when the larvae exit the food to find a place for pupating (Texada, Koyama and Rewitz, 2020). Still, the size of the imaginal discs increases through the three larval growth periods, the non-feeding period and the first day of pupation (Garcia-Bellido and Merriam, 1971; Bryant and Levinson, 1985).
The *Ilp8* gene is expressed during the larval stages in the imaginal discs with a slight decrease during moults (Garelli *et al.*, 2012), while strongly expressed in the cuticle epidermis of the white pupa (Heredia *et al.*, 2021). The temporal requirement of *Ilp8* will also inform where *Ilp8* is required in the growing imaginal discs or within the exterior epidermis.

To do this experiment, we combined a validated *Ilp8* RNAi (*UAS-Ilp8-RNAi*) transgene with the temperature-sensitive Gal80 (*UAS-Gal80^{ts}*) expressed under the control of a ubiquitous *tubα-Gal4* (**Figure 14A**). The silencing of *Ilp8* only during the embryonic period has no effect on the FA (**Figure 14A**, fifth line from the top) (**Figure 14B**, upper left). The effects of the silencing of *Ilp8* start to be visible in the larval stages. The knock-down of *Ilp8* between L1-L2 led to significative high levels of FA related to controls (**Figure 14B**, upper centre), but the overall effect was limited (**Figure 14A**, sixth line from the top). When we silenced *Ilp8* during the three larval stages (L1 to L3), we obtained the highest FA (**Figure 14D**), both for size and shape FA (**Figure 14A** third from the top, and **Figure 14B**

above left). We also found that, when *Ilp8* was knocked down until the starts of the pupariation (from embryo to white pupae, WP) the general shape of the wings was different from his control (**Figure 14C**). In fact, the Canonical Variate 2 (CV2, Y axis) showed that the control wings (*Tub-Gal4; Tub-Gal80/+*) and the experimental wings (*Tub-Gal4; Tub-Gal80>Ilp8^{RNAi}*) have different shape (**Figure 14C**, the reds dots, and the greys, on the right, are separated). This doesn't happen when *Ilp8* is knocked down during the metamorphosis (**Figure 14C**), the reds dots and the greys are stacked together). The clearest separation was in the CV1 (X axis). This big separation was probably the temperature effect. The temperature for down regulate *Ilp8* during the larval stages was 29ºC and 18ºC metamorphosis, and it was the reverse for inactivating *Ilp8* during the pupal stages.

We have shown that the homeostatic regulation of ILP8 in controlling the growth of wings imaginal discs takes place during all the three larval stages. This make sense in the light of a constant growth of the imaginal discs until the wandering stage (Bryant and Levinson, 1985). Although these results seem to be in line with the growth of the wings imaginal discs, others says that the role of Ilp8 in maintaining the developmental stability is during the pupal stages, and not during the larval stages (Boulan *et al.*, 2020). The different results could be caused by the narrow period of the switching temperature in respect with the results in this thesis.

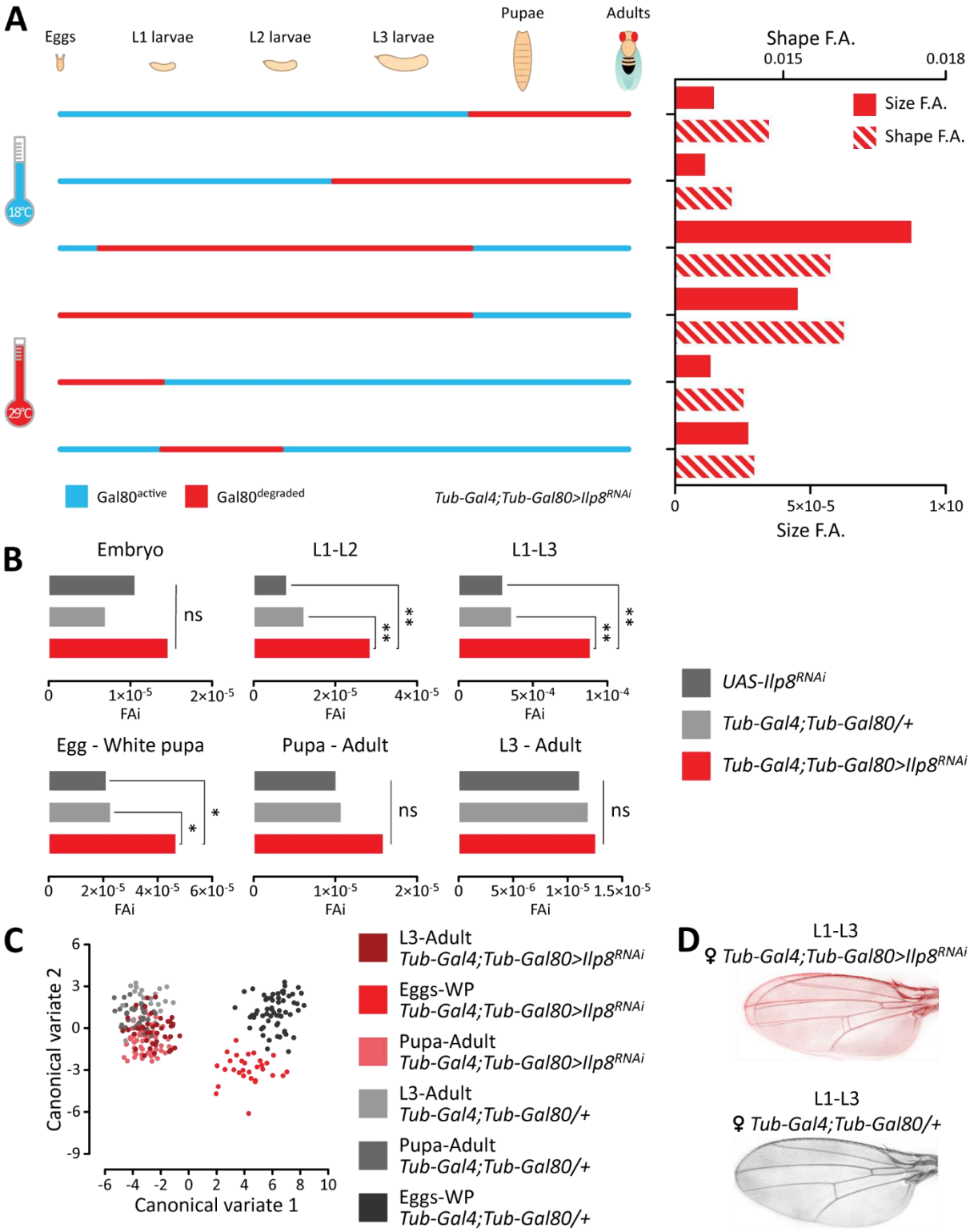

Figure 14. When is Ilp8 necessary during development?

(**A**) The knock down of *Ilp8* in various developmental stages using the temperature sensitive construct *Tub-Gal80*. At 18°C the Gal80 is produced and binds the Gal4 preventing the transcription of *UAS-Ilp8^{RNAi}*, at 29°C the Gal80 was disrupted, activating the transcription of Ilp8^{RNAi} in the selected developmental stages. (**B**) CVA of the wings with the silencing of *Ilp8* of various developmental stages. (**C**) FA of the wings with their controls from the developmental stages in (A). (**D**) Representative wings asymmetry and control flies. L1: 1st instar larva; L2: 2nd instar larva; L3: 3rd instar larva; WP: white pupa. The numbers of animals per genotype was between 20 and 30.

Extensive Left-Right connections in the Lgr3 neural network

Having a bilaterally symmetrical body, with two hands, two legs, or two wings that occur in mirror-image, implies the necessity to employ a strategy whereby the two sides of the body can communicate and integrate left-right body information.

By studying the Lgr3 neuronal network, we noted extensive axonal connections between the left and right Lgr3-expressing neurons (**Figure 15** and **Figure 16**), including the two bilaterally paired neurons in the inferior protocerebrum (**Figure 17D**), which acutely respond to Ilp8 hormone by elevating cAMP reporter (Garelli *et al.*, 2015; Vallejo *et al.*, 2015), and are hypothesized to be the first-order, Ilp8 responsive neurons (Colombani *et al.*, 2015; Garelli *et al.*, 2015; Vallejo *et al.*, 2015).

As a starting point for characterizing left-right connections within the Lgr3 network, we focused on the central brain neurons that we previously defined as Lgr3 responsive neurons based on their activation of a cAMP reporter. Using Brainbow tools (Hampel et al., 2011) for stochastic labelling of paired neurons and MCFO tools (Nern, Pfeiffer and Rubin, 2015) for high-resolution three-dimensional (3D) images of individual neurons, we identified most of central brain Lgr3 responsive neurons and found that like the hyper-responsive Lgr3, many Lgr3-expressing neurons send contralateral projection to innervate their contralateral targets (**Figure 16**, and **Figure 17D**). Also, in the ventral nerve cord (VNC) many neurons send contralateral axons (**Figure 15**). We used previous description of brain compartments to designate these neurons (Cardona *et al.*, 2010; Hartenstein *et al.*, 2015).

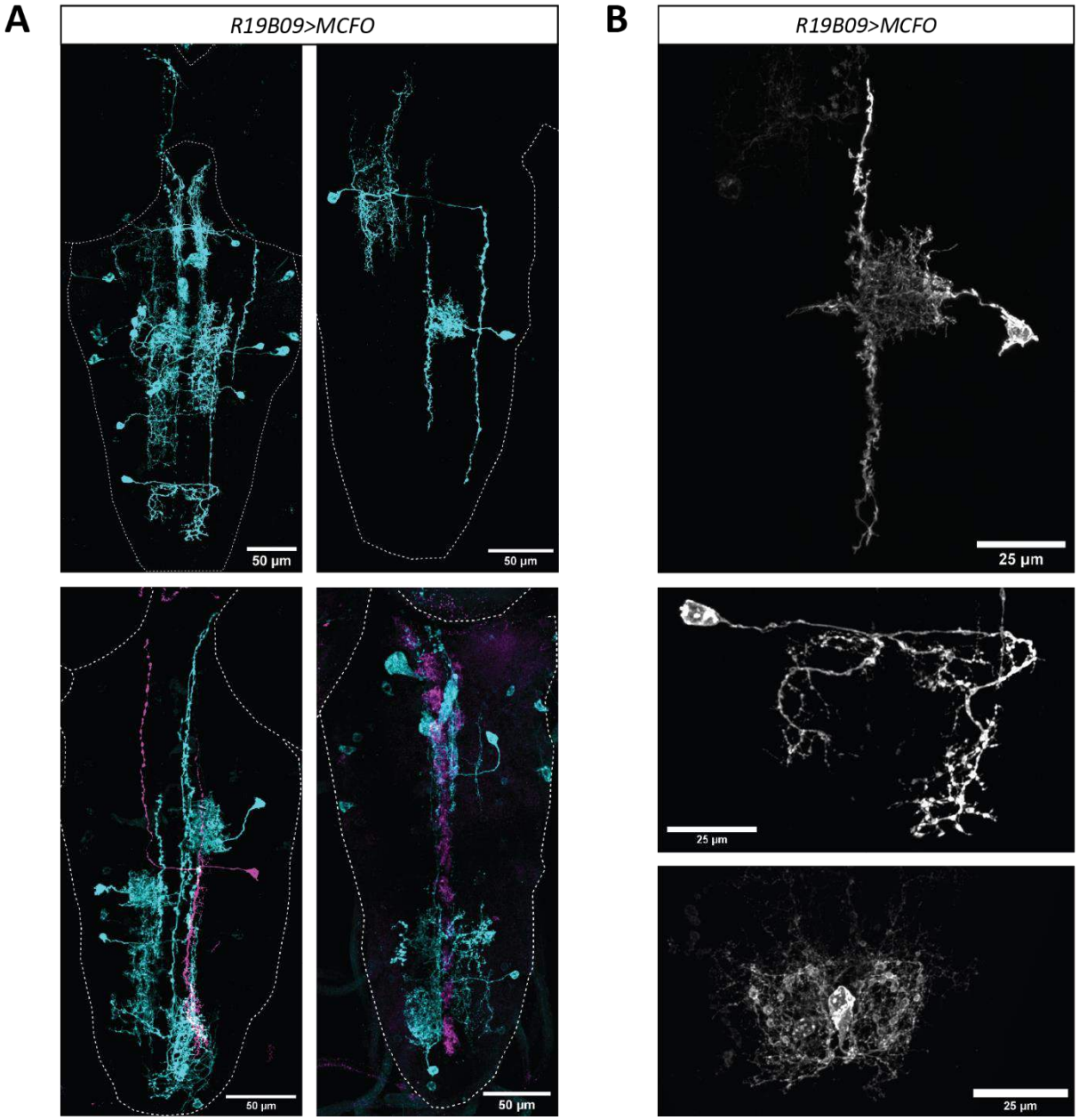

Figure 15. Single cell labelling of the R19B09 enhancer line in the VNC.

(**A**) Sparse labelling of neurons in the VNC. (Top Left) VNC neurons using the MCFO technique, note that a neuron of the VNC reach the anterior part of the pars intercerebralis. (Top right) Two VNC neurons, one with a big contralateral process direct in the lateral-abdominal position, and a Basin neuron in right side. (Bottom left) Basin and Jupiter neurons in the R19B09-Gal4 enhancer line. The Basins are in cyan, and the Jupiter is in magenta. (Bottom right) Posterior VNC neuron with the axon in the proximity of the midline (labelled with Slit). (**B**) (Top) Magnification of a single Basin neuron in the VNC. (Middle) Magnification of the posterior VNC neuron of the top left brain in (A). (Bottom) Magnification of a neuron in the posterior centre of the VNC.

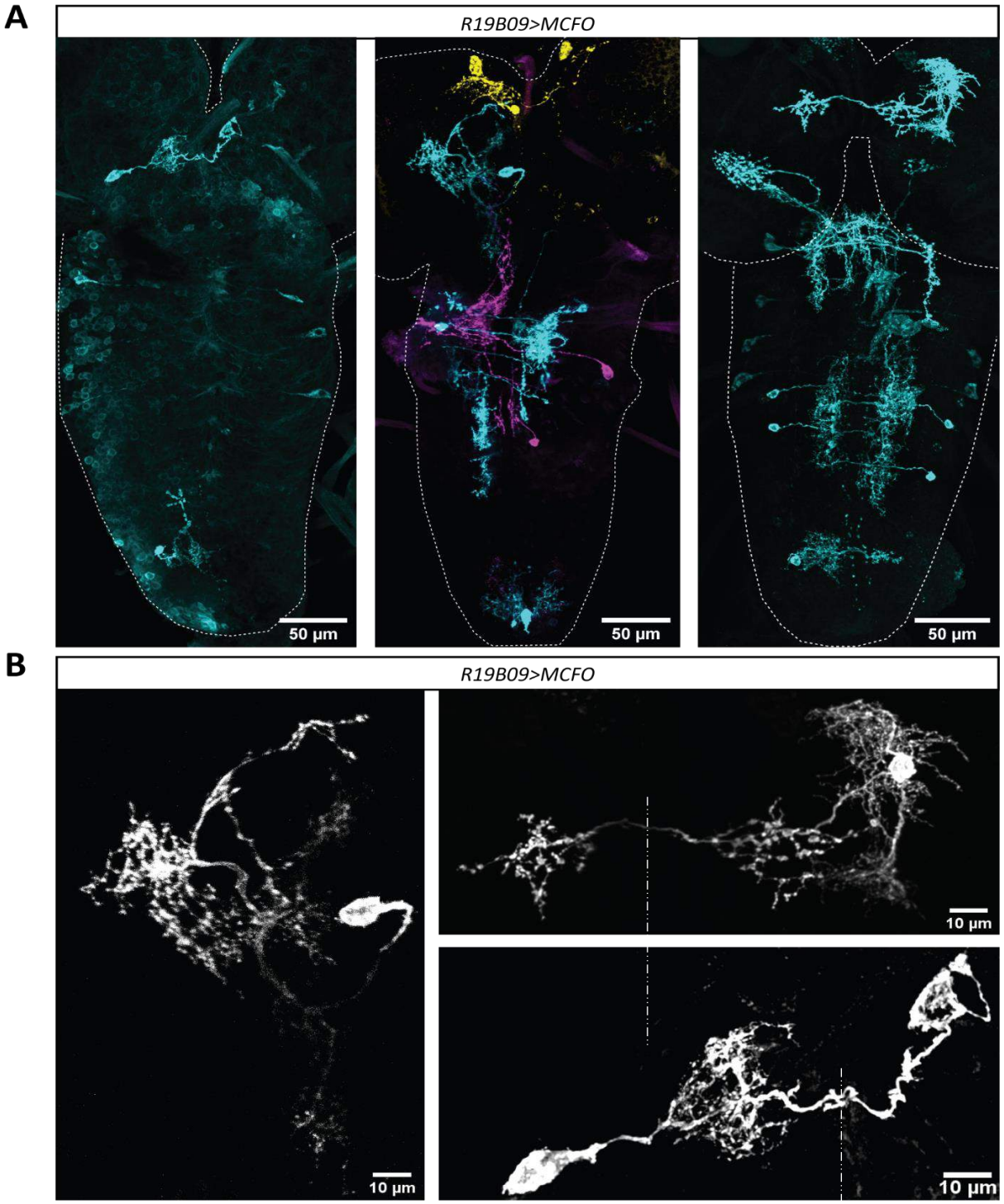

Figure 16. The majority of R19B09 labelled neurons have contralateral projections.

(**A**) (left) An example of a neuron in the sub oesophageal zone crossing the midline. (Centre) example of central brain and VNC neurons. Of the central brain neurons, one in ipsilateral, with a process reaching the SEZ, the cellular body inside the pars-intercerebralis, and with an axon going medio-anteriorly in the pars intercerebralis (in cyan). Another neuron is visible (in yellow) that have contralateral non mirroring axon. This neuron innervates the anterior region of the pars intercerebralis. (Right) In the central brain, a neuron has an axon going contralaterally in a non-mirror region of the left hemisphere. In the SEZ in visible a neuron with a complex structure. In the VNC are visible the Basins, and another contralateral neuron in the abdominal region. (**B**) Magnification of neurons in (A). (Left) the ipsilateral neurons in the protocerebrum of the larval CNS. (Top right) The SEZ neuron shows an enlarged process near the midline and a contralateral axon with a non-mirror target.

Impairing contralateral projections in the Lg3 ensemble decreases developmental stability

Bilaterally symmetric animals represent more than 99% of all living multicellular animal species (Finnerty *et al.*, 2004). In bilateral animals, the integration of left-right inputs is crucial, at least, for sensory and motor functions (Suárez, Gobius and Richards, 2014). This integration works because the left and right sides of the nervous system are connected.

Here we use the Robo signalling pathway to interfere with the contralateral growth of R19B09 neurons in the larva brain. We started with the RNAi of the *roundabout* genes. We didn't see any contralateral effect using the RNAi (Data no shown). So we decided to use the *Robo2* and *Robo3* overexpression used in the paper from Oliva et al (Oliva *et al.*, 2016). The overexpression of *Robo2* was not producing any clear effect in the contralateral projection (data not shown). Moreover, flies overexpressing *Robo2* had normal developmental timing (**Figure S 2A**). Nevertheless, these flies, of both sexes, had bigger wings (**Figure S 2B**, **D**), but no signs of developmental instability (**Figure S 2C**, **E**). The overexpression of *Robo3* induced the loss and the mis-disposition of many contralateral axons in the protocerebrum (**Figure 17C**). Although visible alterations of the anterior commissure, the number of contralateral projections was not statistically different form the control (**Figure 17F**). Moreover, the developmental time was unchanged, as the pupal size and the wings size, and the FA of these fly was very low in both sexes (**Figure S 1**).

Another way to prevent contralateral formations in Drosophila is to use the RNAi of the *comm* gene. We found that removing *comm*, using two different RNAi lines, from the lgr3 neurons (*R19B09-Gal4>Comm*^{RNAi}) prevents the midline crossing of many axons (**Figure 17A**, **B**, and **F**). These flies had a developmental delay of about 8h, and normal pupal size (**Figure 18A**, **B**). In these flies, the dimensions of the wings were reduced in female flies, and with the same tendency in the males (**Figure 18C**, **E**). The male flies show high FA (**Figure 18F**), the female flies show the same tendency, but not significant levels of FA (**Figure 18D**). To verify that the effects of lack of *commissureless* in the developmental instability were a specific effect of the neurons expressing *Lgr3*, we silenced *commissureless* in other two important neurosecretory neural populations, the PTTH neurons, and insulin producing cells (IPCs) (Vallejo *et al.*, 2015). The PTTH neurons are a pair of bilateral neurons that project in the PG assuring the right onset of the metamorphosis (McBrayer *et al.*, 2007). They haven't any visible commissure between them. When we silenced *comm* in the PTTH neurons we found that the flies were normal, as for the dimension of the wings, as for the FA (**Figure S 5**). The IPCs are neurosecretory cell, that produce at least three insulin like peptides (ILPs). These cells are well known for their role in diabetes, and in the growth control. They also have commissural axons between them (Rulifson, Kim and Nusse, 2002; Nässel *et al.*, 2013). We expected a strong effect of *comm* in this population. Although the initial expectations, were in favour to an effect of the silencing, we found that

only the developmental time was accelerated of about 8 hours (**Figure S 4A**). The pupal size, and the adult wing size was unaffected, and the FA was very low (**Figure S 4B**, **C**, **D**, **E**, and **F**). We also over-expressed *Robo3* in the IPCs, and we did not find any defects (**Figure S 3**).

Here we tested if the contralateral connections of Lgr3 neurons (*R19B09*) can affect the right proportions of the two matching parts of the body in populations of flies. We already known that the silencing of Lgr3 in these neurons produces high asymmetry (Colombani *et al.*, 2015, p. 3; Garelli *et al.*, 2015; Vallejo *et al.*, 2015). We found here that, among the genes tested, only *comm* has a role in controlling developmental stability. We saw that the silencing of *comm* prevents many of the bilateral connections, delay the pupariation, reduces the wings' size, and induces FA. Moreover, we saw that the effects were specific of the neuronal population that express *Lgr3*, and not in other populations important for the growth control. These results are also supported by the recent finding of a single cells sequencing, when in a cluster of peridermic neurons there in the expression of *Lgr3* and *comm* (Corrales *et al.*, 2022).

Taken together, these experiments imply that for maintaining the right symmetry during development, the Lgr3 neurons must communicate between the two hemispheres.

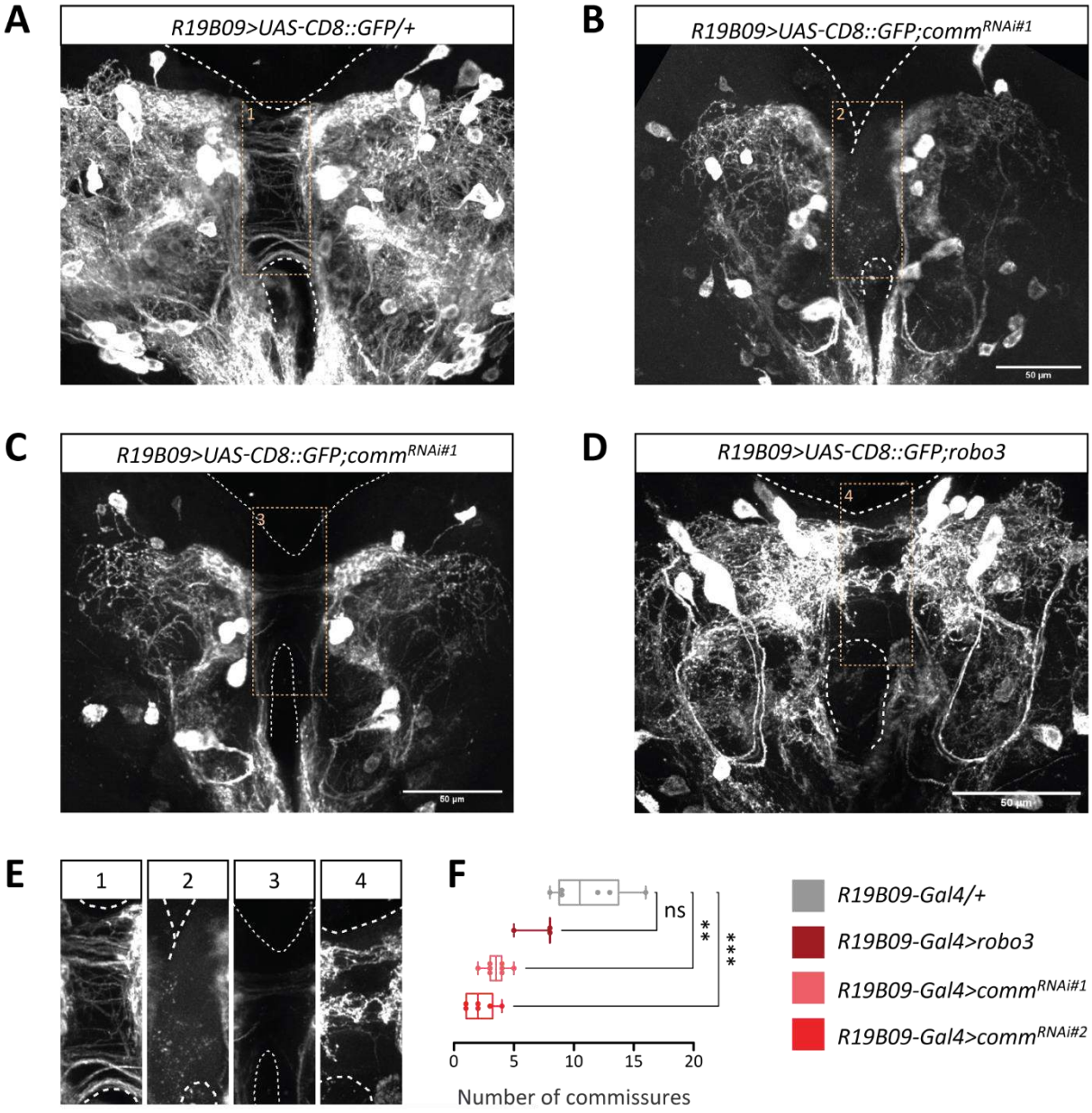

Figure 17. Prevention of contralateral projections in the R19B09 neural ensemble.

(**A, B**) Two different RNA interference line of *commissureless* showed reduction of the number of contralateral axons in the wandering larval brain. The ipsilateral regions seem to be less affected. (**C**) The overexpression of *robo3* affected the positioning of the contralateral projections. (**D**) Wild type brain showed a great number of commissural axons. (**E**) Magnification of the superior commissure of the brain in A, B, C, and D. (**F**) Quantification of the number of visible commissures in the L3 wandering brains of the different genotypes presented in this figure, ***P<0.0001 (Kruskal-Wallis nonparametric test).

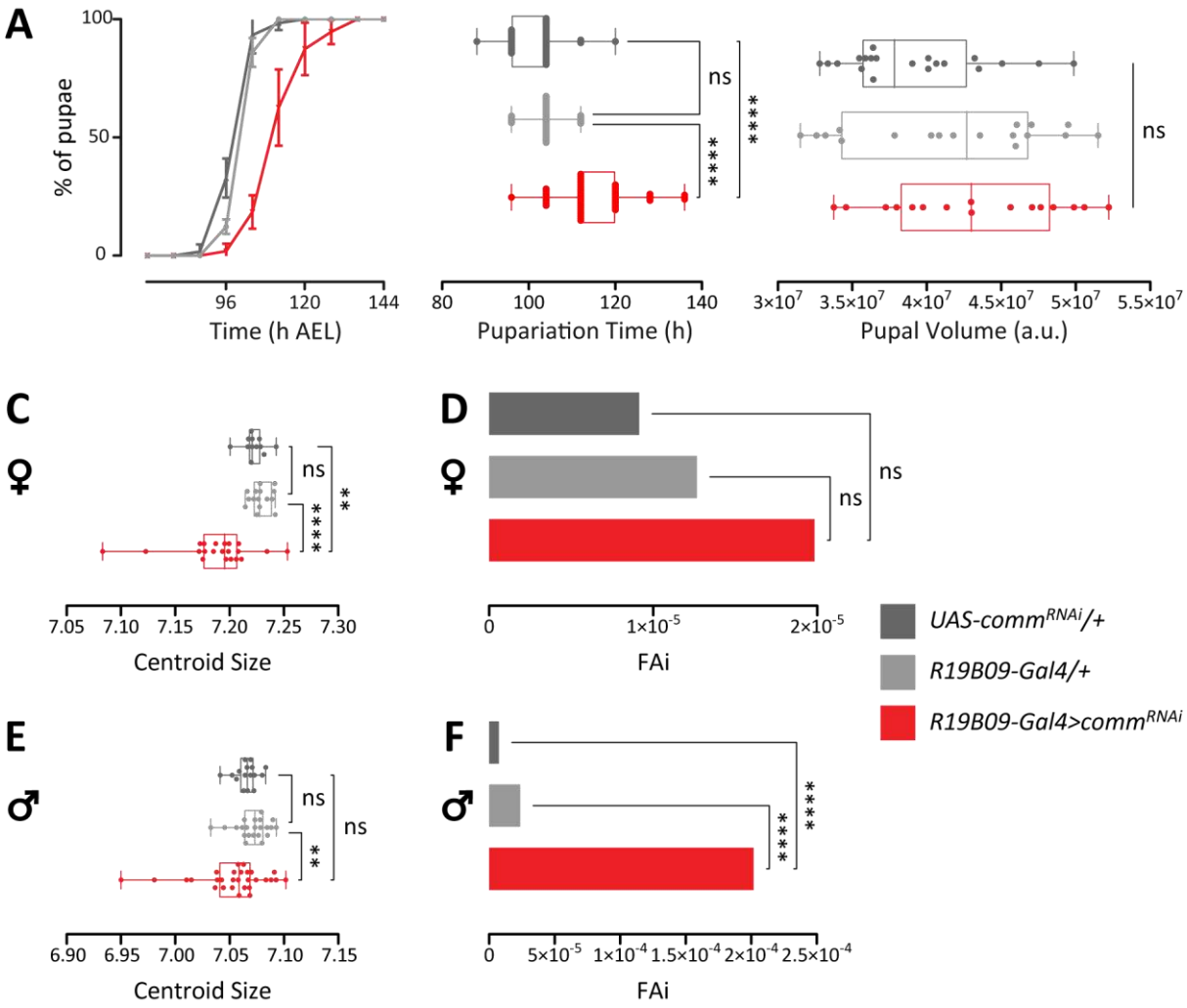

Figure 18. Lgr3 "split-brain" via *comm*^{RNAi} increases FA index.

(**A**) The knock down of *commissureless* significatively increases the developmental time (**** p<0.00001). The number of animals in each genotype is approximately 60. Each data point represents the mean of three biological replicate, and the bars represent the ±SD (Standard Deviation); The statistical test used was the Kruskal-Wallis's test. (**B**) pupal 'volume is unaffected by the silencing of *commissureless* (**C**) Reduced wings 'size in males having defect in the contralateral projections of *R19B09-Gal4* labelled neurons (**D**) Males having defective contralateral projection had slightly increase FA but not significant. (**E**) Not significant reduction of the wing size in females with "split-brain" (**F**) Silencing *commissureless* increases of Fluctuating Asymmetry (FA) in females' flies. ****P<0.0001 (F test). For fluctuating asymmetry analysis, the numbers of animals tested for each sex is from 20 to 30.

Identification of the MAT neurons in the Lgr3 neural ensemble

The Lgr3 enhancer line R19B09 contains more than 200 hundred neurons between VNC and the central brain, but the neurons that Ilp8 acutely activates are only two per hemisphere (Vallejo *et al.*, 2015). So, defining their detailed anatomy could be difficult and is a limit to a better knowledge of this homeostatic system.

We performed extensive single-neuron labelling using various techniques (see other section). By doing so, we could recognize the shapes of many of the neurons in the protocerebrum. Knowing the real morphology of these helped us find the Gal4 lines where some of those neurons were present. We used the database of enhancer lines produced with the project for the Janelia FlyLight facility, where many Gal4 lines with the expression in the larval nervous system are present (Li *et al.*, 2014, p. 4).

We found the R46B11-Gal4. This construct marks two pairs of the bilateral neurons into the dorsomedial region of the dorsomedial protocerebrum, flanking the supraesophageal commissure (**Figure 19A**). It also labels one pair of bilateral neurons in the pars lateralis, with axons reaching the corpora cardiaca (**Figure 19A**). The position of the cellular bodies of these two pairs of bilateral neurons near the midline resembles the place of the somas of the neurons that acutely respond to *Ilp8* overexpression.

We were interested to know if those neurons in the *R46B11* enhancer line were inside the neural ensembled marked with *R19B09-Gal4.* We took advantage of the presence of the *R19B09-LexA* and created a stock for doing an intersection. For doing so, we built flies carrying the constructs *R19B09-LexA; UAS-FRT.stop.mCD8-GFP.H.* Then, we crossed them with males bearing *LexAop2-FLPL; R46B11-Gal4.* We dissected the larvae carrying all four constructs and stained the brains. We verified that the dorsomedial protocerebrum neurons of R46B11-Gal4 were a subset of the R19B09-LexA neurons (**Figure 19C**). We called these neurons Match-maker (MAT) because they respond symmetrically to exogenous Ilp8 when recorded using calcium imaging techniques (see the paragraph Ex vivo whole-brain MAT and GAT neural Ca[2+] responses to ILP8). The MAT are bilaterally symmetric neurons, they have the soma near the supraesophageal commissure, they project ventrally in the subesophageal zone (SEZ), and they have contralateral projections reaching the ipsilateral mirror axon (**Figure 19A,** and **C**).

Later, we crossed the *R46B11-Gal4* with *UAS-DenMark,UAS-syt.eGFP* for labelling dendrites and synapses (Nicolaï *et al.*, 2010). The MAT cells have dendrites positioned ventrally in the SEZ and synapses positioned both ipsilaterally and contralaterally in the medial part of the dorsomedial protocerebrum (**Figure 20A**).

Most sensory neurons send inputs in the SEZ, where the MAT cells have diffuse ventral dendrites. They directly synapse in the dorsomedial protocerebrum, part of the central neuroendocrine system in Drosophila (Hückesfeld *et al.*, 2021). Given the functional anatomy of MAT cells, their presence in the R19B09 ensemble, and their calcium properties, these cells may play a central role in regulating larval growth.

Identification of the GAT neurons in the Lgr3 neural ensemble

Seeking news enhancer lines that label other neurons in the *R19B09* neural ensemble, we identified a new pair of bilateral neurons in the basomedial protocerebrum that could be part of the same neural circuit (**Figure 19B**, and **D**).

We identified the line *R40D06-Gal4*, which strongly labels two neurons where the somas position and morphology similar to Lgr3 neurons. The line R40B06 labelled neurons lay on each side of the basomedial protocerebrum, under the supraesophageal commissure. As in the previous chapter, we used *R19B09-LexA* and created a stock for the recombination-mediated intersection to verify that the *R40D06*-labelled neurons are Lgr3 positive. We built flies carrying the constructs *R19B09-LexA; UAS-FRT.stop.mCD8-GFP.H*. Then, we crossed them with males bearing *LexAop2-FLPL; UAS-R40D06-Gal4*. We genetically demonstrated that these neurons in the basomedial protocerebrum are labelled by both *R40D06* and *R19B09* lines (**Figure 19B**).

These neurons have projections reaching the dorsomedial protocerebrum region near the cell bodies of the MAT neurons (**Figure 19B**). Moreover, these cells have descending projections that go to the anterior part of the subesophageal ganglion (**Figure 19B**). As far as we know, these neurons are entirely uncharacterized. We called these neurons GAT (Give-and-take) because in calcium imaging preparation these bilateral neurons have an oscillatory activity between each other. These are three pairs of bilateral neurons in the *R19B09* ensemble, with their soma in the basomedial protocerebrum and projections reaching the dorsomedial protocerebrum. However, the individual neurons have potentially different properties, as seen in calcium responses to Ilp8 (data not show). The *R40D06-Gal4* line labels a sub-population of the GAT neurons and not all of them.

Finally, we used these Gal4 drivers to define the dendrites and axons using *UAS-syt.eGFP* for labelling both the dendrites and the synapses of the GAT neurons (Nicolaï *et al.*, 2010). As a result, we saw that ventral projections reaching the subesophageal ganglia are dendrites. The synapses are localized in the dorsomedial protocerebrum (near the soma of the MAT cells) and the basomedial protocerebrum (**Figure 20A)**.

Here we have identified the GAT neurons, a subset of the central brain neurons shared with the line *R19B09*. These neurons lay in regions also known as the par intercerebralis and pars lateralis. Moreover, these neurons contact the subesophageal ganglia with their dendrites and synapse in the anterior regions of the brain, raising the possibility that these neurons regulate some aspects of the integration of sensory information (Hückesfeld *et al.*, 2021).

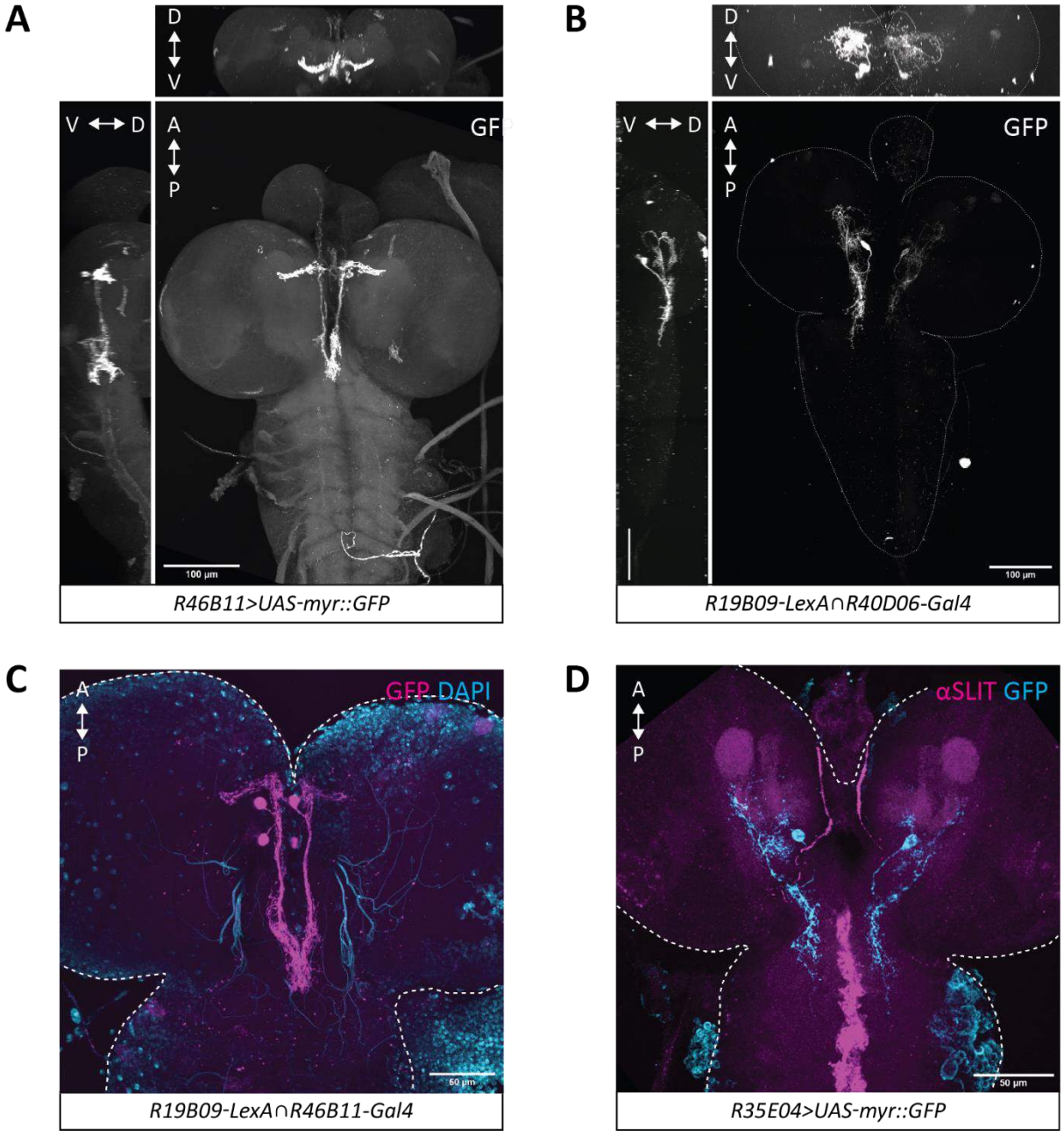

Figure 19. MAT and GAT neurons are part of the neural ensemble of *R19B09*.

(**A**) The enhancer R46B11 shows expression in two pairs of bilaterally symmetric neurons in the central brain of the L3 wandering larvae. We called them the Match-makers neurons (MAT neurons). There are also neuronal processes that reach the VNC from the periphery. The transverse and the sagittal plan are shown. These neurons have a contralateral projection in the anterior part of the pars intercerebralis, the have long process reaching the SEZ, with a wrench-like shape (visible in the sagittal plan) (**B**) Intersectional experiment showing that the GAT (R40D06-Gal4) neurons are a subset of the R19B09-Gal4 labelled neurons. The transverse and the sagittal plan are shown. (**C**) Intersectional experiment showing that the MAT neurons are a subset of the R19B09-Gal4 labelled neurons. (**D**) The enhancer R35E04 is another enhancer labelling the GAT neurons.

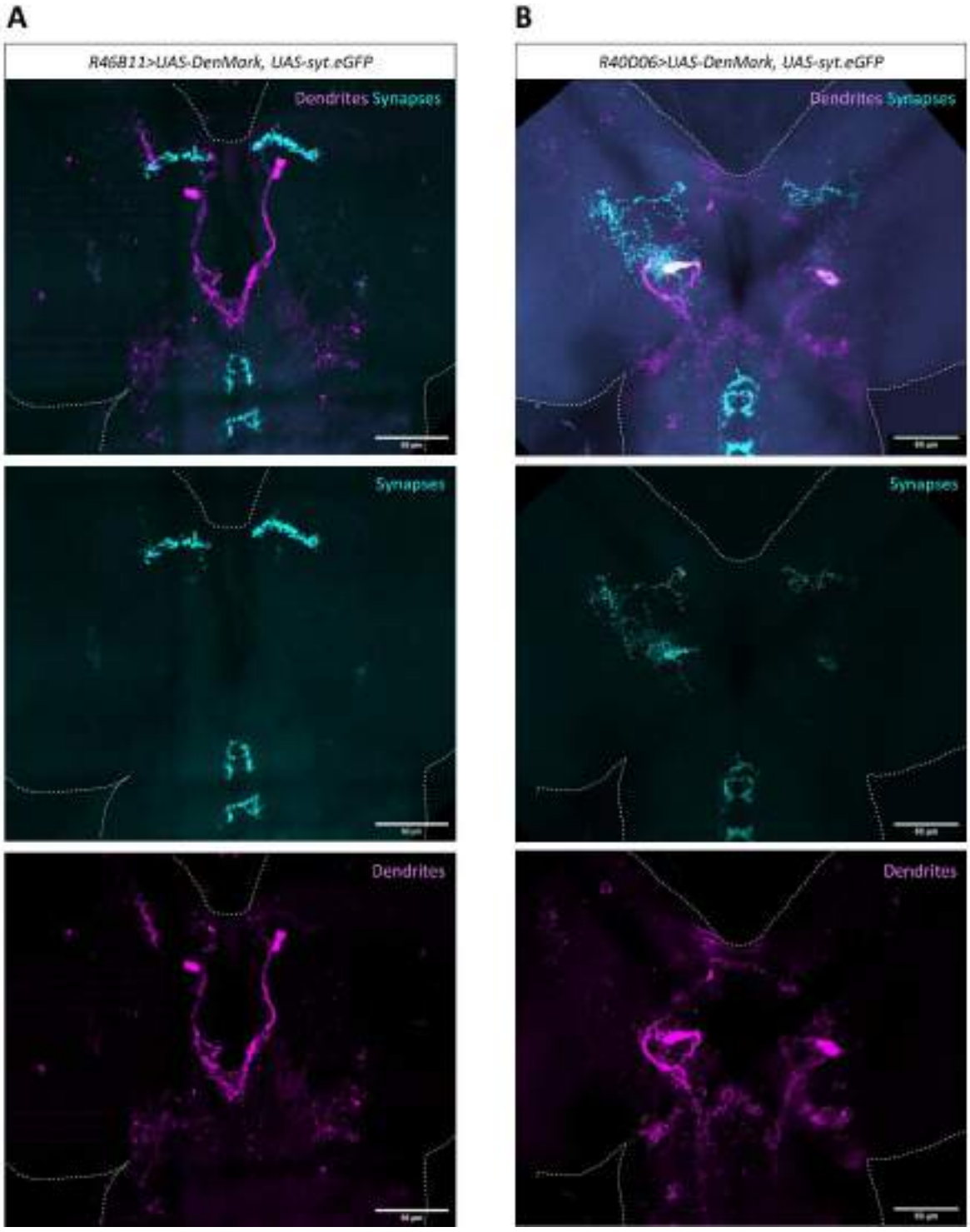

Figure 20. Details of synapses and dendrites in the MAT and GAT neurons.

(**A**) The dendritic and synaptic sites of the MAT. The dendrites of mat neurons are in the SEZ, and the synapses are in the anterior region of the pars intercerebralis. This could indicate that these neurons received inputs form interneurons in the VNC, and output in the neurosecretory region of the brain. (**B**) The dendritic and synaptic sites of the GAT. They have the dendrites that reach the SEZ ipsilaterally, they send their axons in the near the anterior commissure, and in the medial part of the pars intercerebralis.

Ex vivo whole-brain MAT and GAT neural Ca[2+] responses to ILP8 stimulation

To investigate the circuit logic in response to ILP8 stimulation, we performed ex vivo whole-brain calcium recording using the complex R19B09 ensemble but focusing on the MAT and GAT responses.

We used a microfluid chamber for the administration of synthetic ILP8 at the concentration of 50µM in PBS, or PBS alone. We used the *R19B09-Gal4*, which labels all the neurons of interest, and the *UAS-GCaMP6m*. GCaMP6m is a genetically encoded fluorescent Ca[2+] indicator that shows high sensitivity and medium decay kinetics (Chen *et al.*, 2013). We created a fly 'stock which bring both transgenes in homozygosis (*UAS-GCaMP6m; R19B09-Gal4*) and we crossed them with *UAS-Comm^{RNAi}; UAS-Lgr3^{RNAi}*, and with *W1118*.

We initially focused on the MAT neurons, localized near the mid-line of the protocerebrum, in proximity with the supraesophageal commissure. These are the neurons that acutely responds to Ilp8 *in vivo* by increasing the intracellular cAMP levels (Vallejo *et al.*, 2015). Because LGR3 is a G protein-coupled receptor we expect to see an increase in the calcium levels after applying the synthetic ILP8 to the *ex-vivo* brains. MAT neurons show increased Ca[2+] after the application of ILP8 (**Figure 21A**). To make sure the response was specifically due to ILP8, we recorded brains by applying PBS alone, and we were not able to see any response (**Figure 21C**). We double checked that the activity of MAT neurons was due to the LGR3 receptor by knocking down it with *UAS-Lgr3^{RNAi}*(*R19B09>UAS-GCaMP6m; UAS-Lgr3^{RNAi}*), and we saw no activity of MAT neurons (**Figure 21C**).

We also recorded the activity of the GAT neuron when applying ILP8 to the preparation. We observed a clear and reproducible activation of these 3 pairs of bilateral neurons (**Figure 21A**, **D**). We confirmed the specificity of that activation by stimulating brains with PBS alone, or by knocking down the Lgr3 receptor (**Figure 21E**). This activity was not expected, as there were no clues to find other neurons responding to ILP8 beyond the acutely responders MAT neurons.

The evoked response to ILP8 of GAT cells is delayed when compared with the MAT of 80/100 seconds (**Figure 21A**). The MAT neurons respond symmetrically, instead the GAT neurons respond asymmetrically between the brain hemispheres (**Figure 21B**).

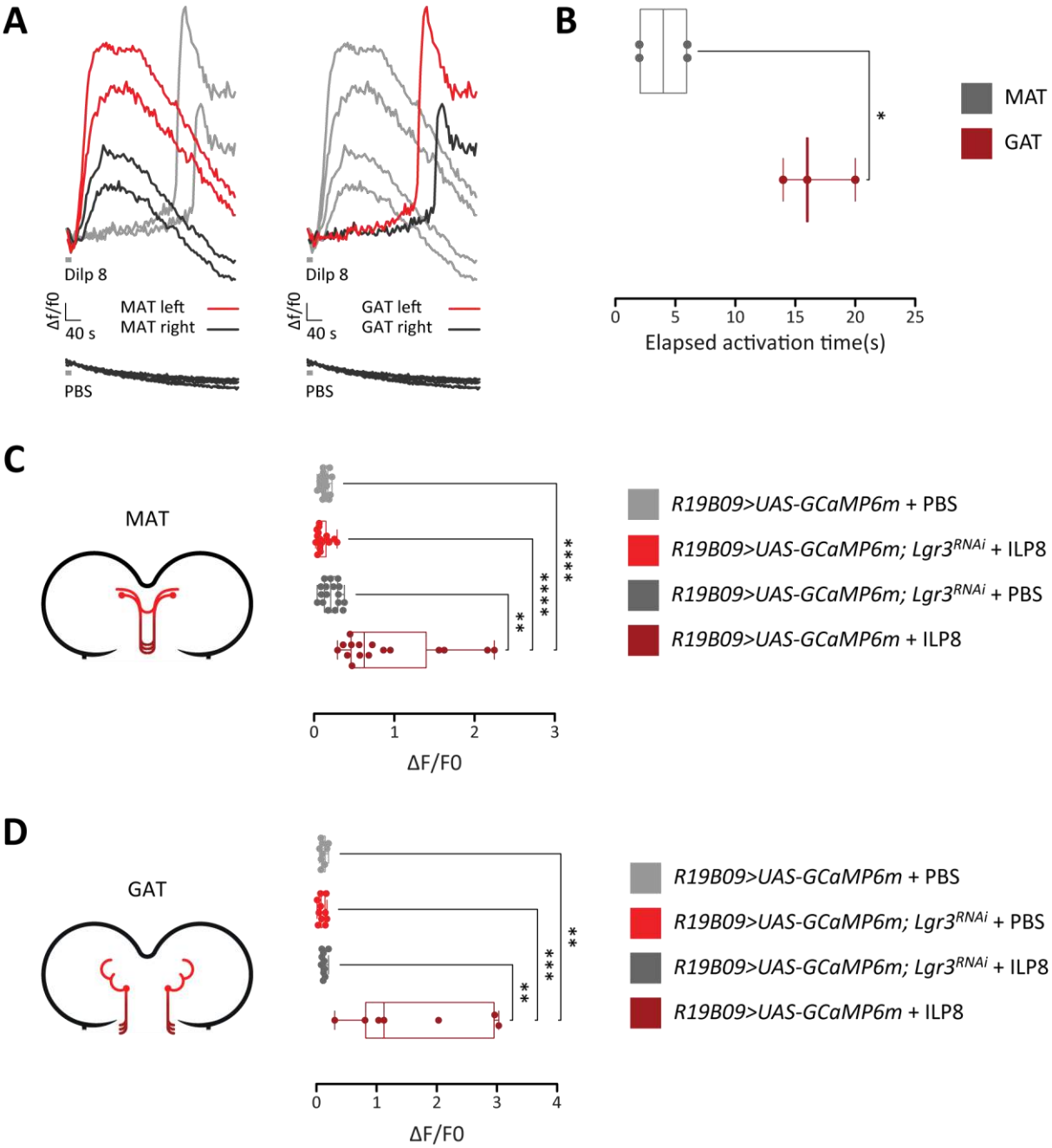

Figure 21. Activity of MAT and GAT cells.

(**A**) Activation of MAT and GAT neurons upon the administration of ILP8. We administrated synthetic ILP8 at the concentration of 50µM in PBS, or PBS alone. (Left panel) Activation of MAT neurons upon the administration of ILP8. (Right panel) activation of GAT neurons upon the administration of ILP8. Note that both neurons are part of the *R19B09* neural ensemble. (**B**) Elapsed time of the L-R peak of activation in the MAT and GAT neurons. *P<0.05 (Mann-Whitney test). (**C**) Resume of the activation of MAT neurons in WT and Lgr3^{RNAi} brains. **P<0.01, ***P<0.001 (Kruskal-Wallis' test). (**D**) Resume of the activation of GAT neurons in WT and Lgr3^{RNAi} brains. **P<0.01, ***P<0.001 (Kruskal-Wallis' test).

GAT Ca[2+] responses in "split-brains" and intact brains uncover the potential importance of inhibitory commissural interneurons

The results described in the previous chapters support the role of inter-hemispheric communication in sensing/correcting body bilateral symmetry. Therefore, to investigate whether inter-hemispheric communication and asymmetry are related to the activity of the MAT and GAT neurons, we knocked down commissureless (*R19B09>UAS-GCaMP6m*; *UAS-Comm^{RNAi}*), and we performed calcium recordings.

Upon ILP8 stimulation, we saw a reduced, but not absent, activity in the MAT neurons. Remarkably, in the "split-brain", GAT neurons had an atypical activity with spontaneous, seemingly synchronous calcium (see **Figure 22A**, **B**, **C**, and **D** to compare *Comm^{RNAi}* and intact brain calcium responses). The most parsimonious explanation is that commissural inhibitory interneurons within the Lgr3 ensemble normally maintain tonic inhibition of GAT neurons, which is released upon Ilp8 stimulation in a non-synchronous manner in the Left and Right Gat neurons. Although perhaps preliminary to conclude, we wish to mention that we frequently observed that the *GAT-Gal4* driver is slightly asymmetric, which typically has a higher expression on the left side of the brain, perhaps indicating that the brain is anatomically asymmetric. Indeed, the asymmetric response to Ilp8 is hard-wired because, in the ex vivo whole-brain recording, we dissect the brain from the sensory connections. Therefore, sensory input cannot explain the lag in the response between the left and right GAT. Similar arguments explain the central pattern generators for locomotion in *ex vivo* isolated brains in other species. Oscillations of the GAT neurons in brains lacking most of the contralateral projections were high-frequency and near-symmetric between the two brain hemispheres (**Figure 22C**, **D**).

Moreover, by knocking down Lgr3 or comm in the Lgr3 (*R19B09-Gal4*) neural ensemble, we saw high levels of the fluorescence of the calcium sensor GCamP6m compared with the control brains, with more dramatic changes in the flies lacking comm (**Figure 22E**, **F**).

We thought that a lack of contralateral inhibitory connections by a commissural neuron in the *R19B09* neural ensemble could cause unusual oscillations that we saw in GAT neurons. This could also explain the high fluorescence spotted in GAT neurons when comm was absent. If this is true, then a forced activation of the *R19B09*, which comprises the GAT neurons, should compromise the homeostatic growth of those animals.

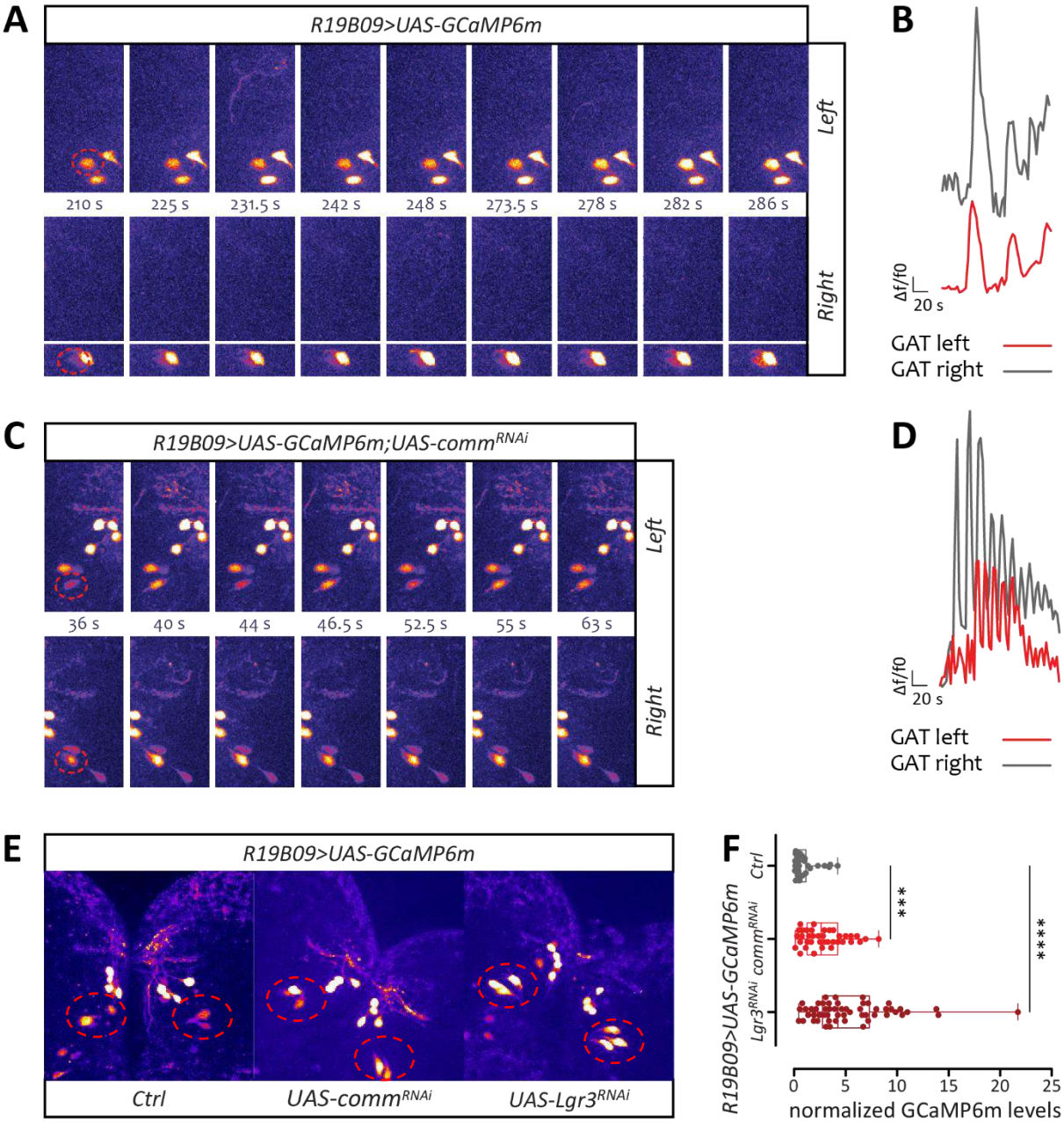

Figure 22. The activity of GAT neurons in the "split-brain" condition.

(**A**) Lgr3 control brain expressing the calcium sensor *GCaMP6m*. (**B**) Activity representation of GAT neurons in the control brain, showed in (A), upon the administration of ILP8. Note the oscillatory response. (**C**) Oscillations of left and right GAT neurons upon the removal of *commissureless* ("split-brain") from the Lgr3 neuronal ensemble. (**D**) Activity representation of the oscillation in the "split-brain" condition of the GAT cell bodies, highlighted in (C). Note the uncoupled (spontaneous) and fast oscillations. (**E**) Example of GAT neurons in the first frame of the recording showing the differences in the CGaMP6m in *R19B09>UAS-comm^{RNAi}* and *R19B09>Lgr3^{RNAi}*. (**F**) Quantification of the mean intensity of the first 5 frames from brains with *commissureless* or *Lgr3* knocked down, and controls (*R19B09-Gal4>UAS-CaMP6m*). **** P<0.0001, ***P<0.001 (Kruskal-Wallis' test).

Enforced symmetrical activation of *R19B09* neurons with TrpA1 channel increases FA

We next investigated whether perception (of mismatches) and compensation arise from the collective asymmetrical activity of neurons within the Lgr3 ensemble (labelled by R19B09 Lgr3 enhancer). Specifically, we sought to determine whether the differential neuronal activity is functionally relevant for buffering left-right asymmetries. To this end, we assayed FA in flies in which all Lgr3 neurons were enforced to be symmetrical activated using the warmth-gated ion channel TRPA1 (Viswanath *et al.*, 2003; Hamada *et al.*, 2008; Pulver *et al.*, 2009). TRPA1 is the D. melanogaster ortholog of the mammalian transient receptor potential channel TRPA1 (Hamada *et al.*, 2008).

Previously TRPA1 stimulation of defined neurons has been successfully used to disrupt aspects of locomotion behaviours that are relevant to symmetric movements in the larvae (Heckscher *et al.*, 2015; Clark *et al.*, 2018). For example, during larval locomotion, the left and right sides of each segment must contract simultaneously to produce forward movements, but unilateral movements such as turning involve asymmetric contractions mediated by commissural interneurons (Clark *et al.*, 2018).

We expressed TRPA1 in Lgr3 neurons using *R19B09-Gal4* and shifted control (*R19B09-Gal4/+*) and experimental (*R19B09>TRPA1*) animals from 23º (no-stimulation) to 29ºC (TRPA1 stimulation) at the defined developmental time points (**Figure 23**). In the animals with TRPA1 expressed in Lgr3 neurons, we observed a small but not statistically significant temperature-dependent increase in FA in animals shifted to 29ºC from early L3 to adulthood (**Figure 23A,** and **B**, right). The activity of TRPA1 from L1 to white pupa yielded highly asymmetric female flies, establishing a functional association between neuronal activation "symmetry" and FA (**Figure 23A**, right).

Flies with the forced activation of TRPA1, from L1 to white pupa, also show an increase in the wings size in both sexes (**Figure 23A**, and **B**, left), pointing to a role of the activity of these neurons in regulating the body's size.

We hypothesized that the ability of the larvae to buffer minor (e.g., unilateral) deviations from bilateral symmetry might depend on the capacity of Lgr3 neurons to perceive even minute variations in circulating Ilp8 peptide across the body. As such, the TRPA1 activity must necessarily interfere with this capacity. In the human population, fluctuating asymmetry covaries positively with exposure to environmental stresses and disease status (Livshits and Kobyliansky, 1991), supporting the association between increased FA and disease stress and fitness (Meissner *et al.*, 2016).

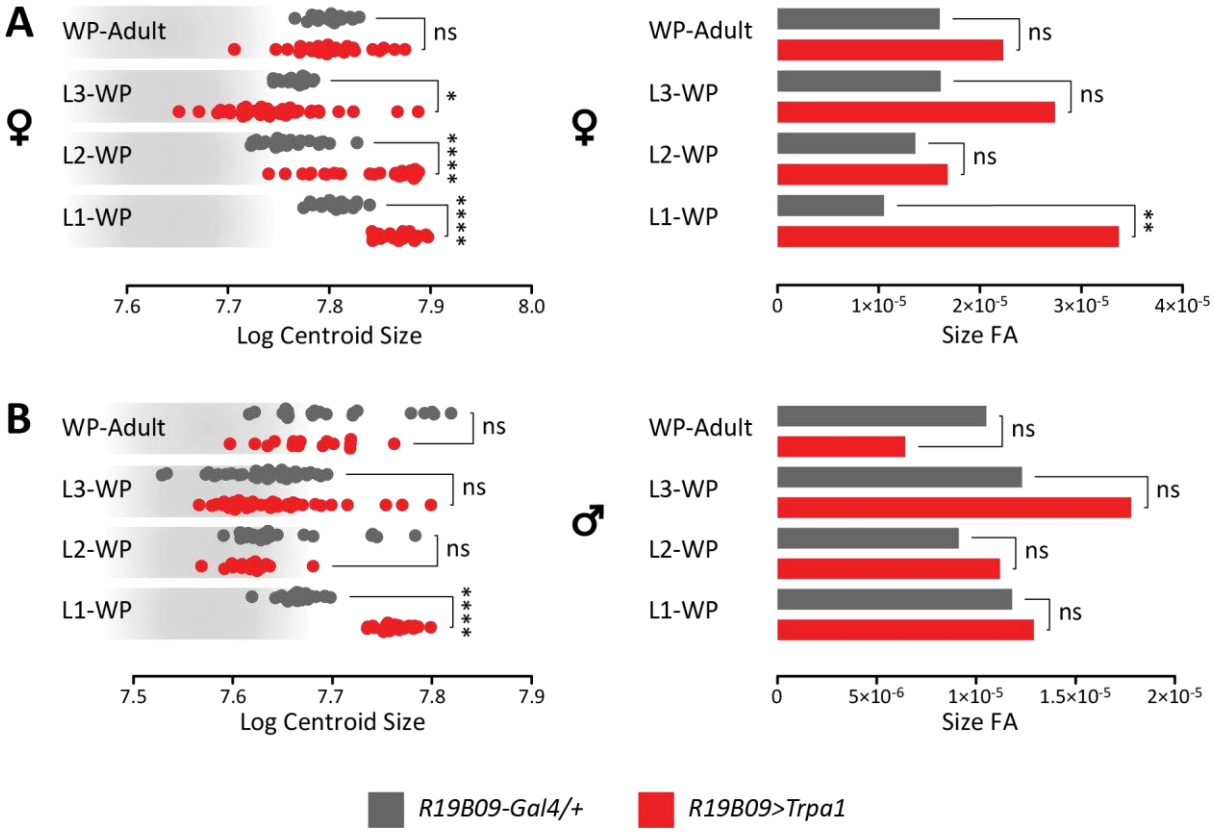

Figure 23. TRPA1 Symmetrical activation of R19B09 neurons with Trpa1 increases FA.

(**A**) The activation of TRPA1 between L1-WP and L2-WP in Lgr3 neuronal ensemble increases wings' size in female flies. ****P<0.0001 (one-way ANOVA). (**A**, right) High levels of FA appeared when Lgr3 neuronal ensemble was activated from L1 to WP in female flies **P<0.001 (F test). (**C**) The activation of TRPA1 also increased the wings' size of male flies during L1 to WP ****P<0.0001 (one-way ANOVA). (**D**, right) No changes in FA levels in male flies with TRPA1 activation. L1: 1st instar larva; L2: 2nd instar larva; L3: 3rd instar larva; WP: white pupa.

MAT and GAT neurons ensure growth homeostasis through Lgr3

After showing that MAT and GAT neurons are part of the neural ensemble labelled with R19B09 enhancer fragment and that both populations respond to ILP8, we asked if these neurons could have a role in the developmental stability. Previous studies have already shown that the mutants for Lgr3 have high FA (Colombani *et al.*, 2015, p. 3; Garelli *et al.*, 2015, p. 3; Vallejo *et al.*, 2015). Moreover, the knockdown of Lgr3 in the brain (*Elav-Gal4*) and in the neurons of the Lgr3 enhancer R19B09-Gal4 have a huge increase in FA (Vallejo *et al.*, 2015). If MAT and GAT neurons have a role in the growth homeostasis, we expect an increase in FA after removing Lgr3 from these cell populations. We started testing the MAT neurons for FA upon the silencing of Lgr3 (*R46B11>Lgr3*^{RNAi}). We observed that female flies had high FA with respect to the controls (*R46B11-Gal4/+* and *Lgr3*^{RNAi}*/+*) (**Figure 24C**, left). We also saw the same tendency in males, albeit the result was not significant for both the control lines (**Figure 24C**, right). Females' wings size was also affected; the flies carrying *R46B11>Lgr3*^{RNAi} had bigger wings size (**Figure 24B**, left , although the pupariation time was unchanged (**Figure 24E**). We also tested the GAT neurons using *R40D06-Gal4* for FA upon the silencing of Lgr3 (*R40D06>Lgr3*^{RNAi}) (**Figure 25C**). We detected high levels of FA in both males and females with respect to the controls (*R40D06-Gal4/+*, and *Lgr3*^{RNAi}). We did not detect any change in the wings dimension for both sexes (**Figure 25B**), and no change in the developmental time (**Figure 25E**).

Here to understand the role of MAT and GAT neurons in controlling growth homeostasis, we suppress *Lgr3* using *R46B11-Gal4* and *R40D06-Gal4*, respectively (**Figure 24** and **Figure 25**). We find that MAT neurons have a sex dimorphic role in controlling wing size (**Figure 24B**), despite no differences in developmental time, and in the control of developmental noise (FA), through the receptor LGR3 (**Figure 24C**). We also show that GAT neurons have a central role in the control of growth homeostasis through the expression of *Lgr3*. GAT cells have high significant FA in both sexes, meaning that their role is not sex-dimorphic, as it seems to be for the MAT cells (**Figure 25C**).

These results highlight the importance of *Lgr3* in the control of growth homeostasis and demonstrate how the lack of *Lgr3* in the MAT or GAT neurons is sufficient to induce FA.

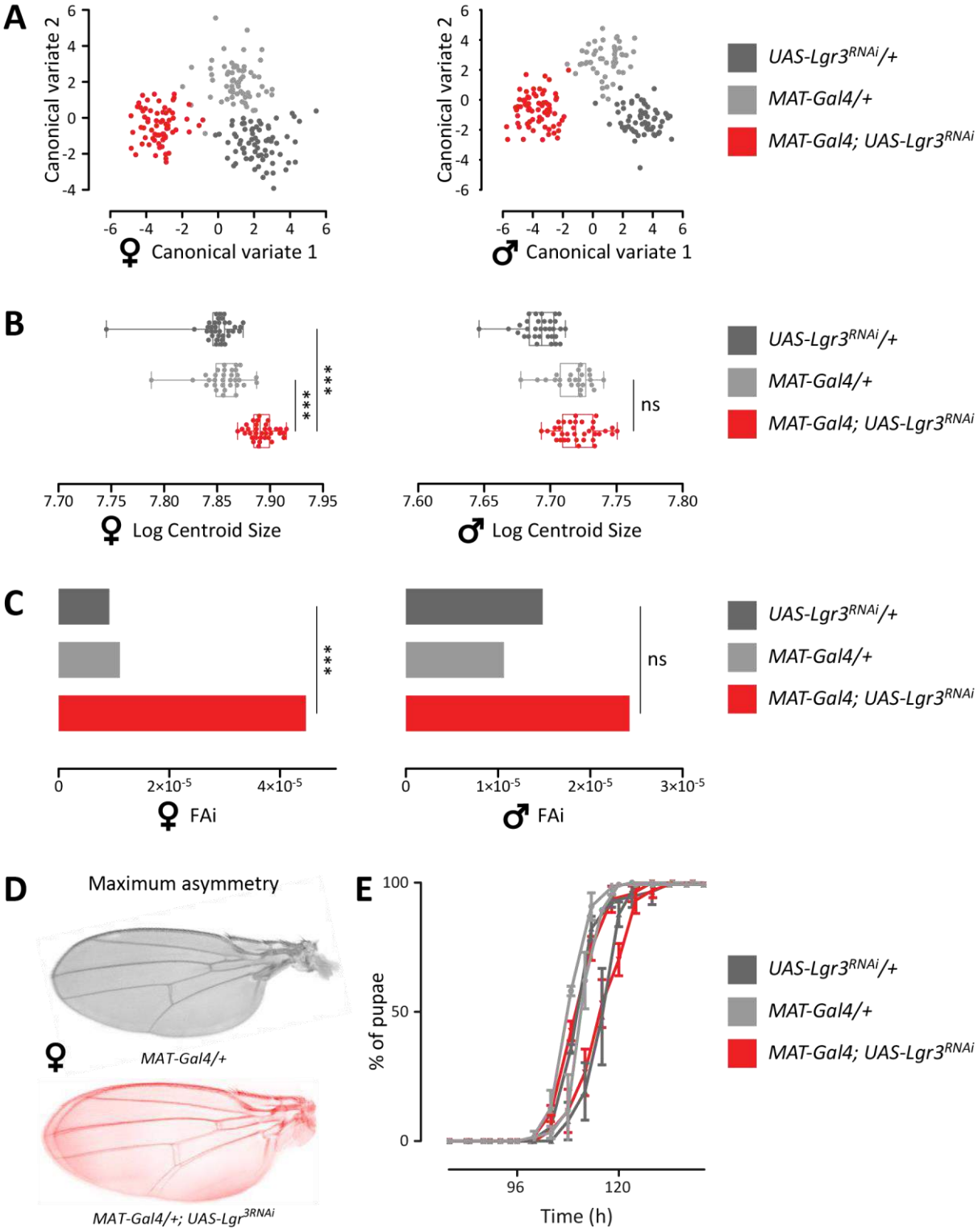

Figure 24. MAT neurons contribute to ensuring developmental stability and body size, not affecting developmental timing.

(**A**) CVA representing the separation of three genotypes in female (left panel) and male flies (right panel). (**B**, left) Increased wings' size of the female flies upon the knock down of *Lgr3* in the MAT neurons. (**B**, Right) No changes in the wings' size in male flies with the silencing of *Lgr3*. (**C**, left) The FA index of female flies. ***P<0.0001 (F test). (**I**, right) FA index in male flies. n.s. (F test). (**D**) Example of FA in control (*MAT-Gal4/+*) and experimental (*MAT-Gal4; UAS-Lgr3^{RNAi}*) female flies. (**E**) The developmental time in unaffected by the silencing of *Lgr3* in the MAT neurons.

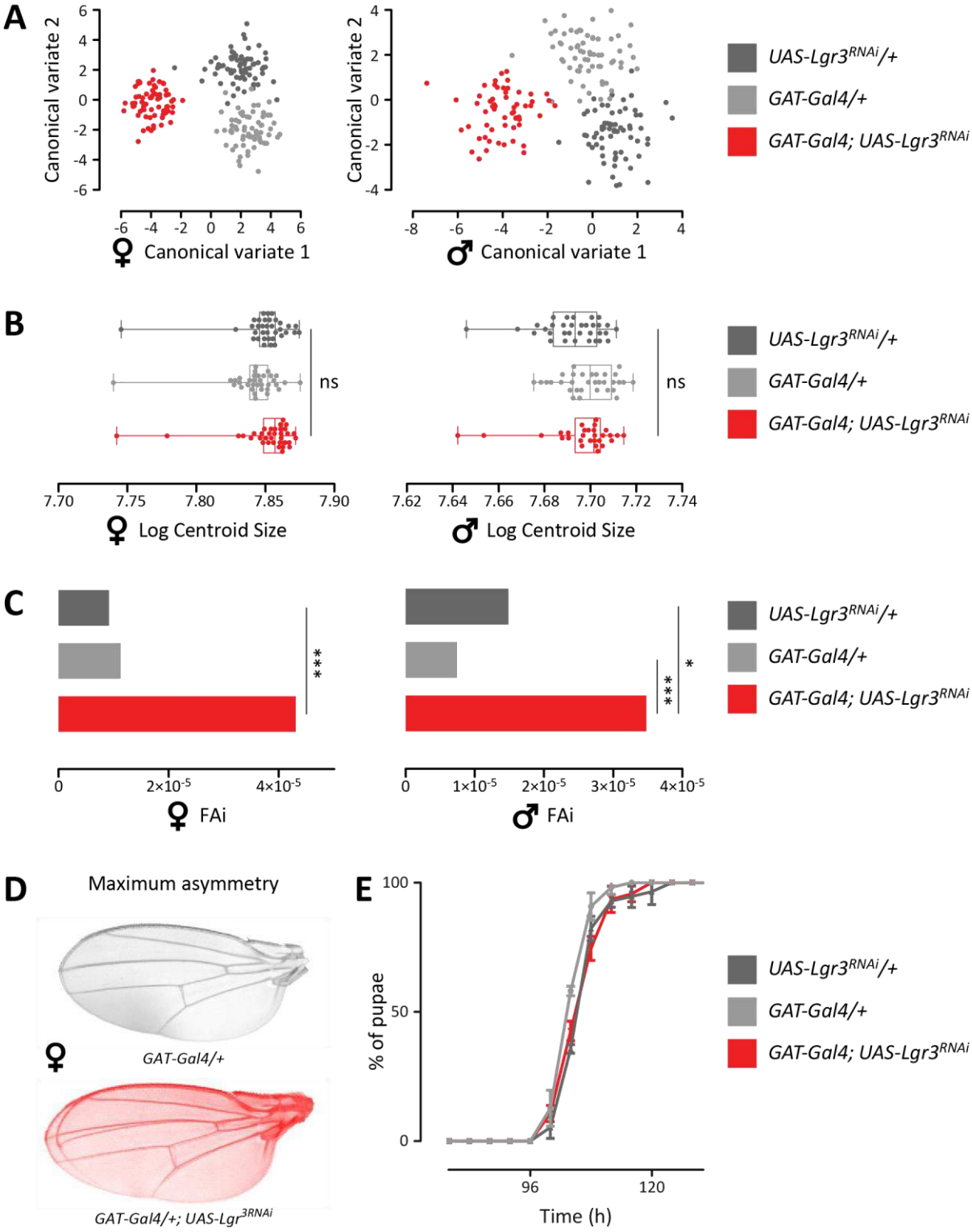

Figure 25. GAT neurons contribute to ensuring developmental stability, not affecting developmental timing.

(**A**) CVA representing the separation of three genotype in female (left panel) and male flies (right panel). (**B**, left) Wings' size of the female flies upon the knock down of *Lgr3* in the MAT neurons. (**B**, right) Wings' size in male flies with the silencing of *Lgr3*. (**C**, left) The FA index of female flies. ***P<0.0001 (F test). (**C**, right) FA index in male flies. *P<0.05. **P<0.001(F test). (**D**) Example of FA in control (*GAT-Gal4/+*) and experimental (*GAT-Gal4; UAS-Lgr3^{RNAi}*) female flies. (**E**) The developmental time in unaffected by the silencing of *Lgr3* in the MAT neurons.

The decoupling of the FA from the developmental timing

An acute damage in an imaginal disc, a tumour, or growing larvae in EMS supplemented food promote high expression of *Ilp8* (Colombani, Andersen and Léopold, 2012; Garelli *et al.*, 2012). These high levels of ILP8 delay the pupariation of *Drosophila melanogaster* larvae, allowing damaged tissues to recover (Garelli *et al.*, 2012; Vallejo *et al.*, 2015). This mechanism is regulated in the central nervous system by LGR3 expressing neurons that interact with both the Insulin producing cells (IPCs) and the Ptth neurons (Colombani *et al.*, 2015; Vallejo *et al.*, 2015). It also seems that the neurons regulating the developmental timing were the same that are regulating the homeostatic growth of the two side of the body (Colombani *et al.*, 2015; Vallejo *et al.*, 2015). However, when we looked at the time to pupariation of the "split brain" flies the developmental delay induced by ILP8 was still present, despite the high levels of FA in these population (**Figure 18E**). This result means two things: 1) The Lgr3 mediated delay is mediated by ipsilateral neurons; 2) The mechanisms of delay and homeostatic growth rely on two different neural population expressing the *Lgr3* gene.

We asked if the MAT and GAT neurons, both regulating the perfect bilateral symmetry of the wings, could also regulate the time to pupariation of flies overexpressing *Ilp8*. We crossed the flies with the MAT neurons labelled (*R46B11-Gal4*) with flies carrying the $Lgr3^{RNAi}$ (*UAS-*$Lgr3^{RNAi}$), and with flies carrying the $Lgr3^{RNAi}$ and the *Tub-Ilp8* transgene (*Tub-Ilp8; UAS-*$Lgr3^{RNAi}$) with all the controls. We conducted this experiment using the flyGear and we set up the recording every 4 hours. We found that the silencing of *Lgr3* in the MAT neurons had no effect on the developmental timing (**Figure 26A**, and **B**). Moreover, MAT neurons did not regulate the delay induced by ILP8, as the time to pupariation between control flies overexpressing *Ilp8 (Tub-Ilp8; UAS-*$Lgr3^{RNAi}$*/+*) is undistinguishable from the flies lacking the receptor (LGR3) in the MAT cells (*Tub-Ilp8; R46B11> UAS-*$Lgr3^{RNAi}$) (**Figure 26A**, and **B**). This result was unexpected, because the MAT neurons are the high ILP8 sensitive *Lgr3* expressing neurons (labelled with *R19B09-Gal4*) (Vallejo *et al.*, 2015).

We decided to conduct the same experiment using the GAT enhancer line (*R40D06-Gal4*). As for the experiment before, we crossed the Gal4 line with the $Lgr3^{RNAi}$ flies (*R40D06 >* $Lgr3^{RNAi}$) and with the line overexpressing *Ilp8* coupled with $Lgr3^{RNAi}$ (*Tub-Ilp8; R40D06> UAS-*$Lgr3^{RNAi}$) with all the controls needed. We found no differences between flies lacking Lgr3 in the GAT neurons from the control flies (**Figure 26C**, and **D**). The GAT neurons are an ipsilateral neural population and, albeit these neurons also express Lgr3, they are not capable to mediating the delay caused by ILP8.

Garelli et al., 2015 showed that the knockdown of *Lgr3* in cholinergic neurons (using *Chat-Gal4.7.4*) rescues the delay in pupariation. We repeated the timing experiment and recapitulated their result (*Tub-Ilp8; ChaT-Gal4.7.4, UAS-GFP.S65T> UAS-*$Lgr3^{RNAi}$ rescued the delay induced by *Tub-Ilp8*, data not

shown). GAT and MAT cells didn't colocalize with the *ChaT-Gal4* enhancer line (**Figure S7B, B'**). Moreover, the use of *ChaT-Gal80* crossed with *R19B09; UAS-CD8::GFP* was not repressing the expression of the CD8::GFP in many *R19B09* labelled neurons (including MAT and GAT) (**Figure S7A**).

The regulation of the developmental timing and the developmental noise are both regulated by Lgr3 (as it is show by using *Elavl-Gal4* and *R19B09-Gal4*). Despite the tight link between these two developmental processes, both the MAT and GAT neural population doesn't rescue the developmental timing induced by *Ilp8* overexpression, suggesting that these two homeostatic mechanisms are regulated by different neuronal populations.

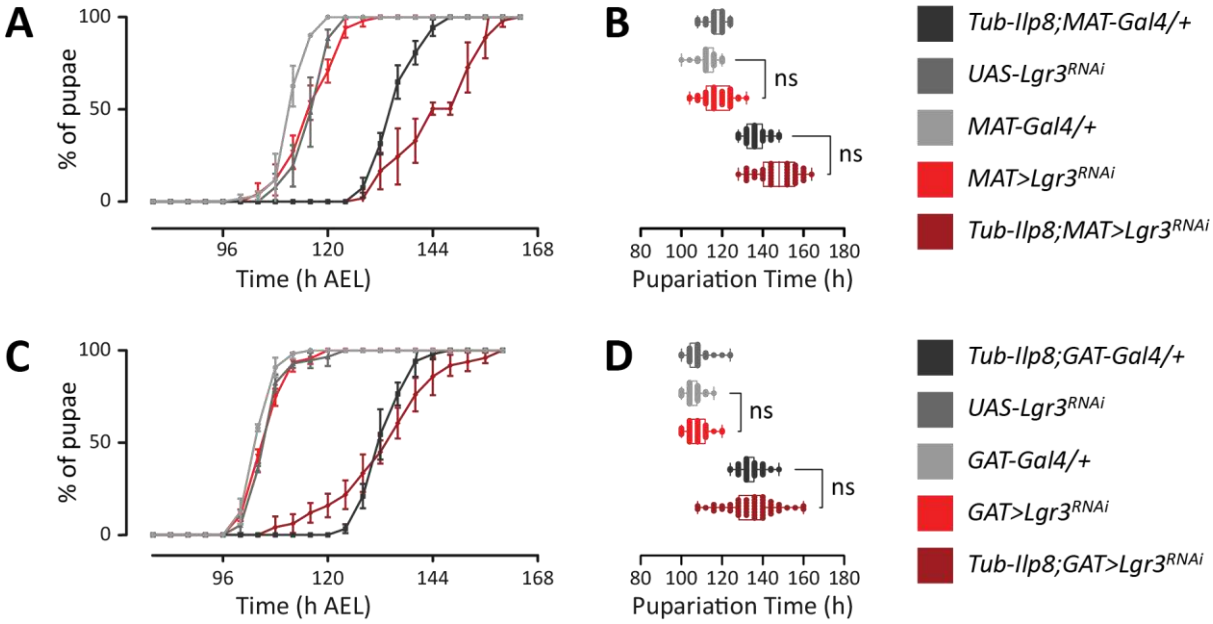

Figure 26. MAT and GAT neurons are not involved in the ILP8-mediated developmental timing/checkpoint.

(**A**) Percentage of puparium formation over time of GAT neurons with *Lgr3* silenced. (**B**) Box blot representing the time to pupariation of GAT neurons with *Lgr3* silenced. (**C**) Percentage of puparium formation over time of MAT neurons with *Lgr3* silenced. (**D**) Box blot representing the time to pupariation of MAT neurons with *Lgr3* silenced. For all the graphs representing the pupariation time in expressed as the percentage of pupae counted every 4h using the last version of flyGear. The number of animals in each genotype is approximately 60. Each data point represents the mean of three biological replicate, and the bars represent the ±SD (Standard Deviation).

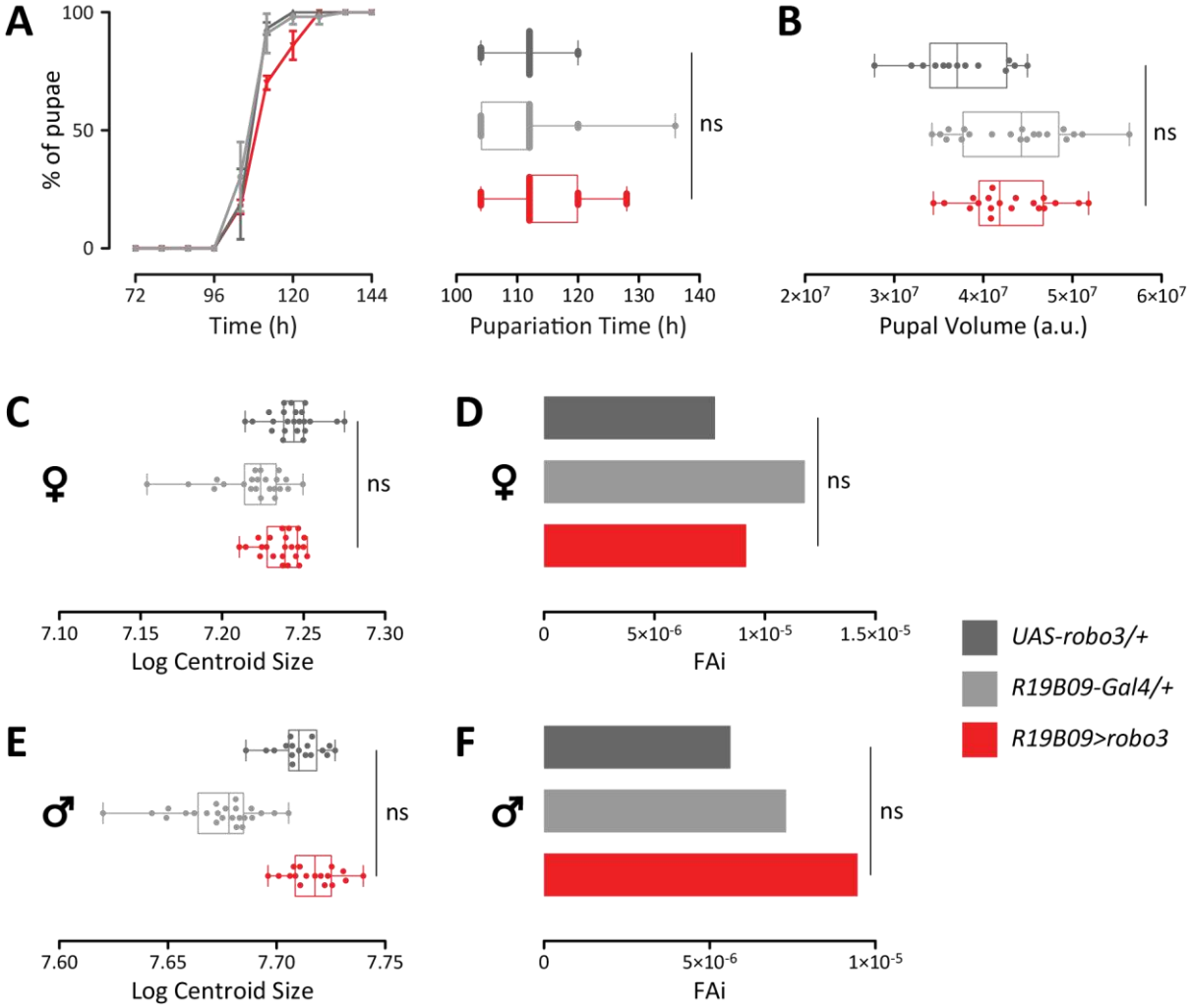

Figure S 1. The overexpression of *robo3* had no effect in developmental instability.

(**A**) The overexpression of *robo3* did not change the developmental time (**B**) pupal volume is unaffected by the overexpression of *robo3* (**C**) Unchanged wings size of the male flies (**D**) Centroid size FA of the males (**E**) Unchanged wings 'size of the females (**F**) Centroid size FA of the female flies. For all the graphs representing the pupariation time in expressed as the percentage of pupae counted every 8h. The number of animals in each genotype is approximately 60. Each data point represents the mean of three biological replicate, and the bars represent the ±SD (Standard Deviation); The statistical test used was the Kruskal-Wallis's test. For fluctuating asymmetry analysis, the numbers of animals tested for each sex was from 20 to 30.

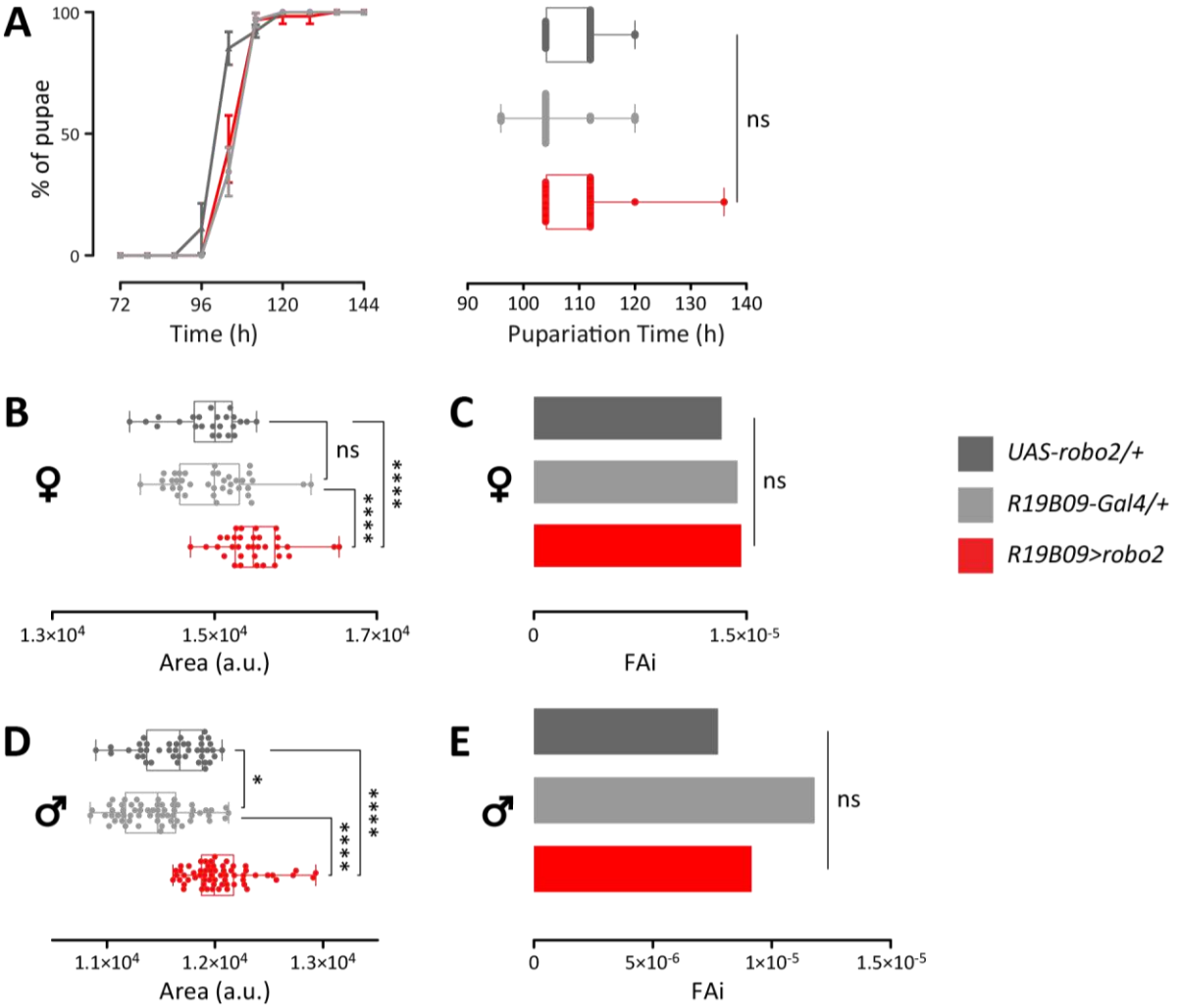

Figure S 2. Robo2 overexpression increases wings 'size.

(**A**) The overexpression of *robo*2 did not alter the developmental time (**B**) Increased wings area of the females. (**C**) The Fluctuating asymmetry is unchanged in females. (**D**) Increased wings area of the males. (**E**) The fluctuating asymmetry of males is unaffected. For all the graphs representing the pupariation time in expressed as the percentage of pupae counted every 8h. The number of animals in each genotype is approximately 60. Each data point represents the mean of three biological replicate, and the bars represent the ±SD (Standard Deviation); The statistical test used was the Kruskal-Wallis's test. For fluctuating asymmetry analysis, the numbers of animals tested for each sex is from 20 to 30.

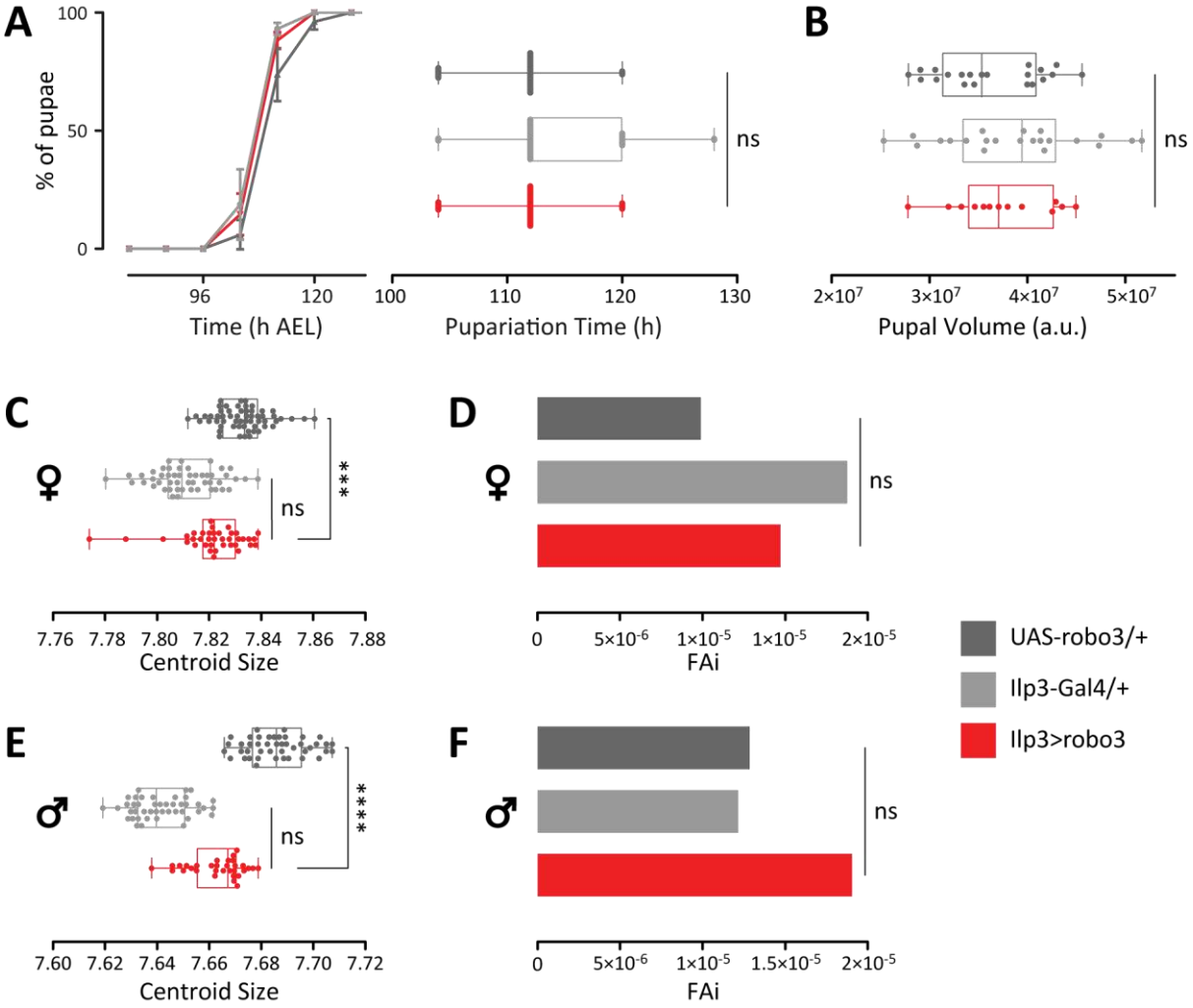

Figure S 3. robo3 overexpression in the insulin producing cells.

(**A**) The overexpression of *robo3* did not change the developmental time (**B**) pupal volume is unaffected by the overexpression of *robo3* (**C**) Unchanged wings size of the male flies (**D**) Centroid size FA of the males (**E**) Unchanged wings 'size of the females (**F**) Centroid size FA of the female flies. For all the graphs representing the pupariation time in expressed as the percentage of pupae counted every 8h. The number of animals in each genotype is approximately 60. Each data point represents the mean of three biological replicate, and the bars represent the ±SD (Standard Deviation); The statistical test used was the Kruskal-Wallis's test. For fluctuating asymmetry analysis, the numbers of animals tested for each sex is from 20 to 30.

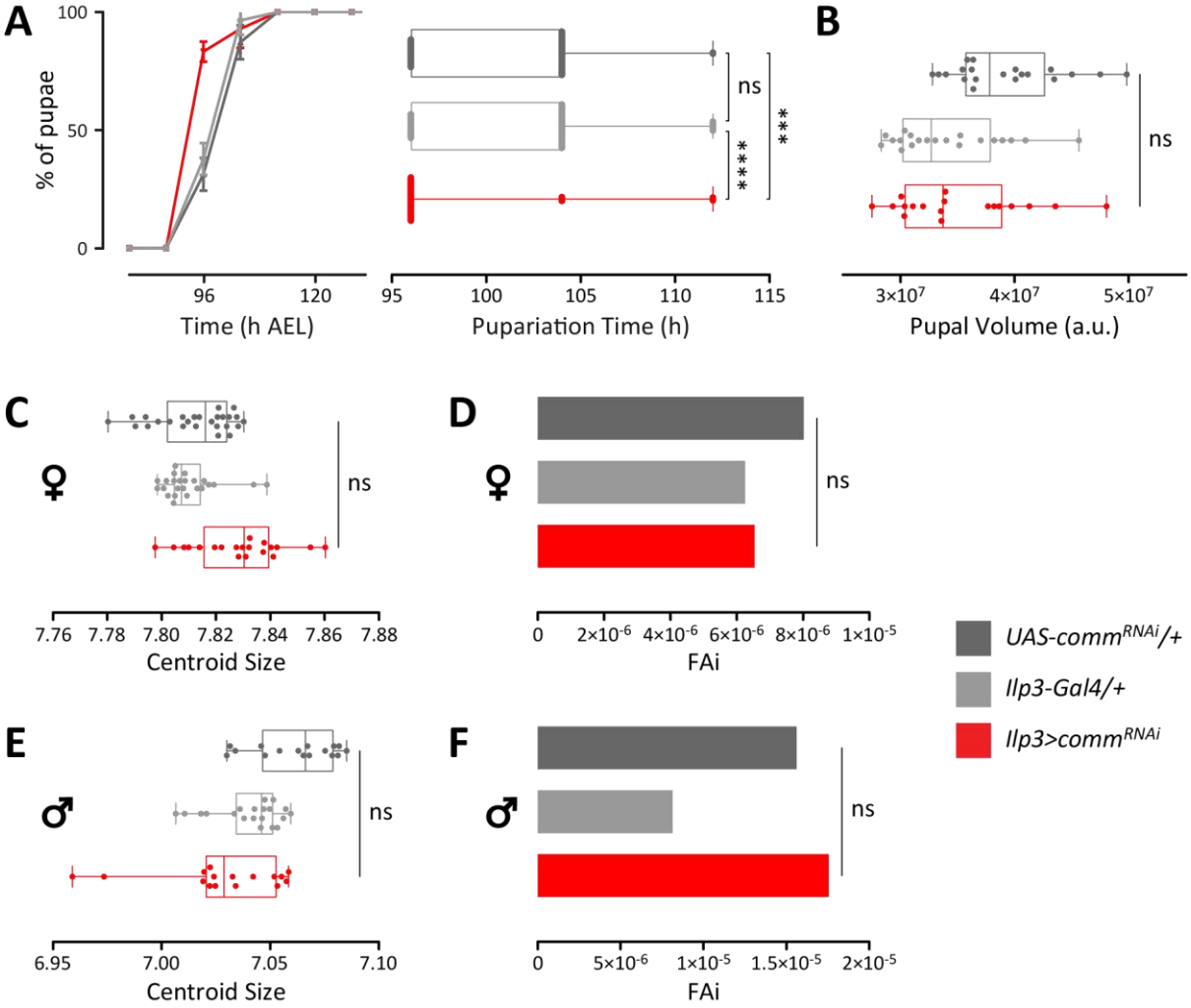

Figure S 4. The knock down of *commissureless* in the insulin producing cells.

(**A**) The knock down of *commissureless* significatively decreased the developmental time (**** p<0.0001). (**B**) pupal 'volume is unaffected by the silencing of *commissureless* (**C**) Wings 'size in females flies (**D**) Fluctuating asymmetry in females (**E**) Wings 'size in males flies (**F**) Fluctuating Asymmetry in males' flies. For all the graphs representing the pupariation time in expressed as the percentage of pupae counted every 8h. The number of animals in each genotype is approximately 60. Each data point represents the mean of three biological replicate, and the bars represent the ±SD (Standard Deviation); The statistical test used was the Kruskal-Wallis's test. For fluctuating asymmetry analysis, the numbers of animals tested for each sex is from 20 to 30.

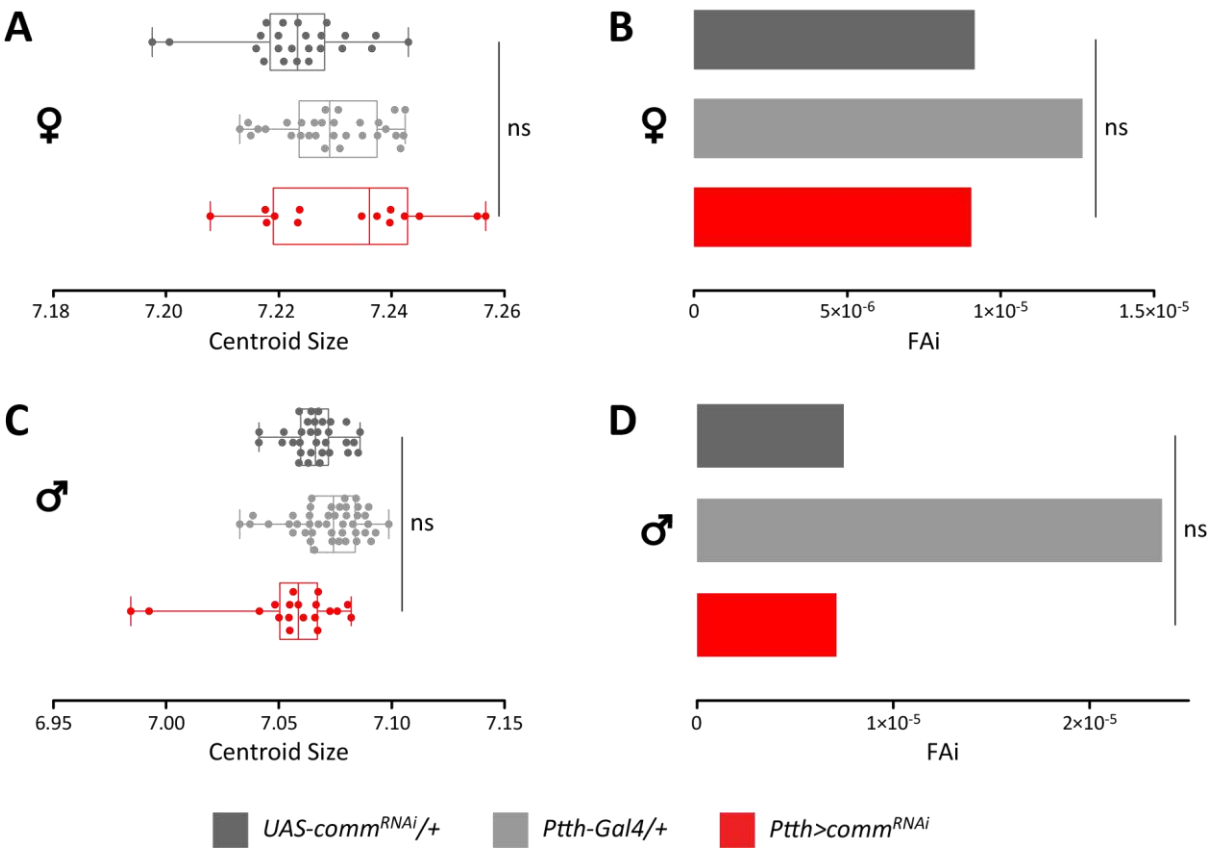

Figure S 5. Silencing of *commissureless* in Ptth neurons.

(**A**) Wings 'size in females flies (**B**) Fluctuating asymmetry in females (**C**) Wings 'size in males flies (**D**) Fluctuating Asymmetry in males' flies. For fluctuating asymmetry analysis, the numbers of animals tested for each sex is from 20 to 30.

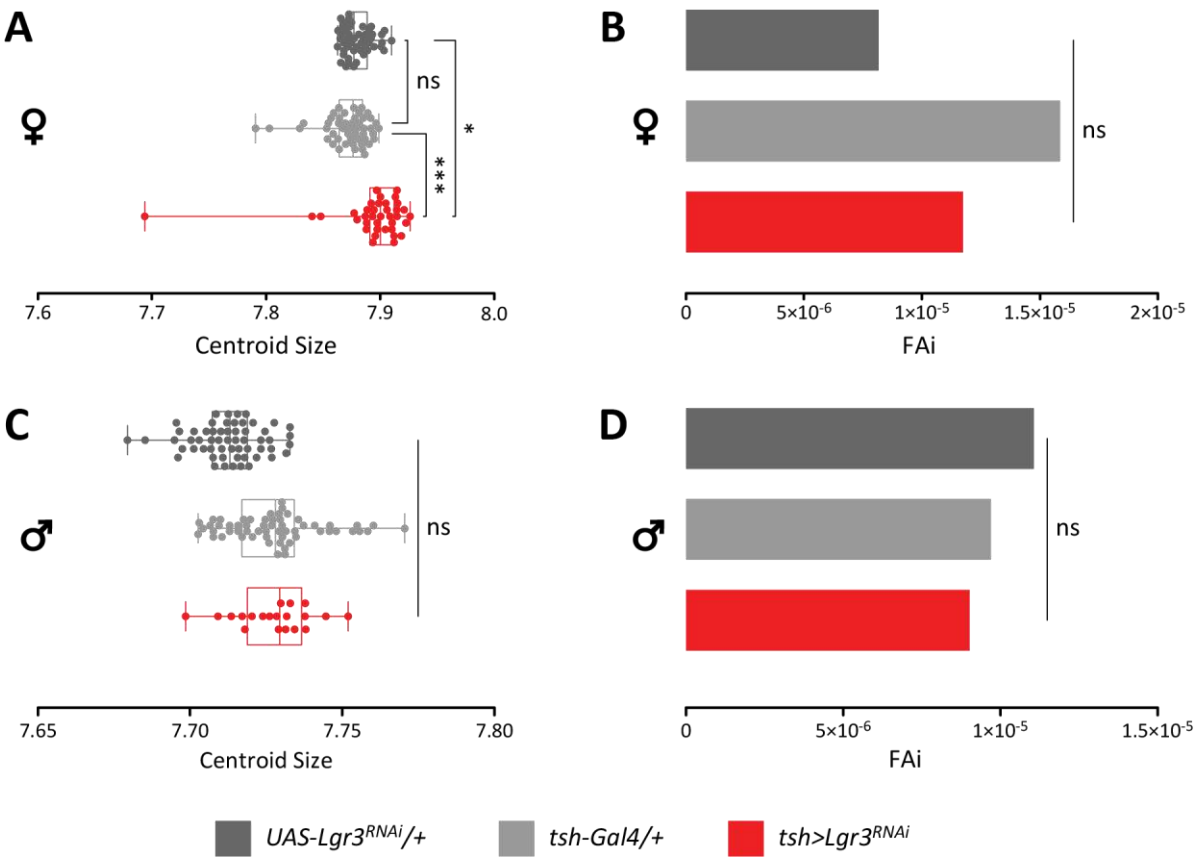

Figure S 6. Silencing of Lgr3 in the ventral nerve cord neurons.

(**A**) Slightly increase in wings' size in female flies lacking *Lgr3* in the VNC (**B**) Fluctuating asymmetry in females (**C**) Wings size in males' flies (**D**) Fluctuating Asymmetry in males' flies. For fluctuating asymmetry analysis, the numbers of animals tested for each sex is from 20 to 30.

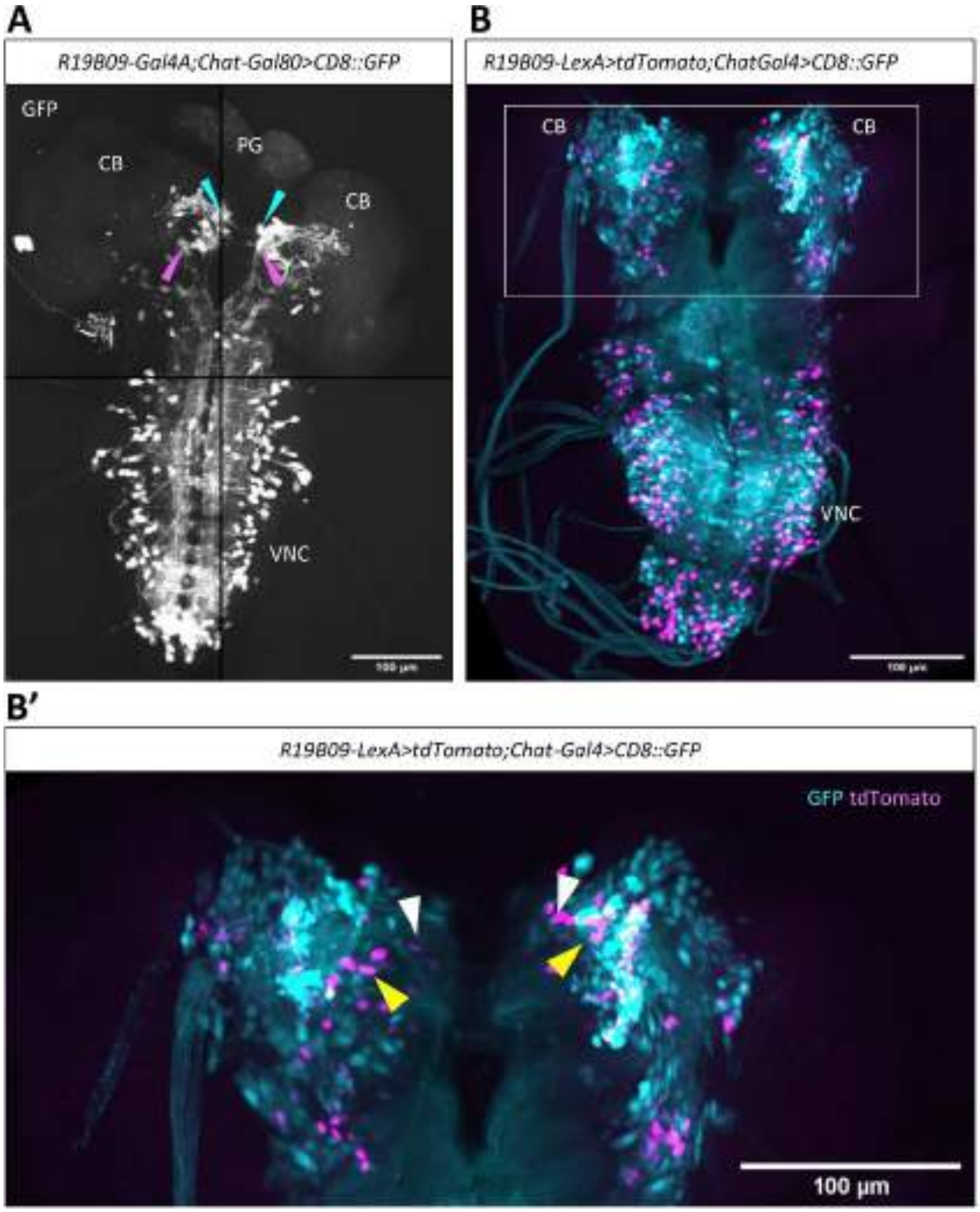

Figure S 7. MAT and GAT neurons are not cholinergic.

(**A**) *ChaT-Gal80* did not repress the GFP expression of *R19B09* neurons. Cyan arrowheads indicate the cell bodies of MAT neurons, and magenta arrowheads indicate the cell bodies of GAT neurons. (**B** and **B'**) Few cells colocalized between R19B09-LeA and Chat-Gal4. Note that the MAT (white arrowheads) and GAT neurons (yellow arrowheads) were in the medial protocerebrum and did not colocalize with neurons where the expression of CD8::GFP was induced.

Discussion

flyGear

The flyGear prototype

We are working with engineers to develop a prototype to commercialize and implement the software analysis using Artificial Intelligence (AI). Our mission is that flyGear becomes the standard of counting larvae and pupae for developmental timing experiments. We have extensively validated flyGear robot in the laboratory, and data obtained using flyGear or manually is included in this thesis work in other sections.

We have recently obtained a public and competitive grant from the *Generalitat Valenciana* to start producing a prototype to market flyGear as a small laboratory robot and also produce a larger version (100 tubes or more) for CRO (Contract Research Organizations) and start-up companies interested in preclinical trials using the *Drosophila melanogaster*. We are now collaborating with an enterprise of the *Comunidad Valenciana* to complete the final prototype in such a way that will be aesthetically attractive for the beta testers, and fully functional.

Competitors

Several possible solutions for development time automation has been reported (Schumann and Triphan, 2020b; Seong *et al.*, 2020b; Memeo *et al.*, 2021). None of the solutions reach exactness and precision of the manual scoring, and scaling the number of animals is either not possible (Schumann and Triphan, 2020b; Memeo *et al.*, 2021) or expensive (Seong *et al.*, 2020b). For example, the Ki-Hyeon Seong et al. (2020) solution uses 96-well microplates inserted into a scanner (Seong *et al.*, 2020b) and scaling involves buying more scanners — which has an estimated cost (according to the authors' specifications) of around 14.000 €. We compare the two best solutions with the flyGear solution. Both PEDtracker (an automatic staging approach for *Drosophila melanogaster* larvae) (Schumann and Triphan, 2020b) and DIAMonDS (the *Drosophila* Individual Activity Monitoring and Detection System) (Seong *et al.*, 2020b) use single-use disposable plastic microplates. In both solutions, the researchers must place the embryos manually in each well, which is tedious, time-consuming, and can perturb the embryos.

The PEDtracker (Schumann and Triphan, 2020b) uses a tracking system based on an earlier device, the LarvaLodge (Szuperak *et al.*, 2018), in which individual larvae are monitored over time. Another pain that creates the PEDtracker setup is that, unlike manual work, this automated device can only monitor up to 20 larvae simultaneously for several hours, which is insufficient for most routine developmental timing experiments. More importantly, the well-size is too small to ensure smooth and healthy development. This problem is so far insurmountable in this configuration. The food dries up, causing starvation of the larvae, which negatively impacts development time (Beadle, Tatum and Clancy, 1938; Bakker, 1959; Ormerod *et al.*, 2017; Juarez-Carreño *et al.*, 2021). They also have the problem of

humidity that causes, on the one hand, the appearance of mould and, on the other, the fogging of the glass that covers the plate that houses the larvae, which occludes the video image, causing the system to fail in animal tracking. These important limitations are reflected in the Tables in the article (Schumann and Triphan, 2020b). In addition, a 14-day experiment generates about 60,480 images with this system, which hints at a potential problem for complex experiments. Lastly, the processing uses ImageJ and manual analysis implemented with R in RStudio.

DIAMonDS setup (Seong *et al.*, 2020b) is superior to PedTracker, but has also important limitations. The DIAMonDS configuration uses single-image processing between continuous images to distinguish animals' active phases (e.g., larvae) from stationary phases (e.g., egg, pupae). The system infers not identify the transition points. Like PEDtracker, DIAMonDS configurations require that a single egg or a young larva is placed manually into each well of a 96- or 384-well microplate containing suitable fly media. The scalability of DIAMonDS is costly, and the equipment occupies a large space. A single scan harbours only three microplates and can simultaneously measure only ≤288 flies and 1-3 experimental conditions. The flyGear setup can simultaneously monitor 20 experimental conditions or genotypes and ≤2000 flies per flyGear. The flyGear robot uses standard fly tubes that researchers typically use to rear larvae and flies and has the potential to reduce carbon emissions and plastic waste (see the economic and environmental impact) by using reusable glass tubes, fully compatible with our robot. Thus, our solution is more environmentally sustainable. The flyGear is fully automatised, unlike the other solutions. Moreover, in flyGear, the animals are housed in tubes (4 mm diameter) with 2-3 ml of food.

Thus, flyGear does not have the moisture-related mould and food drying problems of the PEDtracker and DIAMonDS configurations. In addition, flyGear exactly reproduce the manual task and increases accuracy because it can score at shorter intervals (defined by the users) and can increase reproducibility between laboratories, whether they use automatic or manual measurement. The flyGear permits high control of external variables to perform equally or better than the manual task.

The neural substrates and circuitry logic for body symmetry-assurance

The temporal requirement for Ilp8 in keeping left-right body symmetry

Using well-controlled temporal silencing of *Ilp8* genes using a validated RNAi, we discovered that *Ilp8* is required across the larval stages to assure perfect body symmetry. Because the adult structures like the wing grow extensively throughout the larval period, these data support a model of continuous monitoring of growth and variation by the brain Ilp8-Lgr3 system. This model is further supported by our findings that constitutive activation of Lgr3 neurons in the *R19B09* ensemble via the TRPA1 tempo-sensitive allele is sufficient to cause increased fluctuating asymmetry in the resulting adult flies. Furthermore, our ex vivo brain calcium imaging indicates that Lgr3 neurons are highly responsive to stimulation by ILP8 and that genetic manipulation of Lgr3 commissures affects larval Lgr3 neuronal calcium spiking and responses.

Nonetheless, we detected a modest increase in left-right body asymmetry when *Ilp8* was only suppressed during the pupal stages. However, this fluctuating asymmetry level is not statistically significant and could result from genetic background or the effect of temperature.

Our data also indicate that the neuronal substrate for body symmetry and the developmental time checkpoint in response to injury and tumours are distinct. Moreover, the *Ilp8*-mediated checkpoint for body growth and symmetry in pupae by the group of Gontijo involves neurons different from those identified in this thesis as the core neurons in LR symmetry (Heredia *et al.*, 2021). Our data do not support checkpoint control of body symmetry, and neurons driven by the enhancer *R18A01-GAL4* of Gontijo do not respond to ILp8 stimulation (Vallejo et al., 2015). Therefore, while Ilp8 has different roles and responses during physiological growth and response to pupal programmes, body symmetry requires continuous larval Ilp8.

We have yet to know the reason for the discrepancy in the results of Leopold and us with temperate-sensitive Gal80 in (Boulan *et al.*, 2020, p. 8). Moreover, the version of the same article published in 2022 uses a light-sensitive Gal4, raising questions about how the light could affect feeding larvae (Blanco-Obregon *et al.*, 2022).

However, we use geometric morphometric analyses, which are informative about the shape of the wings. We found that the larvae lacking *Ilp8* during the larval periods can be distinguished from the control wings, supporting the role of *Ilp8* during larval growth. Another possible problem is that it needs to be clarified whether these authors adjust development time to temperature and how they do it. Ultimately, there are differences in the experimental methods used to silence *Ilp8*.

Left-Right lgr3 neurons communication during larval development

Here we show that most Lgr3 neurons have contralateral projections—both the neurons in the CB and those in VNC.

We found that interfering with the growth of the Lgr3 neurons has a huge effect on developmental stability. The resulting adults presented high FA and interindividual variability. This high FA means that the Lgr3 neurons must share information between the two hemispheres during growth to maintain the right proportions and symmetry. Few studies have investigated this aspect of development so far. However, a recent paper found that, in the axolotl, the nerves connected to the CNS control limb regeneration and its final size (Wells *et al.*, 2021).

We found that among the genes tested, only *comm* has a role in controlling developmental stability. We found that the silencing of *comm* prevents many of the bilateral connections, delays the pupariation, reduces the wings size, and induces FA. These effects were specific to the neuronal population that expresses *Lgr3* and not in other populations essential for growth control (IPC, Ptth neurons). Recent findings from single-cell sequencing support these results: a cluster of peptidergic neurons there is the expression of *Lgr3* and *comm* (Corrales *et al.*, 2022).

We found that GAT neurons had uncontrolled oscillations in the “split-brain” phenotype. The lack of contralateral projections also affected the GAT neurons' activity. It could be that contralateral inhibitory Lgr3+ neurons are tightly controlling their activity. This lack of coordination between the left-right GAT neurons is similar to what happens in mammals upon the destruction of the contralateral inhibitory interneurons of the central pattern generator (Lanuza *et al.*, 2004).

We mimic the uncontrolled activity seen in “split-brain” flies by forcing the activation of the Lgr3+ neurons. This continuous activation of Lgr3 neurons (*R19B09>UAS-TRPA1* at 29°C) increases developmental instability.

These experiments suggest that the Lgr3 neurons must communicate between the two hemispheres to maintain the left-right symmetry during larval development.

The minimal FA circuit

It was previously described that the circuit implies the symmetrical homeostatic growth was regulated by a pair of neurons in the central brain with the enhancer line *R19B09*. However, this enhancer line has more than 200 neurons, which makes it difficult the identification of the correct morphology of the neurons causing the FA phenotype. Therefore, we decided to investigate neuronal morphologies by labelling single neurons of the neuronal ensemble. Then we conducted a manual investigation, coupled with intersectional genetics, to find unequivocally new enhancer lines that restrict the numbers of affected neurons.

Most sensory neurons send inputs in the SEZ, where the MAT and GAT cells have the diffuse ventral dendrites, and they directly synapse in the dorsomedial protocerebrum, part of the central neuroendocrine system in *Drosophila* (Hückesfeld *et al.*, 2021). This anatomical localization, with dendrites in the SEZ and synapses in the basomedial protocerebrum, suggests that sensory inputs could modulate the response of these second-order interneurons to pass this information to the endocrine system.

Given the functional anatomy of MAT and GAT cells, their presence in the *R19B09* ensemble, and their calcium properties, these cells may play central in the regulation of larval growth. These results highlight the importance of *Lgr3* in controlling growth homeostasis and demonstrate how the lack of *Lgr3* in the MAT and GAT neurons is sufficient to induce FA.

Single-cell sequencing identified a cluster of possible “homeostatic growth” neurons

The single-cell sequencing analysis of the larval CNS (Corrales *et al.*, 2022) found that in the cluster of putative peptidergic CNS neurons (supplementary spreadsheet 2, cluster “64 Pept N”), there is an enrichment of *Lgr3*, *comm*, *tsh*, *Xrp1*, and *Dll*. All these genes we found have some roles in the Lgr3 neural ensemble. We showed how *comm* regulates the developmental stability. We showed how *comm* regulates developmental stability. We also saw how the knock-down of *Lgr3* in VNC (using *tsh-Gal4*) influences the final wings size of female flies. In the GAT line *R35E04-Gal4*, the enhancer fragment “*R35E04*” is part of the *Dll* locus. ILP8 regulates the transcription factor XRP1 (Boulan *et al.*, 2019). Interestingly, all these genes, except *tsh* (enriched in another cluster with *Lgr3*), are enriched in the same cluster of 104 cells. Although the functional significance of this cluster is unknown, based on the observation in this thesis, we suppose it could be the cluster regulating the developmental stability during the development of the adult fruit fly. However, further studies are needed to confirm this hypothesis.

Distinct neural substrates for ecdysone-mediated developmental timing and stability

R19B09 enhancer line mediated the effect of developmental stability and the effect of the developmental timing. Few other enhancer lines can mediate the developmental timing through Lgr3. Garelli et al. (2015) showed that the removal of Lgr3 in cholinergic neurons (using *ChaT-Gal4.7.4*) rescues the EMS-induced delay. We also demonstrated that this enhancer of cholinergic neurons mediates the delay induced by *Tub-Ilp8* when *Lgr3* is downregulated in these neurons (data not shown).

Careful dissection of this enhancer line allows us to find Gal4 line for neurons that are a subset of the Lgr3 expressing neurons. One of this line, the *R46B11-Gal4*, labels the MAT neurons, which were defined the core neurons for both mechanisms. However, our experiments showed that these neurons regulate the developmental stability, but they do not regulate the developmental timing. Another enhancer line, the *R40D06-Gal4*, which labels the GAT neurons, an ipsilateral Lgr3 neurons population, is also important for developmental stability, but not for the developmental time.

Moreover, the fact that MAT and GAT neurons are not shared with the *ChaT* enhancer lines is another proof that these cellular populations are not involved in the control of developmental timing (**Figure S7**).

These two neuronal population, MAT and GAT, received inputs from sensory neurons. It is possible that, the neurons regulating the developmental delay are neurons that do not have dendrites reaching the SEZ, and that are other neurons of the dorsomedial protocerebrum.

Conclusions

flyGear

1. We developed an automation solution for developmental timing and more.
2. Two levels of automation and two choices of image analysis — a simple available choice is the rollout of the tubes. The second chois is the use of a workflow for segmenting the videos and extracts meaningful information. The workflow can be further implemented with machine learning by working with Python.
3. An illustrative experiment with flyGear shows that this robot can precisely track the wandering stage and the pupariation every twenty minutes. As far as we know, this is the first time that a tracking records this two behaviours with a short time window.
4. The innovation was protected with an international patent recognised in 156 states.
5. The flyGear is fully operational and has been used for various experiments of this thesis and others not presented here.
6. We completed an acceleration course from the CSIC called Dinamiza for entrepreneurs to accelerate the transference of innovation to the market.
7. Our flyGear project has been selected for a two-year mentoring course "COMTE-Innovation 2022-2023, from Foundation CSIC to help in the different steps to bring innovation to the market.
8. We won several public grants (total of 180.000€) to produce a manufacturable flyGear and to develop new applications to broaden the potential market.

The neural substrates and circuitry logic for body symmetry-assurance

1. Sensing the Ilp8 hormone by Lgr3 neurons is continuously required from L1 to late L3 to keep bilateral symmetry.
2. Left-right communication via Lgr3 commissural interneurons (CIN) is essential for maintaining perfect bilateral symmetry.
3. The neurons mediating bilateral symmetry are not the same ones mediating the ILP8 checkpoint in response to acute injuries or tumours.
4. The circuit for developmental timing involves cholinergic neurons and does not require CINs or interhemispheric communication.
5. Bilateral symmetry is controlled by MAT (two pairs) and GAT neurons.
6. Gal4 lines *R40D06*, and *R46B11* drive expression in the MAT and GAT neurons, respectively.
7. MAT neurons respond symmetrically to ILP8 peptide, producing synchronous calcium spikes.
8. GAT neurons respond to ILP8 peptide with a delay and asymmetrically.
9. Inhibitory CINs tonically inhibit GAT neurons, enabling asymmetric response to ILP8 peptide.
10. The asymmetric response is hard-wired, as observed in ex vivo brains without sensory input.
11. GAT and MAT neurons provide novel insights into further inputs for sensing and correcting bilateral symmetry.

Conclusiones

FlyGear

1. Hemos desarrollado una solución de automatización para estudiar el desarrollo y otros procesos.
2. Existen dos niveles de automatización y dos opciones de análisis de imágenes — la opción más simple disponible es el despliegue de los tubos. La segunda posibilidad se basa en segmentar los videos y extraer información significativa. Se pueden implementar nuevas funciones con el aprendizaje automático trabajando con Python.
3. Un experimento ilustrativo con flyGear muestra que este robot puede hacer un seguimiento preciso de la etapa de wandering y de pupa. Hasta donde sabemos, esta es la primera vez que un sistema de seguimiento registra estos dos comportamientos en un período de tiempo corto.
4. La innovación fue protegida con una patente internacional reconocida en 156 estados.
5. El flyGear está en pleno funcionamiento y se ha utilizado para varios experimentos de esta tesis y otros que no se presentan aquí.
6. Hemos realizado un curso de aceleración del CSIC llamado Dinamiza para emprendedores con el fin de acelerar la transferencia de innovación al mercado.
7. Nuestro proyecto flyGear ha sido seleccionado para un curso de mentoring de dos años, "COMTE-Innovación 2022-2023", de la Fundación CSIC para ayudar en los diferentes pasos y poder llevar la innovación al mercado.
8. Hemos ganado varias subvenciones públicas (un total de 180.000 €) para producir un flyGear fabricable y desarrollar nuevas aplicaciones para ampliar el mercado potencial.

Los sustratos neuronales y la lógica de los circuitos para la garantía de la simetría corporal

1. La detección de la hormona Ilp8 por parte de las neuronas Lgr3 se requiere continuamente desde L1 hasta finales de L3 para mantener la simetría bilateral.
2. La comunicación izquierda-derecha a través de las interneuronas comisurales Lgr3 (CIN) es esencial para mantener una simetría bilateral perfecta.
3. Las neuronas que median la simetría bilateral no son las mismas que median el punto de control mediado por ILP8 en respuesta a lesiones o tumores agudos.
4. El circuito para la sincronización del desarrollo involucra neuronas colinérgicas y no requiere CIN o comunicación interhemisférica.
5. La simetría bilateral está controlada por neuronas MAT (dos pares) y GAT.
6. Las líneas Gal4 R40D06 y R46B11 impulsan la expresión en las neuronas MAT y GAT, respectivamente.
7. Las neuronas MAT responden simétricamente al péptido ILP8, produciendo picos de calcio sincrónicos.
8. Las neuronas GAT responden al péptido ILP8 con retraso y asimétricamente.
9. Las CIN inhibitorias inhiben tónicamente las neuronas GAT, lo que permite una respuesta asimétrica al péptido ILP8.
10. La respuesta asimétrica está programada, como se observa en cerebros ex vivo sin entrada sensorial.
11. Las neuronas GAT y MAT brindan conocimientos novedosos sobre otras entradas para detectar y corregir la simetría bilateral.

References

Abreu, A.P. and Kaiser, P.U.B. (2016) 'Pubertal development and regulation', *The lancet. Diabetes & endocrinology*, 4(3), p. 254. Available at: https://doi.org/10.1016/S2213-8587(15)00418-0.

Aggarwal, A., Reichert, H. and VijayRaghavan, K. (2019) 'A locomotor assay reveals deficits in heterozygous Parkinson's disease model and proprioceptive mutants in adult Drosophila', *Proceedings of the National Academy of Sciences*, 116(49), pp. 24830–24839. Available at: https://doi.org/10.1073/pnas.1807456116.

Alpatov, W.W. (1929) 'Growth and variation of the larvae of Drosophila melanogaster', *Journal of Experimental Zoology*, 52(3), pp. 407–437. Available at: https://doi.org/10.1002/jez.1400520303.

Alpatov, W.W. (1930) 'Growth of larvae in wild Drosophila melanogaster and its mutant vestigial', *Journal of Experimental Zoology*, 56(1), pp. 63–71. Available at: https://doi.org/10.1002/jez.1400560104.

Bakker, K. (1959) 'Feeding Period, Growth, and Pupation in Larvae Ofdrosophila Melanogaster', *Entomologia Experimentalis et Applicata*, 2(3), pp. 171–186. Available at: https://doi.org/10.1111/j.1570-7458.1959.tb00432.x.

Bangi, E. *et al.* (2019) 'A personalized platform identifies trametinib plus zoledronate for a patient with KRAS-mutant metastatic colorectal cancer', *Science Advances* [Preprint]. Available at: https://doi.org/10.1126/sciadv.aav6528.

Baron, J. *et al.* (1994) 'Catch-up growth after glucocorticoid excess: a mechanism intrinsic to the growth plate', *Endocrinology*, 135(4), pp. 1367–1371. Available at: https://doi.org/10.1210/en.135.4.1367.

Barredo, C.G. *et al.* (2021) 'Timing the Juvenile-Adult Neurohormonal Transition: Functions and Evolution', *Frontiers in Endocrinology*, 11. Available at: https://www.frontiersin.org/article/10.3389/fendo.2020.602285 (Accessed: 21 January 2022).

Beadle, G.W., Tatum, E.L. and Clancy, C.W. (1938) 'Food level in relation to rate of development and eye pigmentation in drosophila melanogaster', *The Biological Bulletin*, 75(3), pp. 447–462. Available at: https://doi.org/10.2307/1537573.

Blanco-Obregon, D. *et al.* (2022) 'A Dilp8-dependent time window ensures tissue size adjustment in Drosophila', *Nature Communications*, 13(1), p. 5629. Available at: https://doi.org/10.1038/s41467-022-33387-6.

Boone, E. *et al.* (2016) 'The Hippo signalling pathway coordinates organ growth and limits developmental variability by controlling dilp8 expression', *Nature Communications*, 7(1), p. 13505. Available at: https://doi.org/10.1038/ncomms13505.

Boulan, L. *et al.* (2019) 'Inter-Organ Growth Coordination Is Mediated by the Xrp1-Dilp8 Axis in Drosophila', *Developmental Cell*, 49(5), pp. 811-818.e4. Available at: https://doi.org/10.1016/j.devcel.2019.03.016.

Boulan, L. *et al.* (2020) 'Dilp8 controls a time window for tissue size adjustment in Drosophila'. bioRxiv, p. 2020.11.09.375063. Available at: https://doi.org/10.1101/2020.11.09.375063.

Brogiolo, W. *et al.* (2001) 'An evolutionarily conserved function of the Drosophila insulin receptor and insulin-like peptides in growth control', *Current Biology*, 11(4), pp. 213–221. Available at: https://doi.org/10.1016/S0960-9822(01)00068-9.

Bryant, P.J. and Levinson, P. (1985) 'Intrinsic growth control in the imaginal primordia of Drosophila, and the autonomous action of a lethal mutation causing overgrowth', *Developmental Biology*, 107(2), pp. 355–363. Available at: https://doi.org/10.1016/0012-1606(85)90317-3.

Buhler, K. *et al.* (2018) 'Growth control through regulation of insulin signalling by nutrition-activated steroid hormone in Drosophila', *Development*, 145(21), p. dev165654. Available at: https://doi.org/10.1242/dev.165654.

Cann, M.J., Chung, E. and Levin, L.R. (2000) 'A new family of adenylyl cyclase genes in the male germline of Drosophila melanogaster', *Development Genes and Evolution*, 210(4), pp. 200–206. Available at: https://doi.org/10.1007/s004270050304.

Cao, W. *et al.* (2017) 'An Automated Rapid Iterative Negative Geotaxis Assay for Analyzing Adult Climbing Behavior in a Drosophila Model of Neurodegeneration', *JoVE (Journal of Visualized Experiments)*, (127), p. e56507. Available at: https://doi.org/10.3791/56507.

Cárdenas, A. *et al.* (2018) 'Evolution of Cortical Neurogenesis in Amniotes Controlled by Robo Signaling Levels', *Cell*, 174(3), pp. 590-606.e21. Available at: https://doi.org/10.1016/j.cell.2018.06.007.

Cardona, A. *et al.* (2010) 'Identifying Neuronal Lineages of Drosophila by Sequence Analysis of Axon Tracts', *Journal of Neuroscience*, 30(22), pp. 7538–7553. Available at: https://doi.org/10.1523/JNEUROSCI.0186-10.2010.

Chan, Y.-M., Feld, A. and Jonsdottir-Lewis, E. (2019) 'Effects of the Timing of Sex-Steroid Exposure in Adolescence on Adult Health Outcomes', *The Journal of Clinical Endocrinology and Metabolism*, 104(10), p. 4578. Available at: https://doi.org/10.1210/jc.2019-00569.

Chatterjee, N. and Perrimon, N. (2021) 'What fuels the fly: Energy metabolism in Drosophila and its application to the study of obesity and diabetes', *Science Advances*, 7(24), p. eabg4336. Available at: https://doi.org/10.1126/sciadv.abg4336.

Chen, T.-W. *et al.* (2013) 'Ultrasensitive fluorescent proteins for imaging neuronal activity', *Nature*, 499(7458), pp. 295–300. Available at: https://doi.org/10.1038/nature12354.

Chen, W. *et al.* (2014) 'Regulation of Drosophila circadian rhythms by miRNA let-7 is mediated by a regulatory cycle', *Nature Communications*, 5(1), p. 5549. Available at: https://doi.org/10.1038/ncomms6549.

Cichewicz, K. and Hirsh, J. (2018) 'ShinyR-DAM: a program analyzing Drosophila activity, sleep and circadian rhythms', *Communications Biology*, 1(1), pp. 1–5. Available at: https://doi.org/10.1038/s42003-018-0031-9.

Clark, M.Q. *et al.* (2018) 'Neural circuits driving larval locomotion in Drosophila', *Neural Development*, 13(1), p. 6. Available at: https://doi.org/10.1186/s13064-018-0103-z.

Colombani, J. *et al.* (2005) 'Antagonistic Actions of Ecdysone and Insulins Determine Final Size in Drosophila', *Science*, 310(5748), pp. 667–670. Available at: https://doi.org/10.1126/science.1119432.

Colombani, J. *et al.* (2015) 'Drosophila Lgr3 Couples Organ Growth with Maturation and Ensures Developmental Stability', *Current Biology*, 25(20), pp. 2723–2729. Available at: https://doi.org/10.1016/j.cub.2015.09.020.

Colombani, J., Andersen, D.S. and Léopold, P. (2012) 'Secreted Peptide Dilp8 Coordinates Drosophila Tissue Growth with Developmental Timing', *Science*, 336(6081), pp. 582–585. Available at: https://doi.org/10.1126/science.1216689.

Comer, J.D. *et al.* (2019) 'Commissural axon guidance in the developing spinal cord: from Cajal to the present day', *Neural Development*, 14(1), p. 9. Available at: https://doi.org/10.1186/s13064-019-0133-1.

Corrales, M. *et al.* (2022) 'A single-cell transcriptomic atlas of complete insect nervous systems across multiple life stages', *Neural Development*, 17(1), p. 8. Available at: https://doi.org/10.1186/s13064-022-00164-6.

van Dam, E. *et al.* (2020) 'Sugar-Induced Obesity and Insulin Resistance Are Uncoupled from Shortened Survival in Drosophila', *Cell Metabolism*, 31(4), pp. 710-725.e7. Available at: https://doi.org/10.1016/j.cmet.2020.02.016.

Das, J.K. *et al.* (2017) 'Nutrition in adolescents: physiology, metabolism, and nutritional needs', *Annals of the New York Academy of Sciences*, 1393(1), pp. 21–33. Available at: https://doi.org/10.1111/nyas.13330.

Davis, R.L. (1993) 'Mushroom bodies and drosophila learning', *Neuron*, 11(1), pp. 1–14. Available at: https://doi.org/10.1016/0896-6273(93)90266-T.

Day, F.R. *et al.* (2017) 'Genomic analyses identify hundreds of variants associated with age at menarche and support a role for puberty timing in cancer risk', *Nature Genetics*, 49(6), pp. 834–841. Available at: https://doi.org/10.1038/ng.3841.

Debat, V. *et al.* (2011) 'Developmental Stability: A Major Role for Cyclin G in Drosophila melanogaster', *PLoS Genetics*. Edited by G. Gibson, 7(10), p. e1002314. Available at: https://doi.org/10.1371/journal.pgen.1002314.

Debat, V. and Peronnet, F. (2013) 'Asymmetric flies: The control of developmental noise in *Drosophila*', *Fly*, 7(2), pp. 70–77. Available at: https://doi.org/10.4161/fly.23558.

Dickson, B.J. and Gilestro, G.F. (2006) 'Regulation of Commissural Axon Pathfinding by Slit and its Robo Receptors', *Annual Review of Cell and Developmental Biology*, 22(1), pp. 651–675. Available at: https://doi.org/10.1146/annurev.cellbio.21.090704.151234.

Domínguez, M. and Casares, F. (2005) 'Organ specification–growth control connection: New in-sights from the Drosophila eye–antennal disc', *Developmental Dynamics*, 232(3), pp. 673–684. Available at: https://doi.org/10.1002/dvdy.20311.

Felicísimo, Á.M. *et al.* (2018) 'Rollout archaeological photography for the graphic documentation of cultural heritage'. Available at: https://digital.csic.es/handle/10261/240639 (Accessed: 27 September 2022).

Felicísimo, Á.M. and Polo García, M.E. (2021) *Heritage documentation techniques and methods*. workingPaper. Universidad de Extremadura, Grupo de Investigación Kraken. Available at: https://dehesa.unex.es:8443/handle/10662/11841 (Accessed: 27 September 2022).

Ferres-Marco, D. *et al.* (2006) 'Epigenetic silencers and Notch collaborate to promote malignant tumours by Rb silencing', *Nature*, 439(7075), pp. 430–436. Available at: https://doi.org/10.1038/nature04376.

Finnerty, J.R. *et al.* (2004) 'Origins of Bilateral Symmetry: Hox and Dpp Expression in a Sea Anemone', *Science*, 304(5675), pp. 1335–1337. Available at: https://doi.org/10.1126/science.1091946.

Friedman, M. (2008) 'The evolutionary origin of flatfish asymmetry', *Nature*, 454(7201), pp. 209–212. Available at: https://doi.org/10.1038/nature07108.

Garcia-Bellido, A. and Merriam, J.R. (1971) 'Parameters of the wing imaginal disc development ofDrosophila melanogaster', *Developmental Biology*, 24(1), pp. 61–87. Available at: https://doi.org/10.1016/0012-1606(71)90047-9.

Garcia-Bellido, A., Ripoll, P. and Morata, G. (1973) 'Developmental Compartmentalisation of the Wing Disk of Drosophila', *Nature New Biology*, 245(147), pp. 251–253. Available at: https://doi.org/10.1038/newbio245251a0.

Garelli, A. *et al.* (2012) 'Imaginal Discs Secrete Insulin-Like Peptide 8 to Mediate Plasticity of Growth and Maturation', *Science*, 336(6081), pp. 579–582. Available at: https://doi.org/10.1126/science.1216735.

Garelli, A. *et al.* (2015) 'Dilp8 requires the neuronal relaxin receptor Lgr3 to couple growth to developmental timing', *Nature Communications*, 6(1), p. 8732. Available at: https://doi.org/10.1038/ncomms9732.

Gazzaniga, M.S. (2005) 'Forty-five years of split-brain research and still going strong', *Nature Reviews Neuroscience*, 6(8), pp. 653–659. Available at: https://doi.org/10.1038/nrn1723.

Geissmann, Q. *et al.* (2019) 'Rethomics: An R framework to analyse high-throughput behavioural data', *PLOS ONE*, 14(1), p. e0209331. Available at: https://doi.org/10.1371/journal.pone.0209331.

Generating Slit Scan Images in Python - Make Art with Python (no date). Available at: https://www.makeartwithpython.com/blog/creating-slit-scan-images-in-python-and-moviepy/ (Accessed: 28 September 2022).

Gilestro, G.F. and Cirelli, C. (2009) 'pySolo: a complete suite for sleep analysis in Drosophila', *Bioinformatics*, 25(11), pp. 1466–1467. Available at: https://doi.org/10.1093/bioinformatics/btp237.

Graham, J.H. *et al.* (2010) 'Fluctuating Asymmetry: Methods, Theory, and Applications', *Symmetry*, 2(2), pp. 466–540. Available at: https://doi.org/10.3390/sym2020466.

Graham, J.H. and Özener, B. (2016) 'Fluctuating Asymmetry of Human Populations: A Review', *Symmetry*, 8(12), p. 154. Available at: https://doi.org/10.3390/sym8120154.

Halme, A., Cheng, M. and Hariharan, I.K. (2010) 'Retinoids Regulate a Developmental Checkpoint for Tissue Regeneration in Drosophila', *Current Biology*, 20(5), pp. 458–463. Available at: https://doi.org/10.1016/j.cub.2010.01.038.

Hamada, F.N. *et al.* (2008) 'An internal thermal sensor controlling temperature preference in Drosophila', *Nature*, 454(7201), pp. 217–220. Available at: https://doi.org/10.1038/nature07001.

Han, P.-L. *et al.* (1992) 'Preferential expression of the drosophila rutabaga gene in mushroom bodies, neural centers for learning in insects', *Neuron*, 9(4), pp. 619–627. Available at: https://doi.org/10.1016/0896-6273(92)90026-A.

Hariharan, I.K. (2012) 'How Growth Abnormalities Delay "Puberty" in Drosophila', *Science Signaling*, 5(229), pp. pe27–pe27. Available at: https://doi.org/10.1126/scisignal.2003238.

Hartenstein, V. *et al.* (2015) 'Lineage-associated tracts defining the anatomy of the Drosophila first instar larval brain', *Developmental biology*, 406(1), pp. 14–39. Available at: https://doi.org/10.1016/j.ydbio.2015.06.021.

Heckscher, E.S. *et al.* (2015) 'Even-Skipped+ Interneurons Are Core Components of a Sensorimotor Circuit that Maintains Left-Right Symmetric Muscle Contraction Amplitude', *Neuron*, 88(2), pp. 314–329. Available at: https://doi.org/10.1016/j.neuron.2015.09.009.

Heisenberg, M. *et al.* (1985) 'Drosophila Mushroom Body Mutants are Deficient in Olfactory Learning', *Journal of Neurogenetics*, 2(1), pp. 1–30. Available at: https://doi.org/10.3109/01677068509100140.

Heisenberg, M. (2003) 'Mushroom body memoir: from maps to models', *Nature Reviews Neuroscience*, 4(4), pp. 266–275. Available at: https://doi.org/10.1038/nrn1074.

Heredia, F. *et al.* (2021) 'The steroid-hormone ecdysone coordinates parallel pupariation neuromotor and morphogenetic subprograms via epidermis-to-neuron Dilp8-Lgr3 signal induction', *Nature Communications*, 12(1), p. 3328. Available at: https://doi.org/10.1038/s41467-021-23218-5.

Hsu, S.Y.T. (2003) 'New insights into the evolution of the relaxin–LGR signaling system', *Trends in Endocrinology & Metabolism*, 14(7), pp. 303–309. Available at: https://doi.org/10.1016/S1043-2760(03)00106-1.

Hückesfeld, S. *et al.* (2021) 'Unveiling the sensory and interneuronal pathways of the neuroendocrine connectome in Drosophila', *eLife*. Edited by S. Sen et al., 10, p. e65745. Available at: https://doi.org/10.7554/eLife.65745.

Hur, J. and Giovannucci, E. (2020) 'Racial differences in prostate cancer: does timing of puberty play a role?', *British Journal of Cancer*, 123(3), pp. 349–354. Available at: https://doi.org/10.1038/s41416-020-0897-4.

Hurley, J.H. (1999) ‘Structure, Mechanism, and Regulation of Mammalian Adenylyl Cyclase *’, *Journal of Biological Chemistry*, 274(12), pp. 7599–7602. Available at: https://doi.org/10.1074/jbc.274.12.7599.

Itskov, P.M. *et al.* (2014) ‘Automated monitoring and quantitative analysis of feeding behaviour in Drosophila’, *Nature Communications*, 5(1), p. 4560. Available at: https://doi.org/10.1038/ncomms5560.

Jen, J.C. *et al.* (2004) ‘Mutations in a Human ROBO Gene Disrupt Hindbrain Axon Pathway Crossing and Morphogenesis’, *Science*, 304(5676), pp. 1509–1513. Available at: https://doi.org/10.1126/science.1096437.

Jindra, M., Palli, S.R. and Riddiford, L.M. (2013) ‘The Juvenile Hormone Signaling Pathway in Insect Development’, *Annual Review of Entomology*, 58(1), pp. 181–204. Available at: https://doi.org/10.1146/annurev-ento-120811-153700.

Jones, M.A. and Grotewiel, M. (2011) ‘Drosophila as a model for age-related impairment in locomotor and other behaviors’, *Experimental Gerontology*, 46(5), pp. 320–325. Available at: https://doi.org/10.1016/j.exger.2010.08.012.

Juarez-Carreño, S. *et al.* (2021) ‘Body-fat sensor triggers ribosome maturation in the steroidogenic gland to initiate sexual maturation in Drosophila’, *Cell Reports*, 37(2), p. 109830. Available at: https://doi.org/10.1016/j.celrep.2021.109830.

Juarez-Carreño, S., Morante, J. and Dominguez, M. (2018) ‘Systemic signalling and local effectors in developmental stability, body symmetry, and size’, *Cell Stress*, 2(12), pp. 340–361. Available at: https://doi.org/10.15698/cst2018.12.167.

Justice, E.D., Barnum, S.J. and Kidd, T. (2017) ‘The WAGR syndrome gene PRRG4 is a functional homologue of the commissureless axon guidance gene’, *PLOS Genetics*, 13(8), p. e1006865. Available at: https://doi.org/10.1371/journal.pgen.1006865.

Justin Kerr (no date) *MAYAVASE.COM, Maya vase database: An archive of rollout photographs created by Justin Kerr*. Available at: http://www.mayavase.com/ (Accessed: 27 September 2022).

Keleman, K. *et al.* (2002) ‘Comm Sorts Robo to Control Axon Guidance at the Drosophila Midline’, *Cell*, 110(4), pp. 415–427. Available at: https://doi.org/10.1016/S0092-8674(02)00901-7.

Kjaerulff, O. and Kiehn, O. (1996) ‘Distribution of Networks Generating and Coordinating Locomotor Activity in the Neonatal Rat Spinal Cord In Vitro: A Lesion Study’, *Journal of Neuroscience*, 16(18), pp. 5777–5794. Available at: https://doi.org/10.1523/JNEUROSCI.16-18-05777.1996.

Klingenberg, C.P. (2010) ‘Evolution and development of shape: integrating quantitative approaches’, *Nature Reviews Genetics*, 11(9), pp. 623–635. Available at: https://doi.org/10.1038/nrg2829.

Klingenberg, C.P. (2015) ‘Analyzing Fluctuating Asymmetry with Geometric Morphometrics: Concepts, Methods, and Applications’, *Symmetry*, 7(2), pp. 843–934. Available at: https://doi.org/10.3390/sym7020843.

Kops, G.J.P.L. *et al.* (1999) 'Direct control of the Forkhead transcription factor AFX by protein kinase B', *Nature*, 398(6728), pp. 630–634. Available at: https://doi.org/10.1038/19328.

Kristan, W.B. (2016) 'Early evolution of neurons', *Current Biology*, 26(20), pp. R949–R954. Available at: https://doi.org/10.1016/j.cub.2016.05.030.

Kyriacou, C.P. and Hall, J.C. (1984) 'Learning and memory mutations impair acoustic priming of mating behaviour in Drosophila', *Nature*, 308(5954), pp. 62–65. Available at: https://doi.org/10.1038/308062a0.

Lam, B.Y.H. *et al.* (2021) 'MC3R links nutritional state to childhood growth and the timing of puberty', *Nature*, 599(7885), pp. 436–441. Available at: https://doi.org/10.1038/s41586-021-04088-9.

Lambrechts, R., Faber, A. and Sibon, O. (2017) 'Modelling in miniature: Using Drosophila melanogaster to study human neurodegeneration', *Drug Discovery Today: Disease Models*, 25–26, pp. 3–10. Available at: https://doi.org/10.1016/j.ddmod.2018.09.004.

Lanuza, G.M. *et al.* (2004) 'Genetic Identification of Spinal Interneurons that Coordinate Left-Right Locomotor Activity Necessary for Walking Movements', *Neuron*, 42(3), pp. 375–386. Available at: https://doi.org/10.1016/S0896-6273(04)00249-1.

Larouche-Bilodeau, C., Guilbeault-Mayers, X. and Cameron, C.B. (2020) 'Filter feeding, deviations from bilateral symmetry, developmental noise, and heterochrony of hemichordate and cephalochordate gills', *Ecology and Evolution*, 10(23), pp. 13544–13554. Available at: https://doi.org/10.1002/ece3.6962.

Lee, D. (2015) 'Global and local missions of cAMP signaling in neural plasticity, learning, and memory', *Frontiers in Pharmacology*, 6. Available at: https://doi.org/10.3389/fphar.2015.00161.

Levin, L.R. and Reed, R. (1992) 'Preferential Expression of the Drosophila rutaga Gene in Mushroom Bodies, Neural Centers for Learning in Insects', *Neuron*, 9(4), p. 9.

Li, H.-H. *et al.* (2014) 'A GAL4 Driver Resource for Developmental and Behavioral Studies on the Larval CNS of Drosophila', *Cell Reports*, 8(3), pp. 897–908. Available at: https://doi.org/10.1016/j.celrep.2014.06.065.

Liao, S. and Nässel, D.R. (2020) 'Drosophila Insulin-Like Peptide 8 (DILP8) in Ovarian Follicle Cells Regulates Ovulation and Metabolism', *Frontiers in Endocrinology*, 11. Available at: https://www.frontiersin.org/articles/10.3389/fendo.2020.00461 (Accessed: 12 September 2022).

Lopes, G. *et al.* (2015) 'Bonsai: an event-based framework for processing and controlling data streams', *Frontiers in Neuroinformatics*, 9. Available at: https://www.frontiersin.org/article/10.3389/fninf.2015.00007 (Accessed: 25 January 2022).

Manuel, M. (2009) 'Early evolution of symmetry and polarity in metazoan body plans', *Comptes Rendus Biologies*, 332(2), pp. 184–209. Available at: https://doi.org/10.1016/j.crvi.2008.07.009.

Mathis, A. *et al.* (2018) 'DeepLabCut: markerless pose estimation of user-defined body parts with deep learning', *Nature Neuroscience*, 21(9), pp. 1281–1289. Available at: https://doi.org/10.1038/s41593-018-0209-y.

Mattila, J. *et al.* (2009) 'Drosophila FoxO Regulates Organism Size and Stress Resistance through an Adenylate Cyclase', *Molecular and Cellular Biology*, 29(19), pp. 5357–5365. Available at: https://doi.org/10.1128/MCB.00302-09.

McBrayer, Z. *et al.* (2007) 'Prothoracicotropic Hormone Regulates Developmental Timing and Body Size in Drosophila', *Developmental Cell*, 13(6), pp. 857–871. Available at: https://doi.org/10.1016/j.devcel.2007.11.003.

McGuire, S.E., Mao, Z. and Davis, R.L. (2004) 'Spatiotemporal Gene Expression Targeting with the TARGET and Gene-Switch Systems in Drosophila', *Science's STKE*, 2004(220), pp. pl6–pl6. Available at: https://doi.org/10.1126/stke.2202004pl6.

Meissner, G.W. *et al.* (2016) 'Sex-specific regulation of Lgr3 in Drosophila neurons', *Proceedings of the National Academy of Sciences*, 113(9), pp. E1256–E1265. Available at: https://doi.org/10.1073/pnas.1600241113.

Mellon, D. and Stephens, P.J. (1978) 'Limb morphology and function are transformed by contralateral nerve section in snapping shrimps', *Nature*, 272(5650), pp. 246–248. Available at: https://doi.org/10.1038/272246a0.

Memeo, R. *et al.* (2021) 'Automatic imaging of Drosophila embryos with light sheet fluorescence microscopy on chip', *Journal of Biophotonics*, 14(3), p. e202000396. Available at: https://doi.org/10.1002/jbio.202000396.

Mirth, C., Truman, J.W. and Riddiford, L.M. (2005) 'The Role of the Prothoracic Gland in Determining Critical Weight for Metamorphosis in Drosophila melanogaster', *Current Biology*, 15(20), pp. 1796–1807. Available at: https://doi.org/10.1016/j.cub.2005.09.017.

Mitchell, K.J. (2018) 'Revealing the Genetic Instructions for Nervous System Wiring', *Trends in Neurosciences*, 41(7), pp. 407–409. Available at: https://doi.org/10.1016/j.tins.2018.04.008.

Musselman, L.P. and Kühnlein, R.P. (2018) 'Drosophila as a model to study obesity and metabolic disease', *Journal of Experimental Biology*. Edited by R.K. Suarez and H.H. Hoppeler, 221(Suppl_1), p. jeb163881. Available at: https://doi.org/10.1242/jeb.163881.

Musso, P.-Y., Junca, P. and Gordon, M.D. (2021) 'A neural circuit linking two sugar sensors regulates satiety-dependent fructose drive in Drosophila', *Science Advances*, 7(49), p. eabj0186. Available at: https://doi.org/10.1126/sciadv.abj0186.

Myat, A. *et al.* (2002) 'Drosophila Nedd4, a Ubiquitin Ligase, Is Recruited by Commissureless to Control Cell Surface Levels of the Roundabout Receptor', *Neuron*, 35(3), pp. 447–459. Available at: https://doi.org/10.1016/S0896-6273(02)00795-X.

Myers, R.E. and Sperry, R.W. (1958) 'Interhemispheric Communication Through the Corpus Callosum: Mnemonic Carry-Over Between the Hemispheres', *A.M.A. Archives of Neurology & Psychiatry*, 80(3), pp. 298–303. Available at: https://doi.org/10.1001/archneurpsyc.1958.02340090034004.

Nässel, D. *et al.* (2013) 'Factors that regulate insulin producing cells and their output in Drosophila', *Frontiers in Physiology*, 4. Available at: https://www.frontiersin.org/articles/10.3389/fphys.2013.00252 (Accessed: 20 September 2022).

Nériec, N. and Desplan, C. (2016) 'Chapter Fourteen - From the Eye to the Brain: Development of the Drosophila Visual System', in P.M. Wassarman (ed.) *Current Topics in Developmental Biology*. Academic Press (Essays on Developmental Biology, Part A), pp. 247–271. Available at: https://doi.org/10.1016/bs.ctdb.2015.11.032.

Nern, A., Pfeiffer, B.D. and Rubin, G.M. (2015) 'Optimized tools for multicolor stochastic labeling reveal diverse stereotyped cell arrangements in the fly visual system', *Proceedings of the National Academy of Sciences of the United States of America*, 112(22), pp. E2967–E2976. Available at: https://doi.org/10.1073/pnas.1506763112.

Nicolaï, L.J.J. *et al.* (2010) 'Genetically encoded dendritic marker sheds light on neuronal connectivity in Drosophila', *Proceedings of the National Academy of Sciences*, 107(47), pp. 20553–20558. Available at: https://doi.org/10.1073/pnas.1010198107.

Nijhout, H.F. (2003) 'The control of body size in insects', *Developmental Biology*, 261(1), pp. 1–9. Available at: https://doi.org/10.1016/S0012-1606(03)00276-8.

Ogg, S. *et al.* (1997) 'The Fork head transcription factor DAF-16 transduces insulin-like metabolic and longevity signals in C. elegans', *Nature*, 389(6654), pp. 994–999. Available at: https://doi.org/10.1038/40194.

Oliva, C. *et al.* (2016) 'Regulation of Drosophila Brain Wiring by Neuropil Interactions via a Slit-Robo-RPTP Signaling Complex', *Developmental Cell*, 39(2), pp. 267–278. Available at: https://doi.org/10.1016/j.devcel.2016.09.028.

Ormerod, K.G. *et al.* (2017) 'Drosophila development, physiology, behavior, and lifespan are influenced by altered dietary composition', *Fly*, 11(3), pp. 153–170. Available at: https://doi.org/10.1080/19336934.2017.1304331.

Palmer, A.R. (1994) 'Fluctuating asymmetry analyses: a primer', in T.A. Markow (ed.) *Developmental Instability: Its Origins and Evolutionary Implications: Proceedings of the International Conference on Developmental Instability: Its Origins and Evolutionary Implications, Tempe, Arizona, 14–15 June 1993*. Dordrecht: Springer Netherlands (Contemporary Issues in Genetics and Evolution), pp. 335–364. Available at: https://doi.org/10.1007/978-94-011-0830-0_26.

Palmer, A.R. (1996) 'From symmetry to asymmetry: Phylogenetic patterns of asymmetry variation in animals and their evolutionary significance', *Proceedings of the National Academy of Sciences*, 93(25), pp. 14279–14286. Available at: https://doi.org/10.1073/pnas.93.25.14279.

Palmer, A.R. (2009) 'Animal asymmetry', *Current Biology*, 19(12), pp. R473–R477. Available at: https://doi.org/10.1016/j.cub.2009.04.006.

Palmer, A.R. and Strobeck, C. (1986) 'FLUCTUATING ASYMMETRY: Measurement, Analysis, Patterns', *Annual Review of Ecology and Systematics*, 17(1), pp. 391–421. Available at: https://doi.org/10.1146/annurev.es.17.110186.002135.

Palmer, A.R., Strobeck, C. and Chippindale, A.K. (1994) 'Bilateral variation and the evolutionary origin of macroscopic asymmetries', in T.A. Markow (ed.) *Developmental Instability: Its Origins and Evolutionary Implications: Proceedings of the International Conference on Developmental Instability: Its Origins and Evolutionary Implications, Tempe, Arizona, 14–15 June 1993*. Dordrecht: Springer Netherlands (Contemporary Issues in Genetics and Evolution), pp. 203–220. Available at: https://doi.org/10.1007/978-94-011-0830-0_15.

Palmer Home Page (2019). Available at: http://www.biology.ualberta.ca/palmer.hp/palmer.html (Accessed: 6 September 2022).

Pan, X., Connacher, R.P. and O'Connor, M.B. (2021) 'Control of the insect metamorphic transition by ecdysteroid production and secretion', *Current Opinion in Insect Science*, 43, pp. 11–20. Available at: https://doi.org/10.1016/j.cois.2020.09.004.

Parslow, A., Cardona, A. and Bryson-Richardson, R.J. (2014) 'Sample Drift Correction Following 4D Confocal Time-lapse Imaging', *JoVE (Journal of Visualized Experiments)*, (86), p. e51086. Available at: https://doi.org/10.3791/51086.

Perrett, D.I. *et al.* (1999) 'Symmetry and Human Facial Attractiveness', *Evolution and Human Behavior*, 20(5), pp. 295–307. Available at: https://doi.org/10.1016/S1090-5138(99)00014-8.

Podratz, J.L. *et al.* (2013) 'An automated climbing apparatus to measure chemotherapy-induced neurotoxicity in *Drosophila melanogaster*', *Fly*, 7(3), pp. 187–192. Available at: https://doi.org/10.4161/fly.24789.

Pulver, S.R. *et al.* (2009) 'Temporal Dynamics of Neuronal Activation by Channelrhodopsin-2 and TRPA1 Determine Behavioral Output in Drosophila Larvae', *Journal of Neurophysiology*, 101(6), pp. 3075–3088. Available at: https://doi.org/10.1152/jn.00071.2009.

Reproductive health in young male adults with chronic diseases in childhood (2013).

Richard, D.S. *et al.* (1989) 'Juvenile hormone bisepoxide biosynthesis in vitro by the ring gland of Drosophila melanogaster: a putative juvenile hormone in the higher Diptera.', *Proceedings of the National Academy of Sciences*, 86(4), pp. 1421–1425. Available at: https://doi.org/10.1073/pnas.86.4.1421.

Richards, G. (1978) 'The relative biological activities of α- and β-ecdysone and their 3 dehydro derivatives in the chromosome puffing assay', *Journal of Insect Physiology*, 24(4), pp. 329–335. Available at: https://doi.org/10.1016/0022-1910(78)90032-X.

Rubin, G.M. (1988) 'Drosophila melanogaster as an Experimental Organism', *Science*, 240(4858), pp. 1453–1459. Available at: https://doi.org/10.1126/science.3131880.

Rulifson, E.J., Kim, S.K. and Nusse, R. (2002) 'Ablation of Insulin-Producing Neurons in Flies: Growth and Diabetic Phenotypes', *Science*, 296(5570), pp. 1118–1120. Available at: https://doi.org/10.1126/science.1070058.

Sarov-Blat, L. *et al.* (2000) 'The Drosophila takeout Gene Is a Novel Molecular Link between Circadian Rhythms and Feeding Behavior', *Cell*, 101(6), pp. 647–656. Available at: https://doi.org/10.1016/S0092-8674(00)80876-4.

Schindelin, J. *et al.* (2012) 'Fiji: an open-source platform for biological-image analysis', *Nature Methods*, 9(7), pp. 676–682. Available at: https://doi.org/10.1038/nmeth.2019.

Schumann, I. and Triphan, T. (2020a) 'The PEDtracker: An Automatic Staging Approach for Drosophila melanogaster Larvae', *Frontiers in Behavioral Neuroscience*, 14, p. 612313. Available at: https://doi.org/10.3389/fnbeh.2020.612313.

Schumann, I. and Triphan, T. (2020b) 'The PEDtracker: An Automatic Staging Approach for Drosophila melanogaster Larvae', *Frontiers in Behavioral Neuroscience*, 14. Available at: https://www.frontiersin.org/article/10.3389/fnbeh.2020.612313 (Accessed: 17 May 2022).

Sedlmeyer, I.L. and Palmert, M.R. (2002) 'Delayed Puberty: Analysis of a Large Case Series from an Academic Center', *The Journal of Clinical Endocrinology & Metabolism*, 87(4), pp. 1613–1620. Available at: https://doi.org/10.1210/jcem.87.4.8395.

Seeger, M. *et al.* (1993) 'Mutations affecting growth cone guidance in drosophila: Genes necessary for guidance toward or away from the midline', *Neuron*, 10(3), pp. 409–426. Available at: https://doi.org/10.1016/0896-6273(93)90330-T.

Seong, K.-H. *et al.* (2020a) 'The Drosophila Individual Activity Monitoring and Detection System (DIAMonDS)', *eLife*. Edited by H.J. Bellen et al., 9, p. e58630. Available at: https://doi.org/10.7554/eLife.58630.

Seong, K.-H. *et al.* (2020b) 'The Drosophila Individual Activity Monitoring and Detection System (DIAMonDS)', *eLife*. Edited by H.J. Bellen et al., 9, p. e58630. Available at: https://doi.org/10.7554/eLife.58630.

Singh, S.R. and Hou, S.X. (2009) 'Multipotent stem cells in the Malpighian tubules of adult Drosophila melanogaster', *Journal of Experimental Biology*, 212(3), pp. 413–423. Available at: https://doi.org/10.1242/jeb.024216.

Smith-Bolton, R.K. *et al.* (2009a) 'Regenerative Growth in Drosophila Imaginal Discs Is Regulated by Wingless and Myc', *Developmental Cell*, 16(6), pp. 797–809. Available at: https://doi.org/10.1016/j.devcel.2009.04.015.

Smith-Bolton, R.K. *et al.* (2009b) 'Regenerative Growth in Drosophila Imaginal Discs Is Regulated by Wingless and Myc', *Developmental Cell*, 16(6), pp. 797–809. Available at: https://doi.org/10.1016/j.devcel.2009.04.015.

Spierer, A.N. *et al.* (2021) 'FreeClimber: automated quantification of climbing performance in Drosophila', *Journal of Experimental Biology*, 224(2), p. jeb229377. Available at: https://doi.org/10.1242/jeb.229377.

Su, T.T. (2019) 'Drug screening in Drosophila; why, when, and when not?', *Wiley interdisciplinary reviews. Developmental biology*, 8(6), p. e346. Available at: https://doi.org/10.1002/wdev.346.

Suárez, R., Gobius, I. and Richards, L.J. (2014) 'Evolution and development of interhemispheric connections in the vertebrate forebrain', *Frontiers in Human Neuroscience*, 8. Available at: https://www.frontiersin.org/article/10.3389/fnhum.2014.00497 (Accessed: 29 March 2022).

Szuperak, M. *et al.* (2018) 'A sleep state in Drosophila larvae required for neural stem cell proliferation', *eLife*. Edited by M. Ramaswami, 7, p. e33220. Available at: https://doi.org/10.7554/eLife.33220.

Tanner, J.M. (1963) 'Regulation of Growth in Size in Mammals', *Nature*, 199(4896), pp. 845–850. Available at: https://doi.org/10.1038/199845a0.

Tanner, J.M. (1981) 'Catch-up growth in man', *British Medical Bulletin*, 37(3), pp. 233–238. Available at: https://doi.org/10.1093/oxfordjournals.bmb.a071708.

Tanner, J.M. (1986) 'Growth as a Target-Seeking Function', in F. Falkner and J.M. Tanner (eds) *Human Growth: A Comprehensive Treatise Volume 1 Developmental Biology Prenatal Growth*. Boston, MA: Springer US, pp. 167–179. Available at: https://doi.org/10.1007/978-1-4613-2101-9_9.

Tennessen, J.M. and Thummel, C.S. (2011) 'Coordinating Growth and Maturation — Insights from Drosophila', *Current Biology*, 21(18), pp. R750–R757. Available at: https://doi.org/10.1016/j.cub.2011.06.033.

Texada, M.J., Koyama, T. and Rewitz, K. (2020) 'Regulation of Body Size and Growth Control', *Genetics*, 216(2), pp. 269–313. Available at: https://doi.org/10.1534/genetics.120.303095.

TriKinetics (no date). Available at: https://trikinetics.com/ (Accessed: 26 September 2022).

Vallejo, D.M. *et al.* (2015) 'A brain circuit that synchronizes growth and maturation revealed through Dilp8 binding to Lgr3', *Science*, 350(6262), p. aac6767. Available at: https://doi.org/10.1126/science.aac6767.

Vallejo, D.M. *et al.* (2022) 'Neuroendocrine control of catch-up growth in Drosophila'. bioRxiv, p. 2022.12.30.522288. Available at: https://doi.org/10.1101/2022.12.30.522288.

Van Hiel, M.B. *et al.* (2015) 'Cloning, constitutive activity and expression profiling of two receptors related to relaxin receptors in Drosophila melanogaster', *Peptides*, 68, pp. 83–90. Available at: https://doi.org/10.1016/j.peptides.2014.07.014.

Villegas, S.N. *et al.* (2018) 'PI3K/Akt Cooperates with Oncogenic Notch by Inducing Nitric Oxide-Dependent Inflammation', *Cell Reports*, 22(10), pp. 2541–2549. Available at: https://doi.org/10.1016/j.celrep.2018.02.049.

Viswanath, V. *et al.* (2003) 'Opposite thermosensor in fruitfly and mouse', *Nature*, 423(6942), pp. 822–823. Available at: https://doi.org/10.1038/423822a.

Vogt, M. (1946) 'Inhibitory Effects of the Corpora Cardiaca and of the Corpus Allatum in Drosophila', *Nature*, 157(3990), pp. 512–512. Available at: https://doi.org/10.1038/157512b0.

Waddington, C.H. (1942) 'Canalization of Development and the Inheritance of Acquired Characters', *Nature*, 150(3811), pp. 563–565. Available at: https://doi.org/10.1038/150563a0.

Wang, L. *et al.* (2016) 'An In Vivo Pharmacological Screen Identifies Cholinergic Signaling as a Therapeutic Target in Glial-Based Nervous System Disease', *Journal of Neuroscience*, 36(5), pp. 1445–1455. Available at: https://doi.org/10.1523/JNEUROSCI.0256-15.2016.

Wells, K.M. *et al.* (2021) ‘Neural control of growth and size in the axolotl limb regenerate’, *eLife*. Edited by K. VijayRaghavan and M. Harris, 10, p. e68584. Available at: https://doi.org/10.7554/eLife.68584.

Wigglesworth, V.B. (1940) ‘The Determination of Characters at Metamorphosis in Rhodnius Prolixus (Hemiptera)’, *Journal of Experimental Biology*, 17(2), pp. 201–223. Available at: https://doi.org/10.1242/jeb.17.2.201.

Wigglesworth, V.B. (1947) ‘The Corpus Allatum and the Control of Metamorphosis in Insects’, *Nature*, 159(4052), pp. 872–872. Available at: https://doi.org/10.1038/159872a0.

Wolpert, L. (2010) ‘Arms and the Man: The Problem of Symmetric Growth’, *PLOS Biology*, 8(9), p. e1000477. Available at: https://doi.org/10.1371/journal.pbio.1000477.

Xu, Y.-Q. *et al.* (2021) ‘Evolution and diversity of axon guidance Robo receptor family genes’, *Journal of Systematics and Evolution*, 59(1), pp. 169–182. Available at: https://doi.org/10.1111/jse.12587.

Yamaguchi, S.T. *et al.* (2022) ‘The regulation of circadian rhythm by insulin signaling in Drosophila’, *Neuroscience Research*, 183, pp. 76–83. Available at: https://doi.org/10.1016/j.neures.2022.07.005.

Zars, T. (2000) ‘Behavioral functions of the insect mushroom bodies’, *Current Opinion in Neurobiology*, 10(6), pp. 790–795. Available at: https://doi.org/10.1016/S0959-4388(00)00147-1.

Zhong, Y., Budnik, V. and Wu, C. (1992) ‘Synaptic plasticity in Drosophila memory and hyperexcitable mutants: role of cAMP cascade’, *The Journal of Neuroscience*, 12(2), pp. 644–651. Available at: https://doi.org/10.1523/JNEUROSCI.12-02-00644.1992.

Acknowledgments

Famiglia: Nonostante ho deciso di allontanarmi da casa mia, vi ho sempre nel cuore. Grazie per tutto il supporto costante che ho avuto da voi tutti da sempre. Mi mancate, vorrei poter stare più vicino a voi. Spero possiate venire qua a vedere la mia tesi e essere orgogliosi di me.

Selene: Sono la persona più fortunata del mondo per averti potuto tenere vicino tutti questi anni. Senza il tuo auto e supporto continuo, questa tesi non sarebbe la stessa cosa. Sei sempre stata con me nei buoni e cattivi momenti. Mi hai supportato quando nessun altro lo faceva. Sei il mio amore. Grazie.

María: Gracias por confiar en mi todos estos años, contigo he aprendido mucho. Te agradezco de haber confiado en mi muchas veces. Espero que podamos seguir juntos una nueva aventura de lo spin-off- Parece un trabajo sin fin, pero nos está dando muchas satisfacciones. Tu humanidad con las personas que trabajan contigo es algo especial.

Javier Morante: Te agradezco la organización de las mayorías de las actividades de este laboratorio. También tu buen humor, y tus bromas.

Dolors: Para mi eres la más cercana compañera de trabajo y amiga que he tenido. Siempre has estado disponible para todo conmigo. Me has ensañado todo lo que se de genética de *Drosophila*. Te echaré mucho de menos.

Juan: Desde que nos conocimos hemos tenido muchas cosas en común. Eres mi mejor amigo de España y una de las pocas personas de las que estoy seguro seguirán en mi vida. Espero para ti lo mejor a pesar estos difíciles años.

Ernesto: Te agradezco tu energía, tu alegría y tu gana de fiesta te hacen una parte muy importante en el laboratorio. También todas las fiestas que hicimos juntos. ¡Eres un super trabajador y compañero de laboratorio!

Daniel: Eres el mejor estudiante que se puede desear. Eres muy listo y un gran trabajador. Estoy seguro de que en ciencia llagarás a ser alguien importante.

Rosa: Gracias Rosa para toda la ayuda que me has dado en estos años, eres una persona clave en el funcionamiento de este laboratorio.

Esther: Fuiste una persona clave del laboratorio. ¡Te agradezco todos los trabajos que has hecho para mantener el laboratorio de molecular en condiciones! Espero que tendrás suerte en tu nueva aventura.

Diana: El laboratorio perdió una pieza clave con tu despedida. Espero lo mejor para ti.

Sergio: Me has enseñado como avanzar en la investigación y como analizar críticamente mi trabajo. Eres un investigador con mucho éxito y tu carrera llegará muy lejos.

Laura: Tu organización, paciencia, tu buen rollo y tu disponibilidad te hacen una persona fundamental en este laboratorio. Agradezco mucho toda la ayuda que me has prestado en estos años.

Irene: Fuiste una de las primeras personas con la que entablé amistad. Siempre me acuerdo del día que nos enseñaste a Selene y mi a hacer el pan de queso.

Alicia: Trabajas con mucha alegría y vitalidad, y siempre estás disponible para ayudarnos. Espero poderte conocer mejor ahora que he vuelto a estar en el laboratorio. Te lo agradezco.

Aurelia: Eres una persona muy positiva y agradezco tu trabajo en el laboratorio. Me ha gustado mucho hablar contigo de la boda y los consejos que nos ha dado a Selene y mi.

Lucia: ¡Siempre has sido una super compañera de trabajo, me encanta haberte conocido! Eres super lista y espero que puedas encontrar tu trayectoria. Te lo mereces.

Isabel: Con tu buen humor, buen rollo, y los ratos pasados juntos los días en el laboratorio se hacen más cortos. Te agradezco tus consejos y todas las ayudas que me has dado. Espero que tu nueva carrera de profesora pueda seguir adelante lo mejor posible.

Mario: Estoy contento de tenerte como nuevo compañero de laboratorio. Eres un investigador muy bueno y una buena persona. Espero de conocerte mejor en el tiempo que me queda por aquí.

Víctor: Contigo he aprendido muchísimo sobre como programar, construir, soldar y muchas cosas más. Explotar condensadores y dejar sin luz toda una planta del INA. Sin ti el proyecto del flyGear no hubiera podido existir, siento que no hayamos seguido el trabajo juntos por culpa de un sistema que lo hace todo muy difícil.

Simon: Thank you for giving me the opportunity to stay in your lab. I discovered the field of neuro evo-devo that I found so fascinating. I have never seen in the same lab so many different model animal! It was a wonderful experience.

Larisa: Thank you for helping me with calcium imaging and for making me feel integrated in the new lab in Fribourg. You are a wonderful person, and I am very grateful for all the nice moment we passed together.